



# **Study on Impact Condition Identification of Composite Laminate Based on Deep Learning and Peridynamics**

Candidate: Chen Hao

Student Number: s274331

School/Department: College of Civil Engineering

Discipline: Engineering

Major: Civil Engineering

Supervisor: Pietro Cornetti







## ABSTRACT

Composite is often subjected to various loads (such as impact load) from outside, resulting in fracture, delamination and other damages. Traditional continuum mechanics theory based on partial differential equation is difficult to deal with discontinuous problems such as fracture and damage because it involves space derivation. Peridynamics (PD) is a nonlocal theory based on integral equation. It uses space integration to describe the material function, which has great advantages in dealing with the above problems. But there is "surface effect" in traditional PD methods. That is, when discretizing the material points, the horizon of the material points in the boundary area is incomplete, which will cause calculation errors. Based on this, the paper analyzes the problem of the problem, a more concise surface correction factor is proposed.

In the design process of composite materials, accurate load information is needed, such as the direction and velocity of external impactor, for example, for aircraft, it is convenient for engineers to design enough strength in appropriate positions, or estimate the residual strength of structures subjected to load and evaluate the probability of its continued use. Therefore, it is of great significance to identify the impact condition based on the damage data, and to improve the design of composite materials and ensure its safe use. Based on this problem, this paper develops a set of impact condition identification model based on deep learning, which can use the impact damage evolution data of composite materials under different impact conditions for training, and realize the identification of unknown impact conditions, so as to provide more detailed reference and basis for improving the design method of laminated plates.

The main contents of this paper include:

(1) Aiming at the problem of impact damage discontinuity of composite laminates, a numerical analysis model of impact damage evolution of composite laminates based on peridynamics theory is established, and the corresponding calculation program is developed. Moreover, in order to solve the problem of incomplete horizon of material points in the boundary region, an improved "surface correction factor" is proposed, which can improve the calculation accuracy. On the basis of the above model, the damage evolution of composite materials under different

impact conditions of cylindrical and spherical rigid bodies is analyzed.

(2) In order to identify the impact condition of composite laminates, a model based on machine learning convolution neural network (CNN) is developed under the framework of TensorFlow and Jupyter Notebook. The recognition model uses the impact damage evolution data of peridynamic composite laminates under different impact conditions for training, realizes the recognition of unknown impact conditions, and can control the relative error within 5% and reach a high accuracy.

**Key Words:** Peridynamics theory, composite laminate, impact damage analysis, Deep learning, TensorFlow

---

# Content

<b>Chapter 1 Introduction</b> .....	1
1.1 Background and significance of the study.....	1
1.2 Current status of related research.....	4
1.2.1 Status of research on peridynamics theory and impact damage.....	4
1.2.2 Status of research on impact condition identification.....	8
1.3 Development and organization of this paper.....	11
<b>Chapter 2 Introduction to Peridynamics Theory</b> .....	13
2.1 Introduction.....	13
2.2 Theoretical framework of peridynamics.....	13
2.2.1 Overview of "bond-based" peridynamics theory.....	14
2.2.1 Overview of "state-based" peridynamics theory.....	20
2.3 Computational methods and solution systems for peridynamics.....	22
2.3.1 Discretization of the equations of motion.....	22
2.3.2 Stability conditions for numerical methods.....	23
2.4 Summary of this chapter.....	24
<b>Chapter 3 Impact damage analysis of laminates based on peridynamics</b> .....	25
3.1 Introduction.....	25
3.2 Development and Computing Environment.....	25
3.2.1 Development environment construction.....	25
3.2.2 Computational flow and algorithm design.....	27
3.3 Modeling of composite laminates and impactors.....	28
3.3.1 Theory of anisotropic composite laminates.....	28
3.3.2 Description of damage to composite laminates.....	31
3.4 Shock theory based on peridynamics.....	32
3.4.1 Shock modeling.....	32
3.4.2 Examples.....	34
3.5 Determination of surface correction factor.....	38
3.6 Geometric model and material parameters.....	41
3.7 Numerical simulation results under impact conditions.....	44
3.7.1 Simulation results of cylindrical impact damage.....	44
3.7.2 Simulation results of round ball impact damage.....	51
3.8 Summary of this chapter.....	58
<b>Chapter 4 Deep Learning Based Impact Condition Identification</b> .....	59
4.1 Introduction.....	59

4.2 Introduction to Deep Learning Theorys.....	59
4.3 Model Selection.....	61
4.3.1 Common Network Models.....	61
4.3.2 Convolutional neural network and image recognition.....	64
4.4 Convolutional neural network construction.....	68
4.4.1 Activation Function.....	68
4.4.2 Hyperparameter setting.....	72
4.4.3 Network Structure.....	76
4.5 Impact condition identification.....	77
4.5.1 Dataset construction and partitioning.....	77
4.5.2 Identification based on the whole dataset.....	81
4.5.3 Identification based on partial dataset.....	85
4.6 Summary of this chapter.....	90
<b>Chapter 5 Conclusion and Outlook</b> .....	92
5.1 Conclusion.....	92
5.2 Outlook.....	93
<b>Reference</b> .....	96

## Chapter 1 Introduction

### 1.1 Background and significance of the study

Composite material is an important product of modern material industry and technology development. It is a new type of material made by combining material components with different properties and attributes according to a certain ratio, level and structure by using advanced material preparation technology. The material components can be divided into Matrix materials and Reinforcement materials according to the different functions in the preparation process, the former is the carrier of the latter, while the latter is the functional or structural complement of the former.

Composites have been used in a wide range of engineering and technical applications, including.

#### (1) Aerospace.

Composites are not only extremely strong, but also more thermally stable than conventional materials, making them ideal for the various extreme environments in which spacecraft are placed. Therefore, they are widely used in components and parts such as fuselage shells and glass of aircraft, wings, antennas of satellites, and shells of launch vehicles.

#### (2) Automotive and delivery engineering.

The automotive industry is more relevant to our daily life than the aforementioned fields, and is also a field where composite materials are very widely used. In addition to better fatigue resistance and mechanical strength, composite components are more resistant to impact than ordinary materials, and can therefore be used in automobile bodies, windshields and other stressed components.

#### (3) Construction industry

With the low price of composite materials and related products, they have been more widely used in the field of construction engineering. At present, the composite materials used in the construction industry are mainly non-metallic, including fiber reinforced materials (glass fiber, carbon fiber, etc.), synthetic resins (rubber), etc. Due to their low density, these materials can significantly reduce the weight of buildings, improve structural design and architectural design, reduce costs and improve economic efficiency.

(4) Other areas

Composite materials can also be used to produce and manufacture a number of other components or equipment, such as helmets and body armor for military and civilian use. In the military, composite materials are also often used in a variety of disaster prevention and hazard avoidance buildings or components.

In summary, composite materials are often used in structural members due to their own characteristics, and therefore, they are also the first to suffer external loads or effects during their use, and once damage occurs to these key parts of the composite material, it can lead to major accidents.

To aircraft, for example, one of the major hazards of aircraft in flight is flying birds and other outside flying objects, due to the relative speed of the two is great, therefore, once the impact of outside flying objects and the aircraft's front windshield and other key parts, it is very likely to break these parts and invade the interior of the body, thus causing accidents.

In construction projects, for example, composite materials are often used in curtain walls of high-rise and super high-rise buildings, and load-bearing elements of buildings, such as floor slabs and roof panels. These components have an obvious characteristic, that is, they are exposed to the external environment and are very vulnerable to various kinds of external effects, such as explosive loads, impact effects, etc. At the same time, once such events occur, they will lead to serious consequences, such as falling curtain walls, collapse of floor panels, etc., resulting in casualties.

For the automotive industry, once the car suffers a sudden impact from the outside world during the high-speed driving process, these parts often bear the brunt, thus threatening the safety of the driver and passengers. A large number of traffic accidents at home and abroad are from external foreign objects, such as stones and other broken car glass or body, threatening the safety of the driver's life. Therefore, the application of composite materials with excellent load-bearing capacity and impact resistance to these parts can greatly protect the safety of pedestrians, thus reducing the danger of traffic accidents to people.

Composite materials almost naturally possess certain defects due to their preparation processes and composition principles, including the differences in the respective physicochemical properties of the constituent materials, and these defects constitute the initial damage of the material, and damage evolution is an important topic in the field of engineering. Damage refers to the material or structure under

external loading or action, from the fine structure defects (such as microcracks, microvoids, etc.) sprouting, expansion and other irreversible changes caused by the deterioration of the macro mechanical properties of the material or structure. From the traditional point of view, damage analysis is mainly handled by the theory of continuous medium mechanics, but this traditional theory is based on partial differential equations, and thus encounters setbacks in dealing with spatially discontinuous problems such as damage and fracture, while Peridynamics (PD) is a non-local theory based on integral equations, which uses spatial integration to describe the action of matter, instead of the traditional continuous medium mechanics. The traditional peridynamics theory has a "surface effect" in the application process, i.e., the incomplete range of the material points located in the material boundary region, and thus the real results are inaccurate. Based on this, a variety of solutions have been proposed, such as modeling the internal region only by the peridynamics method, while the boundary region is simulated by the finite element method; introducing correction coefficients or attenuation factors to correct the material properties (micromodulus), etc. In this paper, based on the related research, a more concise surface correction factor is proposed to improve the model.

In addition, due to the wide application of composite materials, improving the design of composite materials has also become a very important research content. The improvement of the design, in general, needs to be carried out from two aspects, one is the possible external load or action, and the other is the properties of the material itself, however, the current situation is that once an accident occurs, the information we can obtain is often only a series of discontinuous damage data (such as fracture, deformation, etc.) on the structural member (e.g., composite laminate) that suffers from external load or action, and for the impact object before the accident. However, these parameters are important factors that can help us analyze the cause of the accident. For example, when a car is hit by a stone, we can analyze the source of the stone through the cracking of the front windshield, including the direction and speed of flight, so as to help relevant agencies and units clarify. For aircraft, satellites, rockets and other vehicles, we can also analyze the damage on their shells to qualitatively determine the form of impact or quantitatively calculate the size and direction of the impact, so as to provide more basis for engineers in designing the shells of these vehicles.

In summary, in addition to passively studying the damage of composite materials

after being subjected to external loads or effects, and arbitrarily enhancing the strength and other properties of the materials themselves, we should consider whether we can obtain some parameters of the impact based on the existing damage, with emerging technical methods, to help us analyze and restore the information on the working conditions of the impacted materials at the time of impact and before the impact, and invert the information on the form and size of the impact loads on the materials, and other working conditions. It is a more important topic to improve the design of composite materials.

## 1.2 Current status of related research

As a new theory and method in the field of computational mechanics, peridynamics has natural advantages in the direction of solving damage evolution, crack sprouting, fatigue, fracture, etc. Although it has only been proposed for a short period of more than ten years, and has been introduced to China for only about ten years, there are still many scholars at home and abroad who have produced a lot of results in this field.

### 1.2.1 Status of research on peridynamics theory and impact damage

As mentioned earlier, peridynamics theory has a natural advantage in impact damage studies, but traditional PD faces the so-called "surface effect" problem, which means that when discretizing material points, the near-field range of material points in the boundary region is incomplete, which leads to greater computational errors. Therefore, since PD theory was proposed, scholars at home and abroad have carried out extensive research based on it, proposed a variety of improved models, and carried out simulations and tests for a variety of materials and components, and produced a large number of meaningful results.

In terms of foreign scholars' achievements, early in the research, Madenci et al<sup>[1]</sup> combined the PD method with the traditional finite element method, and used finite element modeling for the boundary area, thus avoiding the problem of "boundary effect", and modeled and analyzed the structures such as steel plates based on the above method, and achieved better results.

Florin et al<sup>[2]</sup> proposed a modified "bond-based" peridynamics model based on brittle materials for "boundary effects", simulating the damage evolution and development of multi-layer tempered glass (MgG) under the action of high-speed impact. The damage evolution and development of multi-layer tempered glass (multi-layer glass) under high-speed impact is simulated, and most of the numerical results of<sup>[3]</sup> are reproduced, such as stress waves, crack development, deflection, etc. At the same time, the damage evolution of the three-dimensional structure of multi-layer tempered glass with time is simulated, and the damage and destruction mechanism of this typical brittle material of glass is revealed.

Akbari et al<sup>[4]</sup> investigated the impact response of polymers. They selected poly(methyl methacrylate) (PMMA) as the object of study and developed a modified "bond-based" PD model based on this material to simulate the impact of PMMA beams with initial cracks at different impact velocities and fracture toughness, and the results were in good agreement with other related literature<sup>[5-8]</sup>

Butler et al<sup>[9]</sup> predicted the compressive and impact strengths of carbon reinforced plastic flat laminate with initial circular holes by using the PD method. Baber et al<sup>[10]</sup> proposed an improved "bond-based" peridynamics model, taking into account bond nonlinear shear deformation and "boundary effects", to simulate the deformation and damage of composite laminates under low-velocity impact. The deformation and damage response of composite laminates under low velocity impact was simulated by Baber et al.

Bobaru et al<sup>[11]</sup> proposed a virtual node method for the PD model of elastic materials to reduce the effect of "boundary effect" and compared the effect of various methods and selected the one with the best correction.

Bartlett et al<sup>[12]</sup> improved the virtual node method proposed by Bobaru et al. to make this method applicable to objects with arbitrarily shaped boundaries, which can better eliminate the "boundary effect", and compared the results with those of related literature and achieved better results.

The domestic results mainly focus on the simulation and analysis of complex materials or structures such as concrete, ice bodies, and composite materials. Qing Zhang<sup>[13]</sup> was the first to introduce the concept and method of PD to China, and also the first to conduct related research in China, improving the calculation method of micro-modulus in the traditional PD model, solving the problem of "boundary effect" in the model, and based on this improved PD method, simulating concrete structures

and members under different working conditions, such as Based on this improved PD method, the damage of concrete structures and members under different loading conditions, such as impact<sup>[14-16]</sup>、 tensile<sup>[17]</sup>、 and intrusion<sup>[18]</sup> is simulated with good accuracy.

Cheng et al<sup>[19]</sup> used an improved damage factor with a modification of the conventional intrinsic force function to model and simulate the cracking process of engineered cement matrix composites (ECC) and compared it with relevant tests with good results.

Based on the "bond-based" PD theory, Xiong Weipeng et al<sup>[20]</sup>constructed an improved PD model and realized the simulation of the mechanical behavior of a complex mixture of ice body under the action of high-speed impact by self-programming, reproduced the damage characteristics of the ice ball with high strain rate during the impact process and the complete damage process of the sphere, and accurately simulated the development of surface cracking and overall cracking of the sphere. The surface cracks and the development of the overall cracking were accurately simulated, while the time course curve of the impact force during the impact was identified by the PD program, which was in good agreement with the measured values.

Xiaoping Zhou<sup>[21]</sup> established a "conjugate bond" base PD model based on the traditional "bond base" PD theory, introduced the rotation angle, and derived the relevant parameters to realize the damage characteristics of the rock under the blast impact load, and achieved a The relevant parameters are derived, and the damage characteristics of the rock under the blast impact load are realized with good results.

In the field of composite materials, Guogun Zheng et al<sup>[22]</sup> proposed an improved BPD model for the problem of the limitation of Poisson's ratio in the peridynamics (BPD) model, which can be used both for the simulation of deformation and crack extension of orthotropic anisotropic monolayers and for the prediction of deformation and crack development of carbon fiber composites with high accuracy.

Jinsong Zhang<sup>[23]</sup> derived a new type of iterative formulation for a heavy-headed quasi-static intrusion plate based on the punch extrusion model in finite element theory, and introduced a volume correction factor in the intrinsic force function to establish an impact dynamics model for composite laminates, studied the impact damage problem of composite laminates, and simulated the damage evolution process of various peer brittle materials.

Wang Fuwei et al<sup>[24]</sup> introduced interlaminar shear and long-range force terms on the basis of the traditional laminate model, modified the "boundary effect" in PD theory, and derived the relevant equations and parameters to improve the traditional model, and used the model to simulate the tensile and impact of each homogeneous and each anisotropic laminate, and obtained the The damage evolution of the composite laminates was obtained, and the damage pattern of the composite laminates was further obtained.

Qin Hongyuan et al<sup>[25]</sup> introduced a kernel function correction term reflecting the dimensional effect of the long range force in the matrix bond on the basis of the traditional intrinsic structure model, which solved the problem of "boundary effect" in the traditional PD theory, and simulated the deformation and damage of the composite single-layer plate with higher accuracy than the traditional model. It can simulate the deformation and damage of composite monolayers with higher accuracy than the traditional model.

The application scenarios and environments of composites are often very complex, and a number of domestic scholars have conducted PD simulations for composites in different use environments. Zhao Tianyou <sup>[26]</sup> proposed an improved PD model based on composite materials commonly used on ships, and simulated the damage evolution of composite laminates and reinforced laminates under the action of underwater fragment intrusion laminates and blast impact based on the boundary constraints of laminates and underwater environment, and obtained the damage evolution of laminates under different impact conditions (impact velocity, impactor shape, mass) and lay-up direction; and analyzed the damage evolution law of laminates with reinforced bars. The damage evolution of laminates under different impact conditions (impact velocity, impactor shape, mass, and layup direction) was obtained, and the influence of the size and distribution distance of the reinforcement on the strength of laminates with reinforcement was analyzed. Su Boyang et al<sup>[27]</sup>, also for composite materials in ships, improved the principal structure equation by introducing a hygrothermal elongation correction term describing humidity and temperature, and used this equation to simulate the evolution of impact damage of this material in different hygrothermal environments, and analyzed the effect of impact velocity on the energy absorption performance of composite laminates, and obtained some relevant laws with certain application values, which can be used to improve the design method of composite materials on ships. The impact velocity effects on the

energy absorption performance of composite laminates are analyzed, and some application rules are obtained, which can be used to improve the design method of composite materials on ship hulls.

Due to its good ductility, composite materials are often prepared into a variety of shapes according to the actual use scenarios, and most of the domestic and foreign studies are carried out based on flat structures. Chen Xiaofeng et al. studied the response of curved plates under the impact action based on the study of impact damage of composite flat plates<sup>[28][29]</sup>. A program was written in Fortran to simulate the impact damage evolution of laminates with different impact conditions (velocity and angle) for various lay-up forms of laminates; meanwhile, the impact resistance of sinusoidal curved plate models with different heights was studied and the best performing curved plate height was optimized.

Since the traditional PD theory faces the problem of "surface effect", the current impact simulation studies based on peridynamics are mostly based on the traditional model, and the form of the intrinsic force function is modified, such as the introduction of correction coefficients, attenuation factors, etc. Therefore, we address this problem by introducing a more concise expression for the surface correction coefficients in the model, based on the existing studies. Therefore, to address this problem, we introduce a more concise expression for the surface correction coefficient to simulate and analyze the impact damage of laminated plates based on existing studies.

### 1.2.2 Status of research on impact condition identification

The impact condition refers to the "Inverse problem" based on the above-mentioned impact damage simulation work, and many scholars at home and abroad have started to study this problem, i.e., to identify the impact condition (such as energy, velocity, angle, load, impact force time range and other parameters) based on the known data, such as the observed damage evolution, the various types of impact response (displacement, strain, etc.) monitored by sensors. In this study, the impact conditions (e.g., energy, velocity, angle, load, impact force time range, etc.) are identified based on known data, such as the observed damage evolution, various types of impact responses (displacement, strain, etc.) monitored by sensors. The current research mainly includes the identification of impact velocity and direction, the reconstruction of the time course curve of the impact load, and the localization of the

impact point.

Liu et al<sup>[30]</sup> proposed a time course identification method for impact loads that combines the L-curve criterion (RCBSC-ML) and the cubic spline configuration method (RCBSC), taking into account the inconvenient installation of sensors and so on, and attempted to reconstruct the time course curve of impact loads by approximating the unknown force with a linear combination of cubic spline curves with good results.

Inman et al<sup>[31]</sup> developed a load and damage identification system based on a one-dimensional convolutional neural network (CNN) that is capable of monitoring and localizing vibration damage in structures in real time (Real-time) and predicting the magnitude and location of impact forces.

Guan et al<sup>[32]</sup>, on the other hand, determined the analytical solution of the displacement function of the plate under impact loading based on Reddy's higher-order shear deformation theory and the classical laminate theory, and proposed a set of impact condition models based on this, which can identify the vibration and impact responses in fiber-reinforced metal laminates, and also predict the impact loads and displacements to which the laminate is subjected with high accuracy.

Abraham et al<sup>[33]</sup> used a hybrid learning approach to build a set of neural network models based on the damage data of vehicles in crashes, capable of classifying the severity of traffic accidents according to the type and extent of vehicle damage, thus providing a reference for researchers and engineers in the automotive industry in their designs.

Kalhari et al<sup>[34]</sup> completed a series of impact load reconstruction and impact location determination using a signal processing approach, including for a multi-story tower structure, where the dynamic response signal of the response was measured by multiple sensors, including acceleration sensors, vibrometers, and displacement sensors, and based on this signal and the superposition principle, the magnitude and location of the impact load applied to the tower were reconstructed. In addition, a similar method was used to complete the identification of the impact load time course curve and the impact position localization on the composite sheet in the field of action [35], which achieved high accuracy and engineering application value.

Kawabata et al<sup>[36]</sup> optimized the strain sensor based on the observation spillover minimization criterion and reconstructed the time course profile of the impact load applied to the structure by measuring the obtained low-order modes.

Li et al<sup>[37]</sup> built a program that can identify the car impact velocity (Velocity), angle (Angle) and deviation (Offset) from finite element simulation, combined with deep learning, which carried out the finite element simulation of car collision through ABAQUS, taking the extracted car sound plastic deformation as input, and after training in the model, the output obtained the above. The identification results of the parameters are compared with the real values with high accuracy and good error control.

Fang et al<sup>[38]</sup> used the small mass impact (Small mass impact) theory, and based on the impact force calculation model of plate deflection in this theory and the spring-impact force prediction model based on impact crater, the impact force was predicted using the force, displacement and acoustic emission signals collected by sensors during the impact, and the time course curve and energy spectrum of the impact load were obtained.

Zhu et al<sup>[39]</sup> used ABAQUS to establish a model of low-velocity impact composite laminates in the hemisphere and to approximate the location of the impact loads by using the stress, strain, and vibration modal data of each layup extracted from the software, so that protection against the hazards caused by low-velocity impact and repair of the corresponding damage can be carried out, which has some practical application value.

Yan Gang et al. proposed a recognition technique based on Bayes compressed sensing (Bayes compressed sensing) method<sup>[40]</sup>, which reconstructed the time course of the impact load based on the impact response measured by the sensor, and the shape, duration, and peak value of the time course curve of the recognition result are basically the same as the actual impact load, which has certain applicability.

Jia et al<sup>[41]</sup> proposed a novel regularization method based on the alternating direction multiplier method for the problem of too many dimensions of the identification matrix and severe pathologies during impact loading, and successfully identified impact loads in cantilever beams and high-speed presses.

Su et al<sup>[42]</sup> introduced the Array signal processing technique (ASP) to the field of impact condition identification, and used Wavelet transform (WT) and Multiple Signal Classification algorithm (MUSIC) to achieve the impact localization of composite results with high accuracy and Real-time monitoring is achieved.

With the development of deep learning, related concepts and methods have been introduced into the study of impact condition identification. Shou-Ju Li et al<sup>[43]</sup>

addressed the blast impact loads that may be encountered in protection engineering, and the response of the structure (e.g., displacement, velocity, stress, etc.) was used as input to obtain the impact loads (magnitude of initial pressure) acting on the structure by inversion through the idea of least squares, so that the relevant damage, damage mechanisms and further guidance for the design of the relevant protection structures could be obtained.

Guo et al<sup>[44]</sup> used FBG fiber grating sensor, combined with Wavelet Packet Transform and Correlation coefficient method (Correlation coefficient) to achieve the impact position identification of composite laminates, to a certain extent can be more localized to the exact position or the position adjacent to the exact position, there is Certain application and promotion value. Wang Liheng<sup>[45]</sup> proposed a series of new identification indexes, such as pulse rise time and pulse rise area, based on the pulse strain signal obtained during the impact process, and found that the time-related indexes can be used to identify the damage degree, while the area-related indexes can be used for impact location identification.

Damage evolution of composite materials is a very complex nonlinear problem, and the inverse problem of this problem, impact condition identification based on damage evolution data, also encounters great challenges. Therefore, in this paper, we try to use a deep learning approach to identify unknown conditions based on damage evolution data of composite laminates.

### 1.3 Development and organization of this paper

This paper can be divided into two parts according to the work, the first part is numerical calculation and the second part is deep learning based impact condition identification.

Composite laminates generate complex discontinuities during the damage process, such as fiber fracture, matrix cracking and delamination damage<sup>[46]</sup>. And due to the use of integral form to construct the equations of motion of the object, the peridynamics method is well suited to deal with these discontinuities, and through bond-by-bond destruction, the peridynamics method can effectively simulate the complete process of composite materials from initial damage to final destruction. Therefore, in this paper, the peridynamics method is used to develop the study of progressive damage and deformation characteristics of fiber-reinforced composite

laminates, which are widely used in engineering.

In Chapter 2, some basic theoretical knowledge of the peridynamics theory is briefly introduced<sup>[47-49]</sup>, which mainly includes the basic equations of motion of peridynamics and the physical quantities in the equations, especially some basic theories of the intrinsic force functions, including some different forms of the functions and the improvements and modifications made by domestic and foreign scholars for the traditional intrinsic force functions.

In Chapter 3, firstly, the basic knowledge of composite laminates is introduced<sup>[46, 49]</sup>, including the intrinsic constitutive equations of the plate, and based on this, a rigid body impact damage evolution analysis model of composite laminates based on peridynamics theory is developed for the impact damage discontinuity mechanics problem of composite laminates in combination with the PD method<sup>[47, 50]</sup>, and the corresponding computational program is developed. Moreover, in order to solve the problem of incomplete near-field material points in the boundary region, an improved "surface correction factor" is proposed, which can improve the calculation accuracy. After the calculation system was built, the impact damage evolution of composite laminates under different working conditions (including different shapes, velocities and angles) was simulated, and the impact damage results at each intermediate step were recorded and analyzed.

In Chapter 4, a deep learning-convolutional neural network (CNN)-based recognition procedure was developed in the framework of TensorFlow and Jupyter Notebook to address the problem that the impact damage evolution of composite laminates exhibits nonlinear characteristics and the impact condition recognition encounters great challenges<sup>[51, 52]</sup>. In this chapter, we build a database with 1800 samples by modifying the impact conditions of rigid impact balls and adding "pretzel noise"<sup>[53]</sup> based on the computational procedure in Chapter 3, and use this dataset for training to achieve the recognition of unknown impact conditions, and the relative error of the recognition results is The relative error of the recognition results is controlled within 5%, while the accuracy rate reaches more than 90%, which has certain applicability.

In Chapter 5, we summarize some of the preliminary results obtained in the previous chapters and provide an outlook on some future work.

## Chapter 2 Introduction to Peridynamics Theory

### 2.1 Introduction

The theory of peridynamics was proposed specifically to deal with discontinuities such as damage<sup>[47]</sup>, where traditional mechanics of continuous media<sup>[54, 55]</sup> describes the motion of objects by introducing partial differential equations<sup>[54, 55]</sup>, so that at points of spatial discontinuity, there is a problem of non-existence of partial derivatives. Peridynamics is a new subject in the field of computational mechanics and opens up a new direction for solid mechanics.

In this chapter, the basic framework of the peridynamics theory originally proposed by Professor Silling<sup>[47, 50]</sup>, i.e., the traditional "bond-based" peridynamics<sup>[50]</sup>, including the PD equation of motion, the intrinsic force function, and some modifications and improvements of the traditional intrinsic force function by domestic and foreign authors. However, the "bond-based" peridynamics theoretical approach has obvious drawbacks<sup>[50]</sup>, including material properties (e.g., Poisson's ratio) limitations, etc. Therefore, an improved "Stated-based" peridynamics was briefly introduced afterwards<sup>[57]</sup>. Although the "Stated-based" theory compensates for the shortcomings of the "Bond-based" theory, it has its own limitations, such as the difficulty of mathematical derivation.

Although the "Stated-based" theory compensates for the shortcomings of the "Bond-based" theory, it has its own limitations, such as the difficulty of mathematical derivation.

After that, this chapter continues to introduce the numerical calculation method and solution system of PD, including the discretization of the equations of motion and the corresponding stability condition, i.e., the condition that the discretized equations of motion can converge to a stable solution by the explicit integration method<sup>[47, 58]</sup>, and this stability condition gives the range of values of the time step  $\Delta t$  that we need to set in the subsequent calculations.

### 2.2 Theoretical framework of peridynamics

## 2.2.1 Overview of "bond-based" peridynamics theory

Peridynamics (PD) <sup>[59]</sup> was proposed in 2000 by Professor Stewart A. Silling of Sandia National Laboratories, USA, and has subsequently rapidly become an emerging method for modeling and describing the mechanical behavior of matter by solving spatial integral equations based on the idea of nonlocal action

The early PD theory is called "bond-based" theory, which is generally translated as "bond-based" theory in China, that is, the interaction only considers the axial force between a single material point pair, but the single-parameter model derived from the energy equivalence method has the limitation of Poisson's ratio<sup>[57]</sup>.

The traditional solid mechanics theory is constrained by the local idea, which introduces partial differentiation and spatial derivation in the solution process<sup>[54]</sup> thus requiring spatial continuity of the object, and such requirement leads to greater difficulties in dealing with <sup>[56]</sup>. PD theory, on the other hand, introduces the nonlocal idea <sup>[60-62]</sup>, which is derived from the traditional continuous medium mechanics and classical molecular dynamics <sup>[63, 64]</sup>, which combines the advantages of macroscopic mechanics and microscopic dynamics.

According to the theory of peridynamics, the conventional continuous medium is first discretized into an ensemble of matter points and it is assumed that any matter point occupies a part of space  $R$ . Also, referring to the theory in classical molecular mechanics<sup>[65]</sup>, PD theory assumes <sup>[47, 59]</sup>, that at any moment  $t$ , a material point  $\mathbf{x}$  interacts with other matter points within a certain range  $\delta$  of its surrounding space  $\mathbf{x}'$ . there exists an interaction, as shown in the following figure:

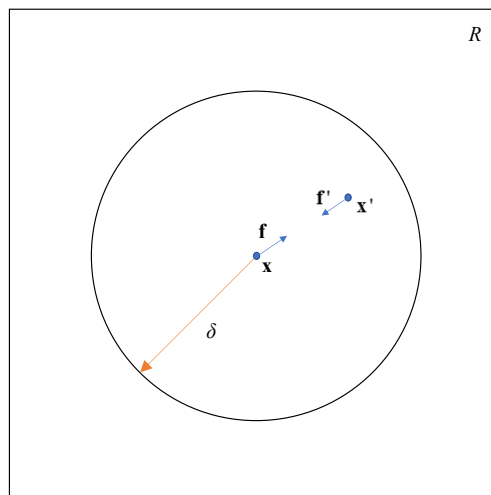


Fig.2.1 Material points and their interactions

This point is similar to the intermolecular forces in molecular dynamics<sup>[65]</sup>, and is the core of PD theory, on which the subsequent construction of equations of motion and mechanical calculations are based. In the above force relation,  $\delta$  is called the horizon of the material point, all such points constitute a region called the "family" of material point as  $H_{(x)}$ , denoted by the following figure:

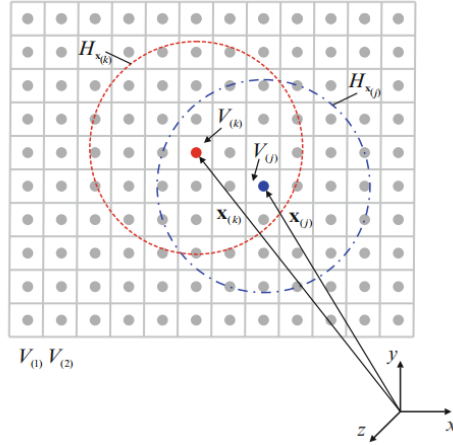


Fig.2.2 range

The material points  $\mathbf{x}_{(k)}$  and  $\mathbf{x}_{(j)}$  occupy a certain volume  $V_{(k)}$  and  $V_{(j)}$  respectively, while their near-field ranges are  $H_{\mathbf{x}_{(k)}}$  and  $H_{\mathbf{x}_{(j)}}$ .

This interaction, which is also known as the near-field kinetic force, can be referred to traditional mechanics<sup>[66-68]</sup> by introducing a function to describe the direction of the magnitude of this force, which is often referred to as the intrinsic force function, the force density function, the force vector function, etc.<sup>[47]</sup>. Similar to the traditional mechanics of continuous media<sup>[67, 68]</sup>, the magnitude of this force is related to the change in the position and relative position of the material point, so that this force function can be denoted as  $\mathbf{f}(\boldsymbol{\eta}, \boldsymbol{\xi})$ , where:  $\boldsymbol{\eta} = \mathbf{u}' - \mathbf{u}$  denotes the relative position of the material point,  $\boldsymbol{\xi} = \mathbf{x}' - \mathbf{x}$  denotes the relative displacement of the material point, and the material points  $\mathbf{x}$ ,  $\mathbf{x}'$ , which each undergo displacement under the interaction, are denoted as  $\mathbf{u}$ ,  $\mathbf{u}'$ , respectively, as follows:

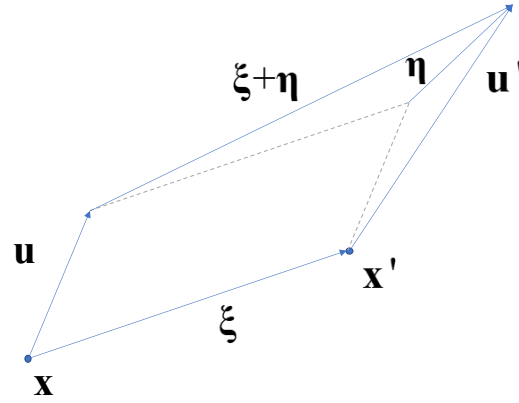


Fig.2.3 Relative position and relative displacement

From the viewpoint of classical Newtonian mechanics, it is clear that the change of the state of motion of a material point is the result of the combined action of external forces as well as the interaction forces between the material points within  $H_{(x)}$ , and therefore, according to Newton's second law <sup>[68]</sup>, we can establish the dynamical equations <sup>[59]</sup> under PD theory as follows:

$$\rho(\mathbf{x})\ddot{\mathbf{u}}(\mathbf{x},t) = \int_H \mathbf{f}(\boldsymbol{\eta},\boldsymbol{\xi},t)dH + \mathbf{b}(\mathbf{x},t) \quad (2.1)$$

Where:  $H$  is the family, expressed as the set of matter points concentrated in the local area of the matter point  $\mathbf{x}$ :  $\{\mathbf{x}' \in R : \|\mathbf{x} - \mathbf{x}'\| < \delta\}$ ;  $\mathbf{b}(\mathbf{x},t)$  is the external load per unit of matter, i.e., the external load density;  $\rho(\mathbf{x})$  is the density.

### force function

The construction of the intrinsic force function is the core and key of peridynamics modeling and has been the focus of research since the birth of PD theory, because it contains the intrinsic information of the material and directly reflects a series of properties of the material itself; therefore, the selection or construction of different intrinsic force functions for different materials <sup>[69, 70]</sup> enables PD theory to simulate different materials <sup>[71]</sup> for static <sup>[72]</sup>, quasi static <sup>[73-76]</sup> or kinematic <sup>[16, 69, 71, 77]</sup> phenomena.

The intrinsic force function itself follows Newton's law in classical mechanics [68] and first satisfies the Linear Admissibility Conditions, i.e.:

$$\mathbf{f}(\boldsymbol{\eta},\boldsymbol{\xi}) = -\mathbf{f}(-\boldsymbol{\eta},-\boldsymbol{\xi}) \quad (2.2)$$

The physical meaning of this equation is that the near-field kinetic forces in the material point pairs and should occur in pairs with equal magnitude and opposite

direction, which is one of the most essential and central features of the "bond-based" near-field kinetic theory<sup>[47]</sup>.

In addition, the principal structure forces should also satisfy the Angular Admissibility Conditions:

$$\mathbf{f}(\boldsymbol{\eta}, \boldsymbol{\xi}) \times (\boldsymbol{\eta} + \boldsymbol{\xi}) = 0 \quad (2.3)$$

This equation states that the intrinsic forces between the material points are parallel to their relative positions, i.e., the lines of action of the forces coincide with the lines of the material points.

Therefore, in summary, in the "bonded base" near-field kinetic theory, we can introduce a scalar function  $F(\boldsymbol{\eta}, \boldsymbol{\xi})$  to describe the intrinsic forces<sup>[47]</sup>, expressed as follows:

$$\mathbf{f}(\boldsymbol{\eta}, \boldsymbol{\xi}) = F(\boldsymbol{\eta}, \boldsymbol{\xi})(\boldsymbol{\eta} + \boldsymbol{\xi}) \quad (2.4)$$

This formula combines the two compatibility conditions mentioned above, where the scalar function  $F(\boldsymbol{\eta}, \boldsymbol{\xi})$  characterizes the magnitude of the intrinsic force and the vector  $(\boldsymbol{\eta} + \boldsymbol{\xi})$  describes the direction of the intrinsic force.

Based on the above description, the study of the present constitutive force function can be reduced to the study of the scalar function. In the very first model proposed by Silling<sup>[47]</sup>, this function is further reduced to a linear function, i.e.:

$$F(\boldsymbol{\eta}, \boldsymbol{\xi}) = c(\|\boldsymbol{\xi}\|)s(\boldsymbol{\eta}, \boldsymbol{\xi}) \quad (2.5)$$

Where,  $s(\boldsymbol{\eta}, \boldsymbol{\xi})$  is the elongation of the material point pair;  $c(\|\boldsymbol{\xi}\|)$  is the micromodulus, which is a concept similar to the elastic modulus in traditional continuum media mechanics and is related to the material itself as a property of the material, and many different micromodulus models have been proposed by scholars for one-dimensional structures (e.g., rods) and two-dimensional structures (e.g., plates), etc.<sup>[78-82]</sup>, as shown in the following figure:

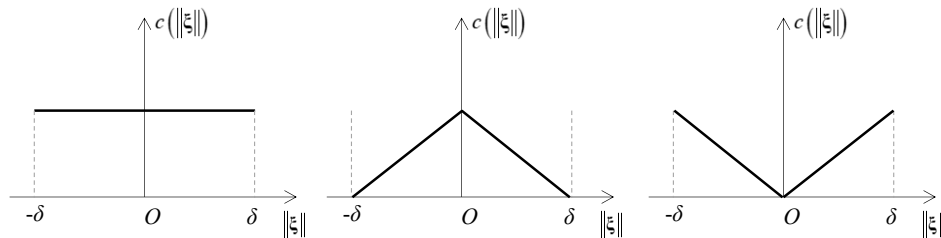


Fig.2.4 One-dimensional structural micromodulus model

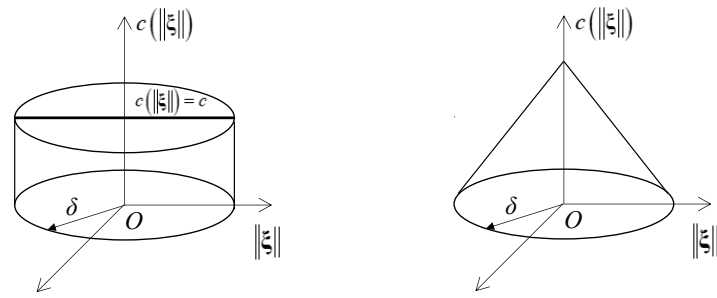


Fig.2.5 Two-dimensional structural micromodulus model

This formulation is a generalization of the classical Hook's Law<sup>[68]</sup> and is therefore formally very concise, and because of this simplicity, PD theory has better results in dealing with some simple problems, especially nonlinear ones.

However, it is also because these micromodular forms are very simple and are stretched in the face of more materials that are slightly more complex in terms of their intrinsic structure (e.g., concrete, composites), therefore, some scholars have introduced various forms of decay terms based on Silling's basic intrinsic force functions<sup>[81-83]</sup> and proposed some kernel function models that can reflect the long-range force properties, which refer to the intermolecular force variations, which can be interpreted as the mesoscopicization of the microscopic model, enabling the PD forces to exhibit decaying properties with distance, as follows.:

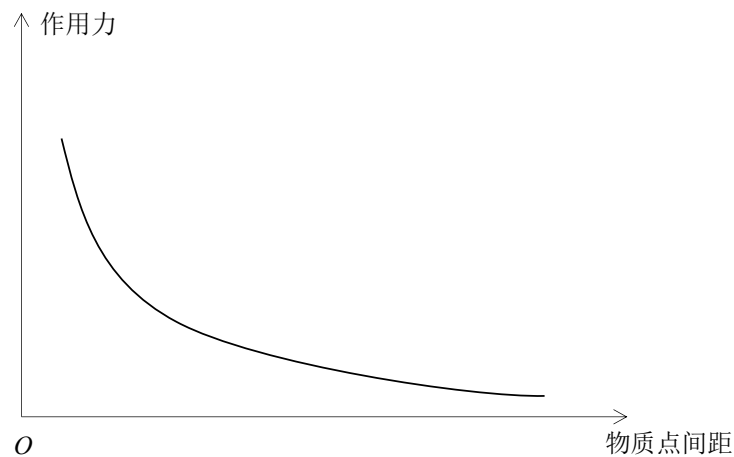


Fig.2.6 Decay of the action force with distance

This modification has improved the accuracy of the PD model and has been more widely used. In China, some scholars constructed a quadratic polynomial-type intrinsic force kernel function under the framework of PD theory<sup>[82]</sup>, which extended

the capability of PD theory in the nonlinear field and could better simulate the response of some nonlinear materials. Some scholars<sup>[70]</sup> also compared different kernel function correction terms and identified the kernel function correction term with the highest accuracy, and applied it to the simulation of cracking test of concrete Brazilian discs, which achieved better results.

### Damage Description

PD theory was originally proposed to describe discontinuous phenomena such as damage, so the definition and description of damage is also a fundamental concept of PD theory. Instead of using the concept of "strain" as in the traditional continuous medium theory<sup>[65]</sup>, PD theory introduces a new concept, namely elongation  $s$ , when considering deformation, and defines elongation as<sup>[47, 84]</sup>, following the definition of strain  $\varepsilon$  in the mechanics of materials.:

$$s(\boldsymbol{\eta}, \boldsymbol{\xi}) = \frac{|\boldsymbol{\eta} + \boldsymbol{\xi}| - |\boldsymbol{\eta}|}{|\boldsymbol{\xi}|} \quad (2.6)$$

The parameters in Eq. are defined as above.

Further, PD theory uses  $\zeta$  to denote the disruption of a given bond at a material point<sup>[47]</sup>, 即:

$$\zeta(\boldsymbol{\xi}, t) = \begin{cases} 1 & s(t', \boldsymbol{\xi}) \leq s_0, t' \in (0, t) \\ 0 & \text{其他} \end{cases} \quad (2.7)$$

Where:  $s_0$  denotes the critical elongation of the material point pair, which for a two-dimensional model can be defined by the following equation<sup>[47]</sup>:

$$s_0 = \sqrt{\frac{G_e}{\left(\frac{6}{\pi} \mu + \frac{16}{9\pi^2} (k - 2\mu)\right) \delta}} \quad (2.8)$$

Where:  $k$  is the bulk modulus of elasticity of the material;  $\mu$  is the shear modulus;  $G_e$  is the critical energy release rate;  $\delta$  is the near-field radius.

The meaning of this formula is very clear: when the relative position between the material point pairs exceeds the critical elongation, the "bond" between the two points is broken and the material is damaged. But this is often the microscopic level of "damage," when the "bond" damage gradually accumulate to form a surface, the material will also produce macroscopic "cracking". Another function was introduced in PD theory to describe this local damage<sup>[47]</sup>:

$$\varphi(\mathbf{x}, t) = 1 - \frac{\int \zeta(\xi, t) dH}{\int_H dH} \quad (2.9)$$

The parameters in Eq. are defined as above.

The statistical significance of the above equation is the ratio of the number of broken bonds to the total number of bonds in the near-field range, with a higher ratio indicating more broken bonds.

### 2.2.1 Overview of "state-based" peridynamics theory

The aforementioned "bond-based" PD theory is the mainstream PD theory nowadays due to its simplicity, procedural simplicity, and fast computational speed, and it has been used for the simulation of various practical problems with different materials and working conditions. However, this theory has a very fatal theory, namely, the Poisson's ratio of the material is fixed under the assumption of online elastic isotropy<sup>[47, 57]</sup>, 1/4 for a one-dimensional structure (rods, etc.), and 1/3 for a two-dimensional material (plates, etc.), it is .

The traditional "bond-based" peridynamics theory suffers from a limited Poisson's ratio, an inherent defect that led Silling et al. to refine it in a paper in 2007. The refined PD theory is called "state-based" theory<sup>[57]</sup>, and overcomes the above-mentioned shortcomings of "bond-based" theory. The "bond-based" theory has overcome these shortcomings.

rofessor Silling proposed the concept of "state" to replace the "tensor" in the traditional theory of continuum mechanics, and the tensor<sup>[49, 85]</sup> and the "state" can be compared and described as follows The comparative description of "state" can be represented in the following figure.

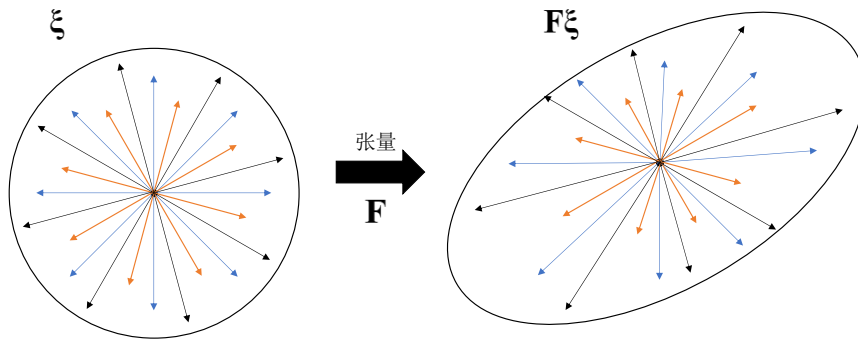


Fig.2.7 Tensor mapping

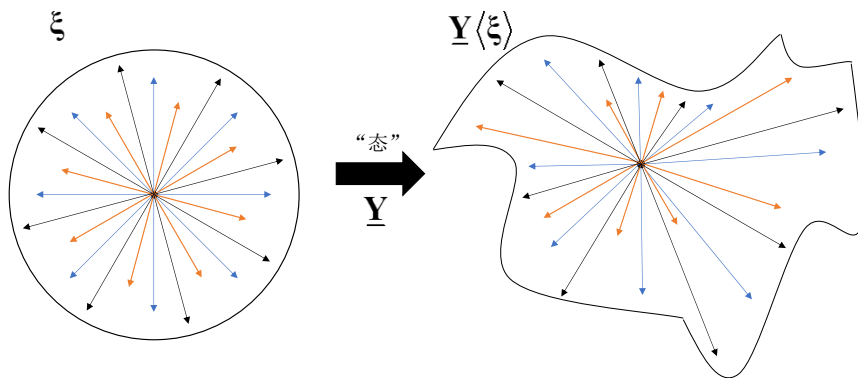


Fig.2.8 "State" mapping

As shown above, "state" was proposed by Silling et al. to compensate for the shortcomings of the traditional tensor concept, which can only map a cluster of vectors  $\xi$  to another cluster of vectors continuously  $F\xi$ ; while "state" can map the vectors to another cluster of vectors  $\underline{Y}\langle\xi\rangle$  discontinuously. The "state" can map the vector discontinuously to another cluster vector. This is consistent with the original purpose of the peridynamics theory, which is to solve the discontinuity problem.

However, the so-called "state" is only a mathematical concept proposed by Dr.

Silling and his co-workers, which is a mapping from a space vector to a tensor set. At present, however, the "state-based" peridynamics theory is mathematically difficult to derive, so the current literature output is much less than the traditional "bond-based" theory.<sup>[85-87]</sup>

## 2.3 Computational methods and solution systems for peridynamics

### 2.3.1 Discretization of the equations of motion

The computational methods of PD theory are also being developed and refined. In the most generalized way, we first consider a uniform discretization of the equation<sup>[47]</sup>, which yields.:

$$\rho(\mathbf{x})\ddot{\mathbf{u}}(\mathbf{x}, t) = \sum_H \mathbf{f}(\boldsymbol{\eta}, \xi, t)\Delta H + \mathbf{b}(\mathbf{x}, t) \quad (2.10)$$

Thus, the integral calculation in the near-field range of the material point is transformed into a volume summation operation for the material point.

Most of the problems described by PD theory are dynamical damage problems, and under dynamical problems, applying the central difference formulation of acceleration<sup>[89, 90]</sup>:

$$\ddot{\mathbf{u}}_i^n = \frac{\mathbf{u}_i^{n+1} - 2\mathbf{u}_i^n + \mathbf{u}_i^{n-1}}{\Delta t^2} \quad (2.11)$$

The dynamic equations can be solved. However, for the static or quasi-static problems, the stiffness matrix can be constructed by imitating the finite element method and then solved by solving a nonlinear system of equations, but this approach generally requires a harsh computer memory machine and has a lower computational efficiency. To solve this problem, the earliest foreign scholars<sup>[47]</sup> effectively solved the quasi-static problem under PD by introducing a damping term. Domestic Shen Feng et al<sup>[91]</sup> borrowed the dynamic relaxation method of solving static problems in classical dynamics, introduced artificial damping, and constructed a graded loading algorithm and related system imbalance judgment criteria, which is the peridynamics method can be applied to the computational analysis of quantitative quasi-static deformation. Dan Huang et al<sup>[82]</sup> modified the original PD theory, considered the relative rotation

of material point pairs, and developed the corresponding discrete, add-in and time-integrated algorithms to realize the simulation of composite crack extension process in typical concrete members. Qing Zhang et al [79] elaborated the solution method of PD micropole model and gave the static solution format of PD micropole model, which improved the computational efficiency without introducing damping terms in solving the static problem and provided a new idea of solving the static problem based on the PD theory.

### 2.3.2 Stability conditions for numerical methods

Although the explicit integral solution method is simpler, this method can only converge the result to a stable solution under certain conditions. Therefore, we need to study the stability conditions of the above equations.

In a related paper<sup>[47]</sup>, Professor Silling et al. obtained stability conditions on the time step  $\Delta t$  by standard von Neumann stability analysis.

First write the displacement <sup>[81]</sup> of the material point  $i$  at the  $n$ -th time step ( $t = n\Delta t$ ) in the form of an exponent:

$$u_i^n = \zeta^n e^{(\kappa k \sqrt{-1})} \quad (2.12)$$

Where,  $\kappa$  and  $k$  are positive real numbers and complex numbers, respectively.

According to the stability requirements of the PD numerical system, there are.:

$$|\zeta| \leq 1 \quad \forall \kappa \in R^+ \quad (2.13)$$

Substitute equation (2.12) into the equation of motion and note that:

$$M_\kappa = \sum_\kappa C(x_k^n - x_i^n) \cos(\kappa k - 1)\Delta V \quad (2.14)$$

It is obtained that:

$$\zeta^2 - 2\left(1 - \frac{M_\kappa(\Delta t)^2}{\rho_i}\right)\zeta + 1 = 0 \quad (2.15)$$

Solving this quadratic equation yields:

$$\zeta = 1 - \frac{M_\kappa(\Delta t)^2}{\rho_i} \pm \sqrt{\left(1 - \frac{M_\kappa(\Delta t)^2}{\rho_i}\right)^2 - 1} \quad (2.16)$$

From equation (2.13),  $|\zeta| \leq 1 \quad \forall \kappa \in R^+$ , it can be derived that:

$$\Delta t < \sqrt{\frac{2\rho_i}{M_\kappa}} \quad (2.17)$$

The above equation should hold for all  $\kappa$ .

Eq. (2.17) is the stability condition for the time step in the numerical method of peridynamics, i.e., for the time step  $\Delta t$  satisfying the equation, the equations of motion can be converged to a stable solution.

## 2.4 Summary of this chapter

In this chapter, the basic theoretical framework of the peridynamics theory, namely, the traditional "bond-based" peridynamics, including the equations of motion, the intrinsic force functions, and some modifications and improvements of the traditional intrinsic force functions by domestic and foreign scholars, is introduced. At the same time, it is pointed out that the "Bond-based" peridynamics theory has obvious shortcomings, including material properties (e.g., Poisson's ratio) limitations, and the improved "Stated-based" peridynamics theory is introduced.

After that, the chapter continues with the numerical calculation method and solution system of PD, i.e., the explicit integration method, and analyzes the stability condition of the method, i.e., the range of values of the time step derived based on the von Neumann stability condition.

## **Chapter 3 Impact damage analysis of laminates based on peridynamics**

### **3.1 Introduction**

Composite materials have been widely used in many engineering fields. This chapter firstly introduces the basic theory of composite laminates, and based on this, an analytical model based on the peridynamics theory of composite laminate rigid body impact damage evolution is established for the problem of discontinuous mechanics of composite laminates impact damage, and a corresponding calculation program is developed. Moreover, in order to solve the problem of incomplete near-field material points in the boundary region, an improved "surface correction factor" is proposed, which can improve the calculation accuracy. After the calculation system was built, the impact damage evolution of composite laminates under different working conditions (including different shapes, velocities and angles) was simulated in the above model, and the impact damage results at each intermediate step were recorded and analyzed.

### **3.2 Development and Computing Environment**

#### **3.2.1 Development environment construction**

The peridynamics theory has been proposed for more than ten years, but the computational resources applicable to the theory are extremely limited, and the computational software and mechanical solution software developed specifically for the PD method are still in the research stage. There are several software developed by domestic scholars that can deal with simple peridynamics problems, such as PdynaComp<sup>[81]</sup> from Shanghai Jiao Tong University, which can deal with the PD theory of damage problems of composite laminates.

At the same time, the computational procedures and algorithms that can effectively improve the computational efficiency are yet to be improved. For general problems, researchers need to design and program their own programs, which is time-

consuming and laborious. For slightly more complex problems, the number of "keys" in the model often reaches millions or even tens of millions, which makes it difficult for general home computers to handle this level of computation and requires the use of more expensive computing resources such as supercomputers.

Among the available computational software that can perform peridynamics, LAMMPS<sup>[47]</sup> was developed by Sandia National Laboratories in the U.S. LAMMPS is called Large-scale Atomic/Molecular Massively Parallel Simulator. Silling et al. developed the PDLAMMPS toolkit on the basis of the original framework, which can directly call the relevant function libraries to complete the modeling and analysis of peridynamics, but this software is based on the LINUX platform, and the building steps and processes are However, this software is based on the LINUX platform, and the steps and procedures are cumbersome, and the computational power is not available on the Windows platform. Therefore, in this paper, we consider using Microsoft's Visual Studio Community with Intel's parallel computing software Intel Parallel Studio for development and computation, and after the installation and integration of the two software, we can directly add the program files of related projects.

Intel Parallel Studio is a professional compiler developed and launched by Intel for parallel computing, supporting programming languages such as Fortran, C++, C, etc. It also inherits a large number of computational libraries commonly used in scientific computing, such as MKL.

Fortran is an old programming language, but it still has a strong vitality in the field of scientific computing due to its fast computation speed, simple syntax, and wide range of related programs. The computational programs in our paper are all based on the Fortran language, and both Visual Studio Community development environment and Intel Parallel Studio parallel computing software have good support for Fortran.

After obtaining the computational results obtained by the above environment, we consider the visualization operation using MATLAB software.

In summary, the computing platform and software development platform used in this paper are as follows.

Table3.1 Table of hardware information of computing platform

Hardware	Type
PC	MSI GE62-2QD Apache

<b>CPU</b>	Intel Core i7-5700HQ(2.7GHz/L3 6M)
<b>GPU</b>	NVIDIA GeForce GTX 960M
<b>RAM</b>	8GB DDR3L 1600MHz
<b>Hard Disk</b>	日立 1TB HDD

The software configuration of the platform is as follows:

Table3.2 Computing platform software information table

<b>Software</b>	<b>Type</b>
<b>OS</b>	Microsoft Windows 10 Basic
<b>IDE</b>	Visual Studio Community 2019
<b>Compilers and solvers</b>	Intel Parallel Studio XE 2019
<b>Plot software</b>	MATLAB

### 3.2.2 Computational flow and algorithm design

The content of this chapter involves PD calculations, including the determination of bond breakage and the calculation of the velocity and displacement of the material point, we can draw the calculation flow of the numerical simulation in this chapter, and the detailed process can be shown by the following flow chart:

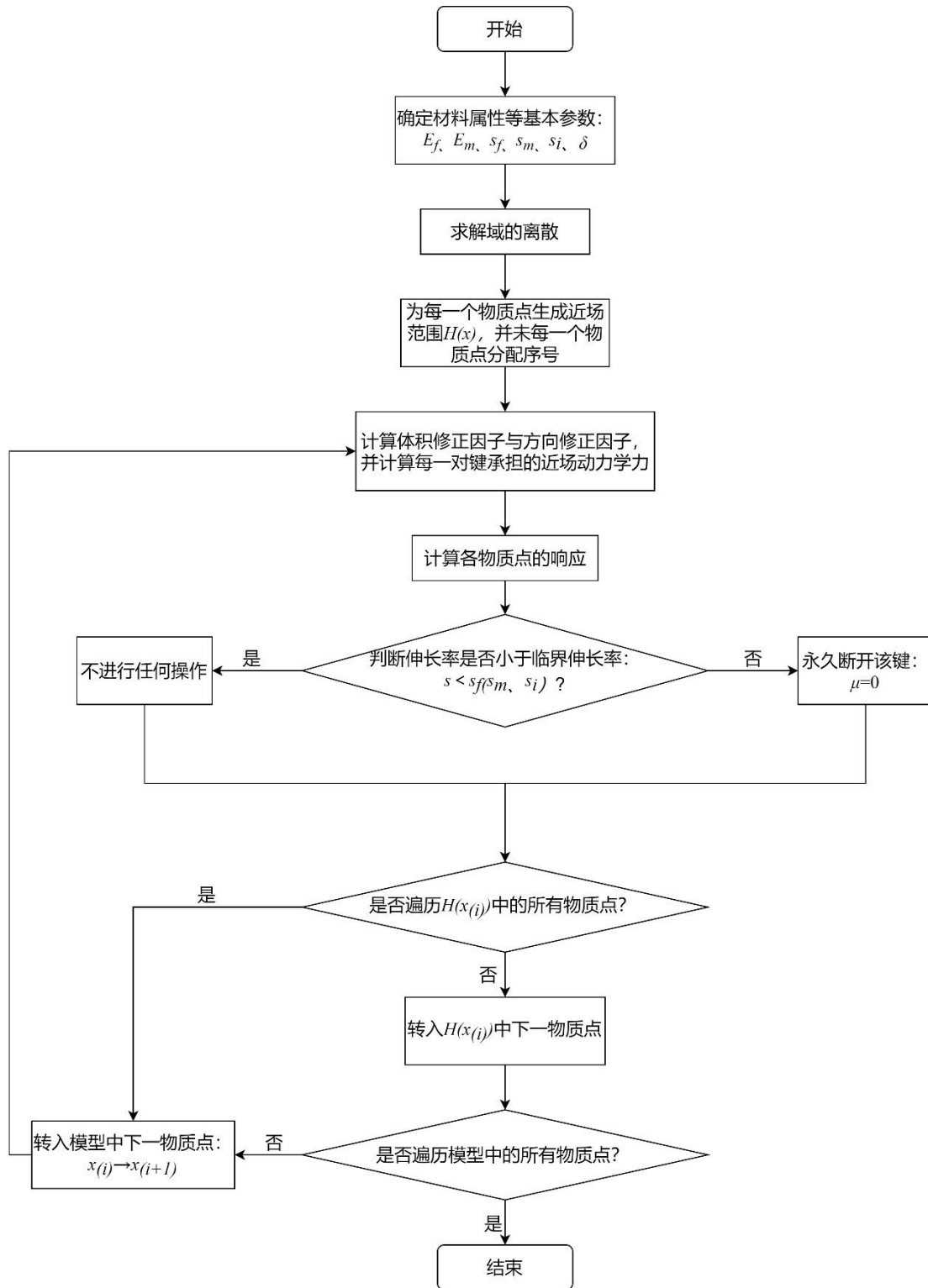


Fig.3.1 Computational flow and algorithm design

### 3.3 Modeling of composite laminates and impactors

#### 3.3.1 Theory of anisotropic composite laminates

With the birth and use of high-strength materials such as carbon fiber, composite materials, a new type of material, have also begun to be widely used in various industrial sectors. Composite materials refer to new materials prepared by using various advanced material preparation technologies and methods to synthesize a variety of materials (components) with different properties and attributes in a certain ratio. Composites have the properties of the original component materials, but often have new properties that these materials do not have, such as alloys, which inherit the strength of the original component metal materials, while far better than the raw materials in terms of fatigue resistance, fire resistance, ductility.。

Composite single-layer panels are generally made by arranging reinforcing fibers (Fiber, such as carbon fiber, glass fiber) in the matrix material at a certain angle, and the common structure of composite single-layer panels can be represented in the following figure:

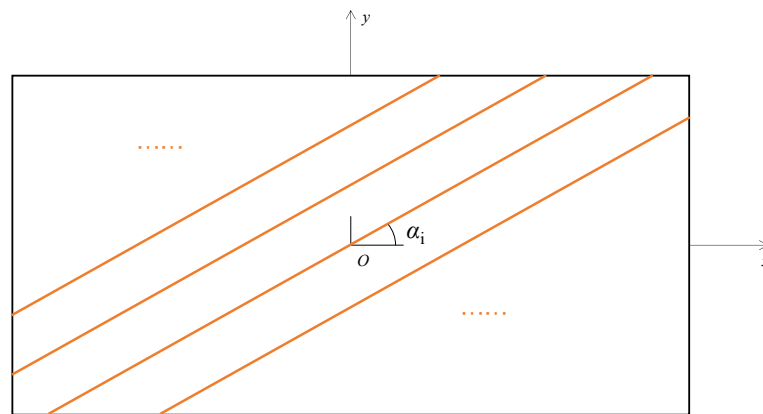


Fig.3.2 复 Schematic diagram of composite single-layer plate structure

The matrix material and the fiber material each have almost completely different material properties <sup>[45]</sup>, the former generally cannot withstand large tensile forces, while the latter has extremely strong tensile properties, the combination of the two makes the formation of composite materials in addition to having notable mechanical properties, often also has some special properties that neither material has, such as strong resistance to vibration, fatigue resistance, etc.

Composite laminates are obtained by bonding single-layer laminates together using certain adhesives and in certain orientations, as shown in the figure below:

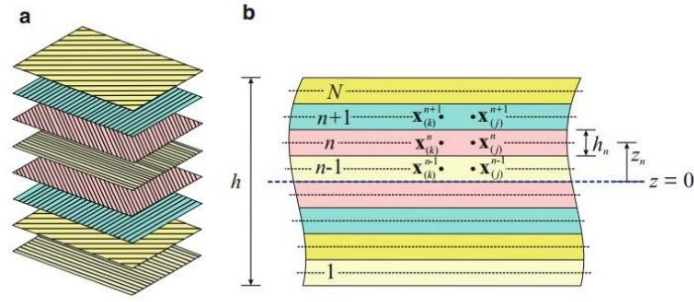


Fig.3.3 Schematic diagram of composite laminate structure

Composite laminates are typically anisotropic materials, meaning that the material has different material properties and strengths in almost all directions, with the strongest along the fiber direction and weaker in the remaining directions.

Classical composite mechanics has a very detailed study of composite laminates. For orthotropic anisotropic composite laminates, the general stress-strain relationship can be expressed as:

$$\boldsymbol{\sigma} = \mathbf{Q} \cdot \boldsymbol{\varepsilon} \quad (3.1)$$

Each quantity in the equation is a tensor.

Expanding gives:

$$\begin{Bmatrix} \sigma_1 \\ \sigma_2 \\ \tau_{12} \end{Bmatrix} = \begin{bmatrix} Q_{11} & Q_{12} & 0 \\ Q_{21} & Q_{22} & 0 \\ 0 & 0 & Q_{66} \end{bmatrix} \begin{Bmatrix} \varepsilon_1 \\ \varepsilon_2 \\ \gamma_{12} \end{Bmatrix} \quad (3.2)$$

Where:

$$Q_{11} = \frac{E_1}{1 - \nu_{12}\nu_{21}} \quad (3.3)$$

$$Q_{22} = \frac{E_2}{1 - \nu_{12}\nu_{21}} \quad (3.4)$$

$$Q_{12} = \frac{\nu_{12}E_1}{1 - \nu_{12}\nu_{21}} \quad (3.5)$$

$$Q_{66} = G_{12} \quad (3.6)$$

The stiffness matrix of the material  $\mathbf{Q}$  consists of four independent elastic constants. Also, considering that the elastic moduli are all positive, the Poisson's ratio  $\nu_{12}$  and  $\nu_{21}$  should also satisfy the relationship satisfying:

$$\frac{\nu_{21}}{E_1} = \frac{\nu_{12}}{E_2} \quad (3.7)$$

$$1 - \nu_{12}\nu_{21} > 0 \quad (3.8)$$

Based on the conventional composite material theory and peridynamics theory, we can develop a PD model for anisotropic composite laminates.

In fiber-reinforced laminates, three types of bonds are considered to be defined - fiber bonds, matrix bonds and interlaminar bonds, where interlaminar bonds also belong to matrix bonds in a broad sense. According to the relevant literature, the bond constants of each of the two bonds and can be given by:

$$c_f = \frac{29(Q_{11} - Q_{22})}{4\pi t \delta^3} \quad (3.9)$$

$$c_m = \frac{8Q_{22}}{\pi t \delta^3} \quad (3.10)$$

### 3.3.2 Description of damage to composite laminates

For composite laminates, we can establish two damage description models, one is the overall damage, which is to record the fracture of all bonds at the material point, including fiber bonds, matrix bonds and interlaminar bonds; the other is the interlaminar damage, which is to record the fracture of interlaminar bonds on both sides of the material point.

As mentioned earlier, PD theory introduces the variable  $\zeta$  to represent the destruction of the material point, i.e.:

$$\zeta(\xi, t) = \begin{cases} 1 & s(t', \xi) \leq s_0, t' \in (0, t) \\ 0 & \text{其他} \end{cases} \quad (3.11)$$

Where:  $s_0$  denotes the critical elongation of the material point pair, which for the plate model can be defined by the following equation.

$$s_0 = \sqrt{\frac{G_e}{\left(\frac{6}{\pi} \mu + \frac{16}{9\pi^2} (k - 2\mu)\right) \delta}} \quad (3.12)$$

Where:  $k$  is the bulk modulus of elasticity of the material;  $\mu$  is the shear modulus;  $G_e$  is the critical energy release rate;  $\delta$  is the near-field radius.

The above equation can be more visually illustrated in the following figure.:

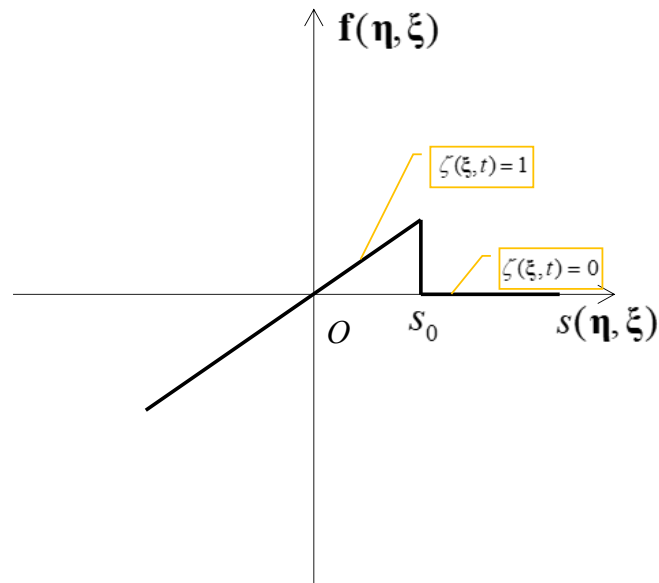


Fig.3.4 Bond breakage

Equation (3.11) shows that at a certain point, when the elongation of the bond is greater than the critical elongation, the bond is permanently fractured.

Introducing another parameter to describe the bond breakage at a given material point:

$$\varphi(\mathbf{x}, t) = 1 - \frac{\int \zeta(\xi, t) dH}{\int_H dH} \quad (3.13)$$

The parameters in Eq. are defined as above.

The statistical concept of Eq. (3.13) describes the proportion of bonds that have been broken in the domain of the material point, and the magnitude of this value implies the extent to which the damage has developed at that point, when the value is 1, it means that all bonds around that point have been broken.

### 3.4 Shock theory based on peridynamics

#### 3.4.1 Shock modeling

Professor Silling et al. proposed a shock theory based on the principle of peridynamics in the related literature, and the shock model contains two parts, i.e., the impactor and the impacted structure (generally regarded as a deformed body). The

latter is the object of our study and analysis and can be discretized by the PD method; for the former, we generally assume that it is an ideal rigid body, i.e., during the whole impact process, the impactor only undergoes rigid body displacement and does not produce any deformation itself, and the PD-based impact model can be shown as follows:

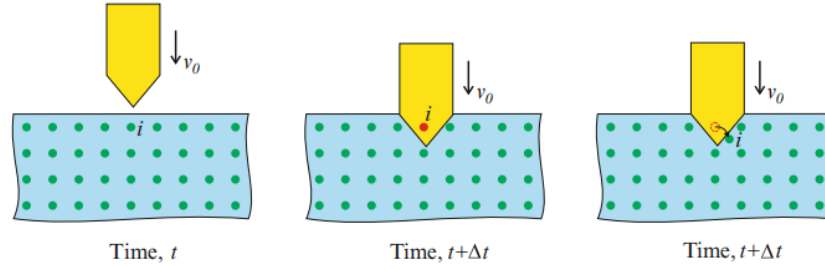


Fig.3.5 Schematic diagram of the impact model based on PD theory

According to the schematic diagram, the impactor collides with the deformed body at a velocity  $v_0$ . The impacted deformed body is controlled by the equations of motion of peridynamics. When the impactor makes contact with the deformed body, a part of the impactor penetrates into the deformed body and occupies the position of some of its original material points (e.g., point  $i$  in the figure). In order to reflect this physical phenomenon, we need to reset the position of the occupied material points. Again, taking point  $i$  in the figure as an example, according to the PD-based impact theory, this point should be transferred outside the impacted body along the shortest path (as shown in the figure above). From there, we can calculate the velocity at the moment  $(t + \Delta t)$  by the following equation:

$$\bar{\mathbf{v}}_{(k)}^{t+\Delta t} = \frac{\bar{\mathbf{u}}_{(k)}^{t+\Delta t} - \bar{\mathbf{u}}_{(k)}^t}{\Delta t} \quad (3.14)$$

Where:

$\bar{\mathbf{u}}_{(k)}^{t+\Delta t}$ ,  $\bar{\mathbf{u}}_{(k)}^t$ : the displacement of the material point at the moment  $(t + \Delta t)$  and the moment  $t$ ;

$\bar{\mathbf{v}}_{(k)}^{t+\Delta t}$ : the velocity at the moment  $(t + \Delta t)$  of matter point;

Similarly, at the moment of time  $(t + \Delta t)$ , the reaction force of the material point  $x_{(k)}$  against the impacting body can be calculated by the following equation:

$$\mathbf{F}_{(k)}^{t+\Delta t} = -1 \times \rho_{(k)} \frac{\bar{\mathbf{v}}_{(k)}^{t+\Delta t} - \bar{\mathbf{v}}_{(k)}^t}{\Delta t} V_{(k)} \quad (3.15)$$

Where:

- $\bar{\mathbf{v}}_{(k)}^{t+\Delta t}, \bar{\mathbf{v}}_{(k)}^t$ : point of material moment by moment  $(t + \Delta t)$  and  $t$  the velocity at the moment of time;
- $\mathbf{F}_{(k)}^{t+\Delta t}$ : the reaction force of the material point  $(k)$  against the impactor;
- $\rho_{(k)}$ : Density at substance point  $(k)$ ;
- $V_{(k)}$ : the volume occupied by the substance point  $(k)$ ;

The inverse force sought to be summed for all material points within the range of the impacting body can be obtained  $(t + \Delta t)$  moment, the reaction force on the impacting body is:

$$\mathbf{F}^{t+\Delta t} = \sum_k \mathbf{F}_{(k)}^{t+\Delta t} \lambda_{(k)}^{t+\Delta t} \quad (3.16)$$

Where:

$$\lambda_{(k)}^{t+\Delta t} = \begin{cases} 1 & \text{冲击物在物体内} \\ 0 & \text{冲击物在物体外} \end{cases} \quad (3.17)$$

That is, if the value is 1, the material point is occupied by the impact and the response of this material point needs to be corrected according to the above process.

The above equation can be used to describe the variation of the velocity of the impacting body movement during the impact.

### 3.4.2 Examples

Professor Silling layer proposed several benchmark problems based on the above impact theory, simulated using the PD method, and visualized the results using MATLAB software, with the following results:

#### **Example 1: Rigid circular plate impact test**

In this example, the rectangular plate is impacted by a rigid circular plate, and the initial positions of both are as follows:

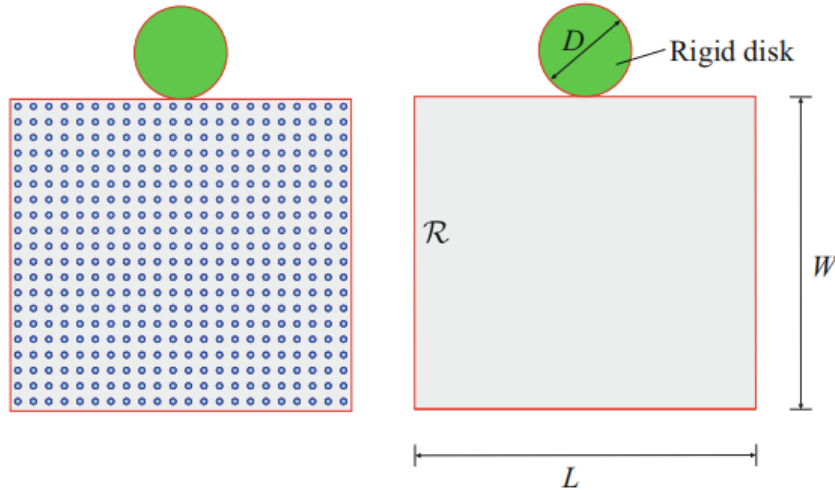


Fig.3.6 Geometric model of the rigid circular plate experiment

The geometric parameters of the steel plates in the experiments are set as follows:

Table3.1 Laminate geometric parameters

参数	备注	数值	单位
$L$	宽	200	mm
$W$	高	100	mm
$h$	总厚度	9	mm

In addition, the material properties of the impacted steel plate are set as follows:

Table3.2 Material properties of steel plates

Property	Note	Value
$E$	Modulus	191MPa
$\nu$	Poisson's ratio	0.33
$\rho$	Density	8000kg/m <sup>3</sup>

The cylindrical impact object is treated as an ideal rigid body, i.e., it does not undergo any deformation under the impact, only rigid body displacement occurs, and its material properties are set as follows:

Table3.3 Material properties of the impactor

Property	Note	Value
$D$	Diameter	50mm
$H$	Height	50mm

Using the PD method for simulation, in this example, we do not consider bond fracture, i.e., the material does not appear to break, so the relevant parameters are set

as follows:

Table 3.4 PD Parameter settings of PD method

Property	Note	Value
$\Delta$	Size of point	1mm
$\delta$	Range	3.015mm
$\Delta t$	Time step	$1 \times 10^{-7}$ s
	Number of steps	2000

After reproducing this experiment using the PD method, the following results were obtained:

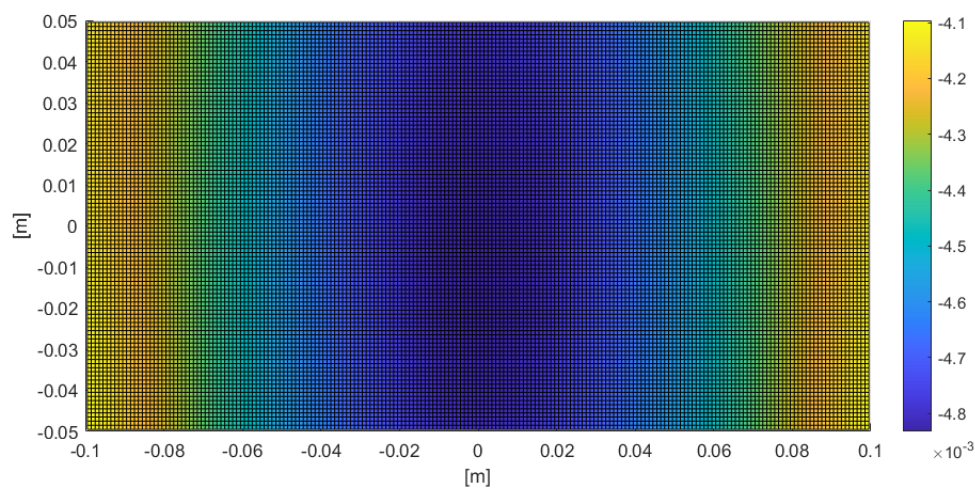


Fig.3.7 Vertical ( $y$ -direction) displacement contour of steel plate

We note that the vertical displacement in the middle of the plate is larger than the sides, which is in accordance with the expected results.

### Example 2: Kalthoff-Winkler impact experiment

Kalthoff and Winkler in 1988 had simulated the crack development of a steel plate with two initial cracks subjected to a cylindrical impact by an experiment. The geometric model of the experiment is shown in Fig:

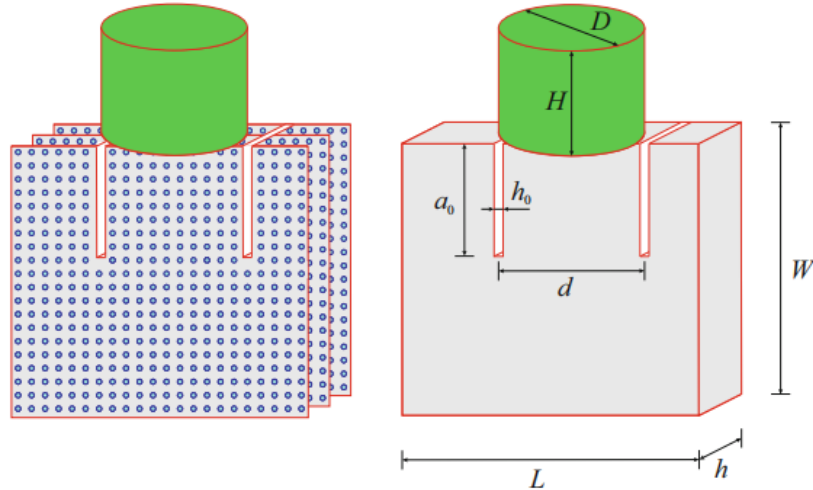


Fig.3.8 Geometric model of the Kalthoff-Winkler experiment

The geometric parameters of the steel plates in the experiments are set as follows:

Table3.5 Laminate geometric parameters

Parameter	Note	Value	Unit
$L$	Width	200	mm
$W$	Height	100	mm
$h$	Thickness	9	mm
$d$	Space of crack	50	mm
$a_0$	Height of crack	50	mm
$h_0$	Width of crack	1.5	mm

In addition, the material properties of the impacted steel plate are set as follows:

Table3.6 Material properties of steel plates

Property	Note	Value
$E$	Modulus	159.96MPa
$\nu$	Poisson's ratio	8.96MPa
$\rho$	Density	0.02

The cylindrical impact object is treated as an ideal rigid body, i.e., it does not undergo any deformation under the impact, only rigid body displacement occurs, and its material properties are set as follows:

Table3.7 Material properties of steel plates

Property	Note	Value
$D$	圆柱直径	50mm

$H$	圆柱高	50mm
-----	-----	------

The simulation is carried out using the PD method, and the relevant parameters are set as follows:

Table3.8 Parameter settings of PD method

Property	Note	Value
$\Delta$	Size of point	1mm
$\delta$	Range	3.015mm
$s_c$	Critical stretch	0.01
$\Delta t$	Time step	$8.7 \times 10^{-8}s$
	Number of steps	1350

After reproducing this experiment using the PD method, the following results were obtained:

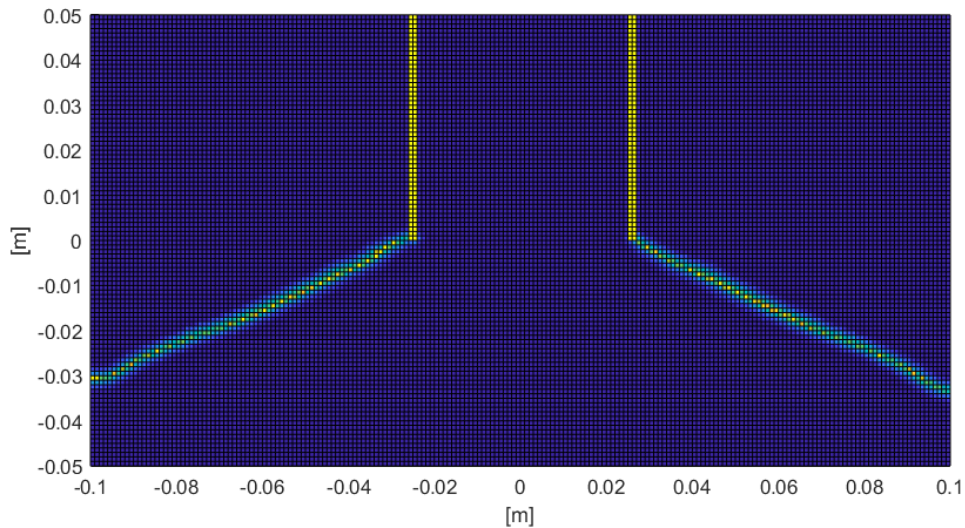


Fig.3.9 Crack development in steel plate with initial cracks

From the above figure, we can observe that, due to the principle of stress concentration, the crack starts to sprout from the initial crack tip and spreads to both sides according to a certain angle; the measurement can be obtained that the angle claimed between the crack and the vertical direction is about  $68^\circ$ , and it is symmetrically distributed.

### 3.5 Determination of surface correction factor

At the beginning of the PD model, some scholars found that the calculation

results of PD often have certain errors with the finite element software or experimental results, mainly due to the incomplete domain of the material point in the boundary region, a phenomenon also known as the "surface effect" (Surface effect), as shown in the following figure:

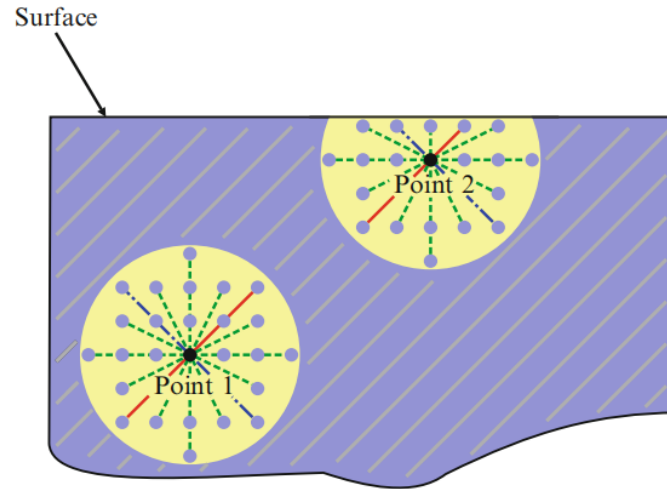


Fig.3.10 "Surface effect"

To make the PD calculations closer to those of conventional continuum media mechanics (CM), some authors<sup>[59, 81, 84]</sup> introduced the concept of long-range forces from molecular physics into PD, while Professor Silling et al. introduced a surface correction factor to correct the microelastic modulus in the literature<sup>[47]</sup>, using the principle of controlling the strain energy density of the two to be equal to determine this factor.

For fiber-reinforced laminate materials, we propose a more concise expression to describe this coefficient based on the above principles, derived as follows.:

Take the  $x$ -direction as an example:

As shown in the figure below, let the fiber direction of the  $i$ -th ply of the laminate be  $\alpha_i$ . An elongation  $\delta$  is given to the laminate along the  $x$ -direction:

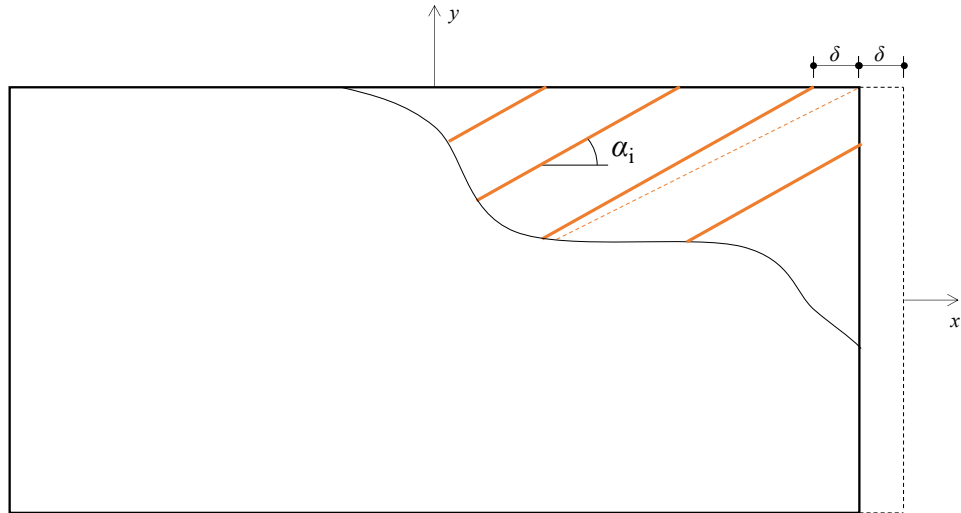


Fig.3.11 Small deformation assumption

Then, from the geometric relationship, the elongation along the fiber direction is:

$$\delta_{f,i} = \delta \cos(\alpha_i) \quad (3.18)$$

In addition, according to the relevant literature [47], the strain energy density of a fiber bond in a laminate under PD theory can be expressed by the following equation:

$$w_{PD,f} = \frac{1}{2} \times \frac{1}{2} \times b_f \times (s(\boldsymbol{\eta}, \boldsymbol{\xi}))^2 \times |\boldsymbol{\xi}| \times \Delta V \times fac \quad (3.19)$$

Where, *fac* is used to describe the decay of the micromodulus with distance, which can be expressed by the following equation [47]:

$$fac = \begin{cases} 1 & r_{ij} < \Delta - \frac{dx}{2} \\ \frac{\Delta + \frac{dx}{2} - r_{ij}}{dx} & \Delta + \frac{dx}{2} \geq r_{ij} \geq \Delta - \frac{dx}{2} \\ 0 & r_{ij} > \Delta + \frac{dx}{2} \end{cases} \quad (3.20)$$

Substituting the relevant variables and simplifying gives:

$$w_{PD,f} = \frac{1}{4} \times b_f \times \left( \frac{\delta \cos(\alpha_i) - |\boldsymbol{\xi}|}{|\boldsymbol{\xi}|} \right)^2 \times |\boldsymbol{\xi}| \times \Delta V \times fac \quad (3.21)$$

Summing over all the bonds in the plate, the strain energy of the laminate is obtained as:

$$W_{PD,f} = \sum w_{PD,f} \quad (3.22)$$

Also, we have the relevant equations in the traditional continuum media

mechanics. According to the knowledge of composite mechanics, the strain energy in the fibers of the laminate and in the matrix can be expressed by the following equation: (3.23)

$$w_{CM,f} = \frac{1}{2}(Q_{11} - Q_{22})\delta^2 \quad (3.24)$$

$$w_{CM,m} = \frac{1}{2}Q_{22}\delta^2 \quad (3.25)$$

Substituting the variables, we have:

$$w_{CM,f,i} = \frac{1}{2}(Q_{11} - Q_{22})(\delta \cos(\alpha_i))^2 \quad (3.26)$$

Thereby, summing the strain energy of all the layers, the strain energy stored in the fibers and matrix in the laminate can be found as:

$$W_{CM,f} = \sum_i^n w_{CM,f,i} \quad (3.27)$$

$$W_{CM,m} = \sum_i^n w_{CM,m,i} \quad (3.28)$$

Where,  $n$  is the number of plies of laminate.

The ratio of  $w_{CM}$  and  $w_{PD}$  is the correction factor, and the correction factors of fiber bond and matrix bond can be obtained as:

$$i_{cor,f} = \frac{W_{CM,f}}{W_{PD,f}} \quad (3.29)$$

$$i_{cor,m} = \frac{W_{CM,m}}{W_{PD,m}} \quad (3.30)$$

### 3.6 Geometric model and material parameters

After determining the surface correction coefficients, we introduce them into the program and perform the numerical simulation work. The composite laminate for the numerical simulation in this paper is in the conventional form, i.e., it consists of composite single-ply sheets superimposed by correlated interactions (e.g., gluing), and interlaminar action bonds are introduced to describe this interlaminar correlation.

In this paper, we will study the damage caused to the laminate by two different

shapes of impact objects, cylindrical and round ball, the relative positions of the two at the beginning of the impact are shown in the following figure:

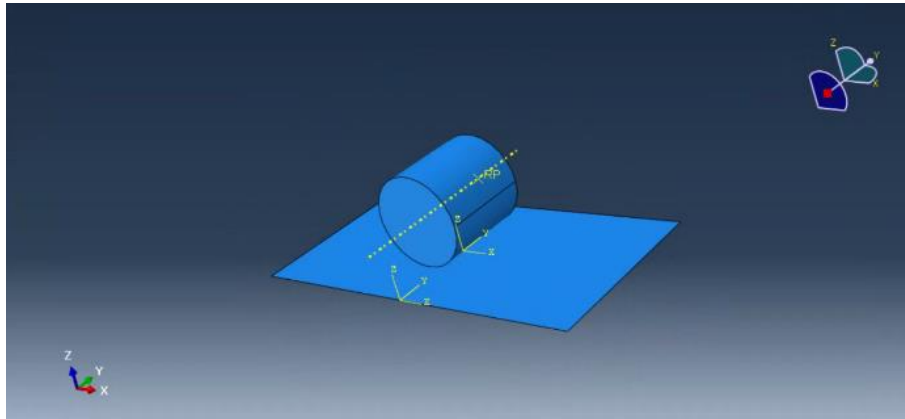


Fig.3.12 Schematic diagram of the initial relative position of the impactor and the laminate

The specific geometric parameters of the laminate model can be summarized as shown below:

Table3.9 Laminate geometric parameters

Parameter	note	Value	Unit
$b$	Width	200	mm
$h$	Height	100	mm
$t$	Total thickness	9	mm
$t_0$	Thickness of layer	1	mm

The specific geometric parameters of the rigid cylinder are as follows:

Table3.10 Cylindrical geometric parameters

Parameter	note	Value	Unit
$\phi$	Diameter	50	mm
H	Height	50	mm

The geometric parameters of the rigid sphere are as follows:

Table3.11 Geometric parameters of the sphere

Parameter	note	Value	Unit
$\Phi$	Diameter	20	mm

The composites used in this paper are all aramid/epoxy (K49/EP) materials, with reinforcing fibers lay out in:

Table3.12 Lay out method of reinforcing fiber

	Direction
Example	[0/45/90/-45/0/-45/90/45/0]

As shown in the picture below::

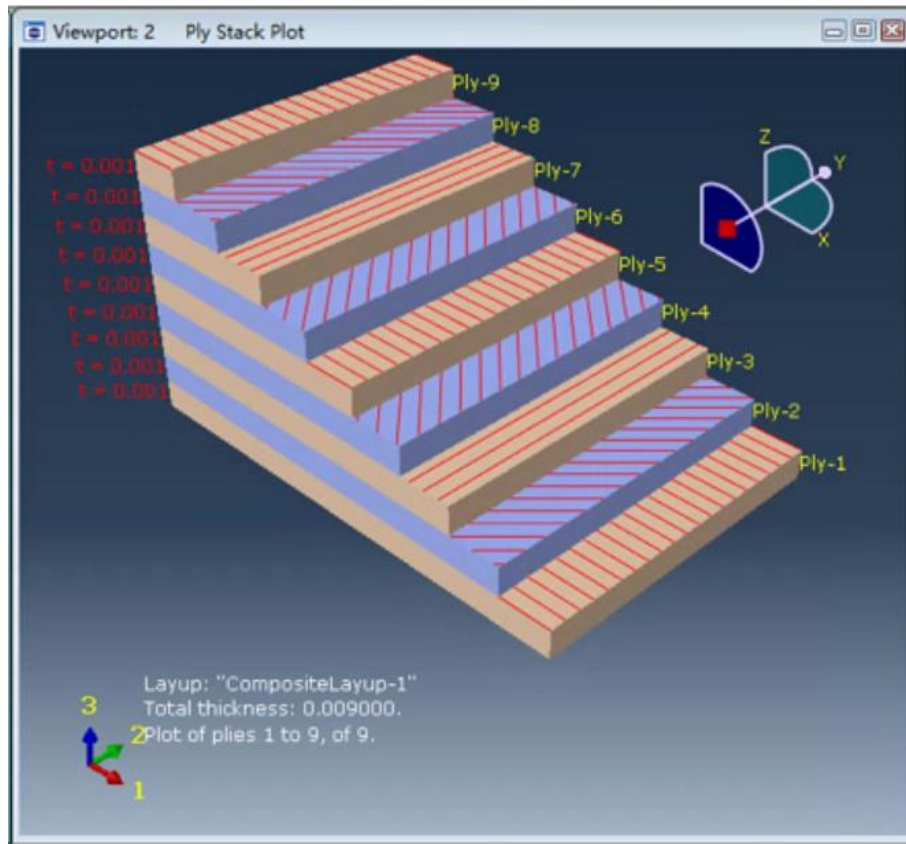


Fig.3.13 Laminate lay out method

In this paper, the following intrinsic model is used for the composite material as shown in <sup>[47]</sup>:

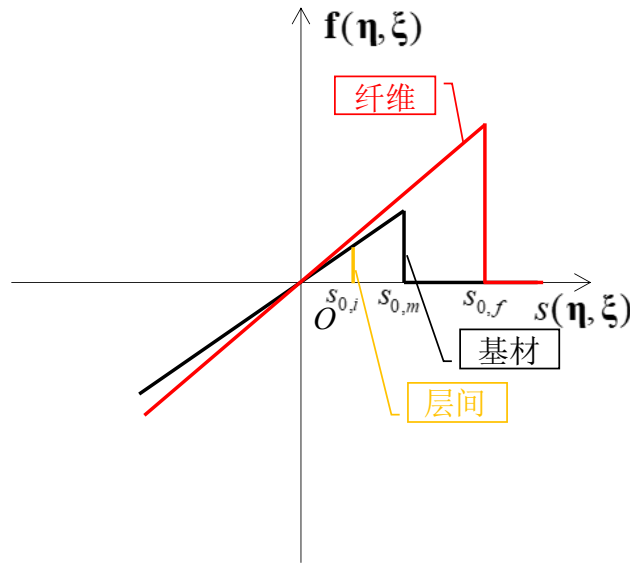


Fig.3.14 Constitutive model of the material

We do not consider the residual bearing capacity of the material after deformation, which is the same in both directions of compression and tension.

Based on data from the relevant literature, the specific material properties are set as follows:

Table3.13 Material properties

Parameter	Note	Value
$E_f$	Modulus-Fiber	159.96MPa
$E_m$	Modulus-Matrix	8.96MPa
$s_f$	Critical stretch-Fiber	0.02
$s_m$	Critical stretch-Matrix	0.01
$s_i$	Critical stretch-Interlayer	0.05

### 3.7 Numerical simulation results under impact conditions

#### 3.7.1 Simulation results of cylindrical impact damage

After determining the relevant parameters and variables, we started to numerically simulate the composite laminate model in the example. The laminate damage includes both intra-ply damage and inter-ply damage, where the intra-ply

damage contains both fiber fracture and matrix cracking, while the intra-ply damage mainly refers to the delamination of two adjacent layers due to extrusion, misalignment, and slip. As mentioned in the previous section, when the deformation of the fiber bond or matrix bond reaches their respective limits, fracture occurs in the phase key, and damage occurs in the region when a large number of bonds break in the region.

We selected the time step of numerical simulation  $8.7 \times 10^{-8} \text{s}$  ( $0.087 \mu\text{s}$ ), The total number of calculation steps is 3000, and the damage evolution of each layer is recorded in the middle of 500, 800, 1000, 2000 and 3000 steps, respectively, and some of the fiber layers with more obvious damage evolution are selected.

### Overall damage

The damage contour can be shown in the following figure.:

(1) 500 step

The damage to the laminate at 500 steps is shown in Fig:

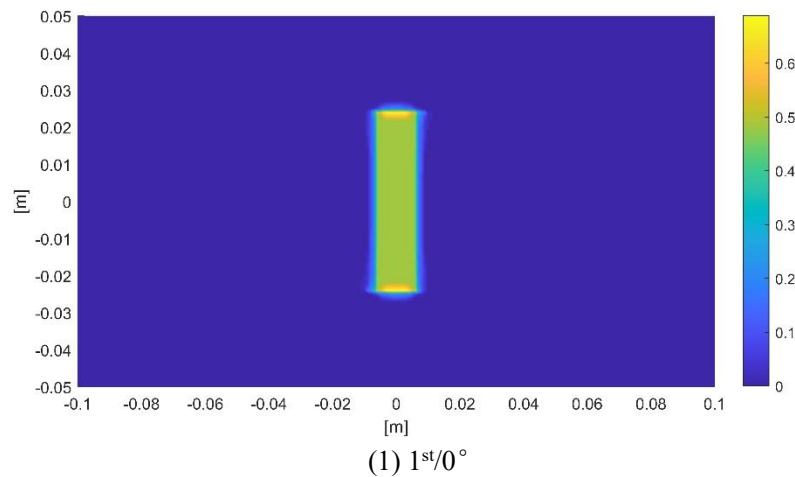


Fig.3.15 Damage cloud at 500 steps

At 500 steps, the impactor has a short stroke and only makes initial contact with the upper surface of the laminate. Therefore, the damage is almost only concentrated in the first layer of the laminate. At the same time, the cylinder will squeeze the laminate during the impact, so although the contact area produces obvious damage, it is not the most serious part of the damage. With the above image, it can be seen that the most serious part of the damage is concentrated at the upper and lower surfaces of the cylinder, which will produce a large tensile stress due to the traction on the plate surface generated by the movement of the laminate, thus causing tensile damage to the substrate material, so the damage is most obvious, which is consistent with our

knowledge and relevant test data.

(2) 800 step

The damage to the laminate at 800 steps is shown in Fig:

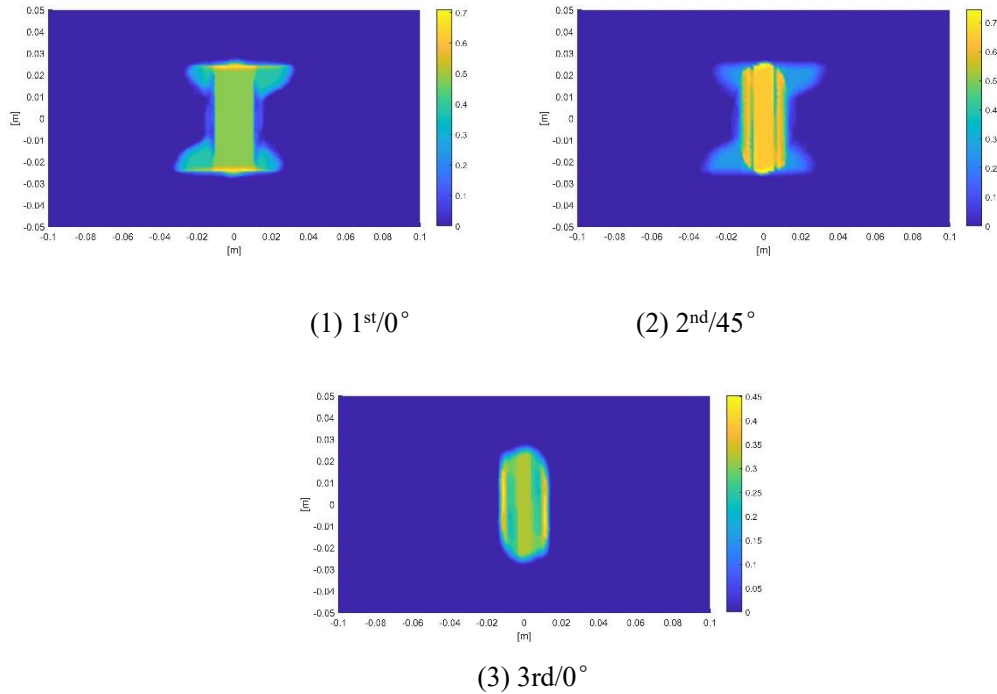
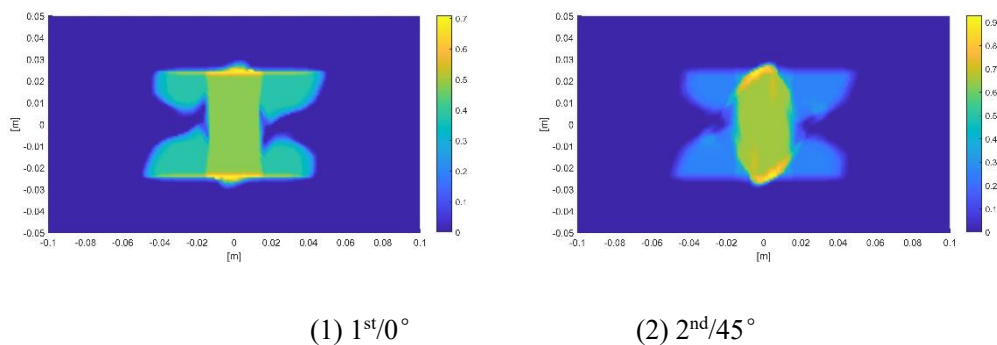
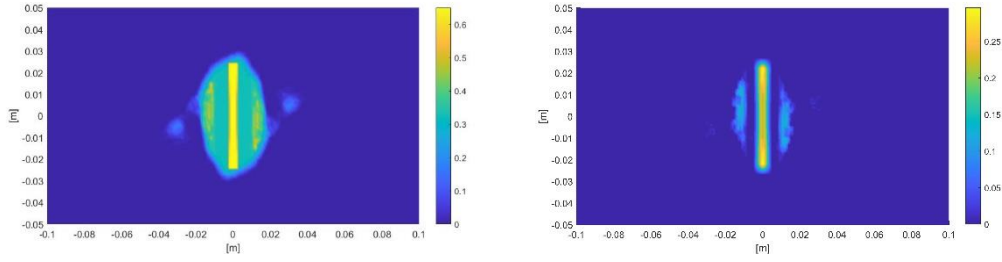


Fig.3.16 Damage cloud at 800 steps

At 800 steps, the damage continued to develop, and the direction of development was roughly the same as the direction of the fibers in this layer; at the same time, along the depth direction of the laminate, the damage began to gradually expand to the first three layers, and the damage in the latter layers was not yet obvious due to the fact that the base had not yet been created with the impact, as well as the extrusion of the column.

(3) 1000 step





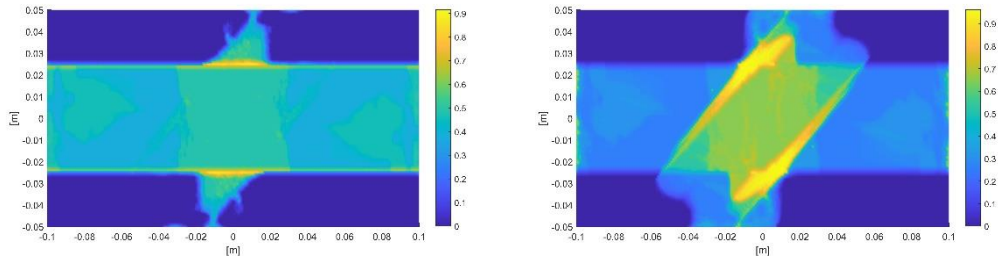
(3) 3rd/0°

(4) 4th/-45°

Fig.3.17 Damage cloud at 1000 steps

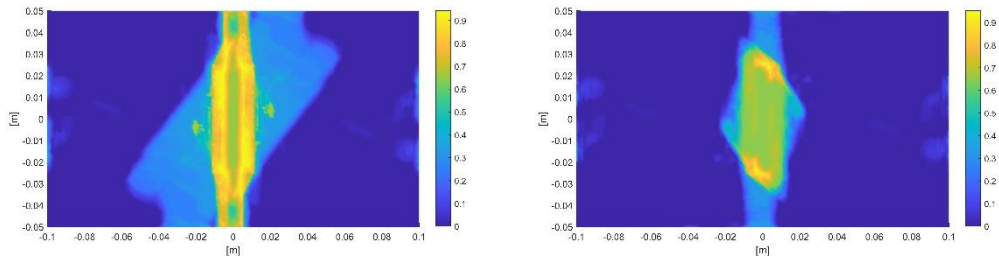
At 1000 steps, we can conclude similarly to the above, that the damage is carried out along the fiber release line of this layer, which is especially evident in the results of the first three layers, with the most severely damaged yellow areas in the first three layers being 0°, 45° and 90°, respectively, in the same direction as the fibers of this layer; at the same time, the damage begins to spread down layer 4 with the motion of the impactor.

(4) 2000 step



(1) 1<sup>st</sup>/0°

(2) 2<sup>nd</sup>/45°



(3) 3rd/0°

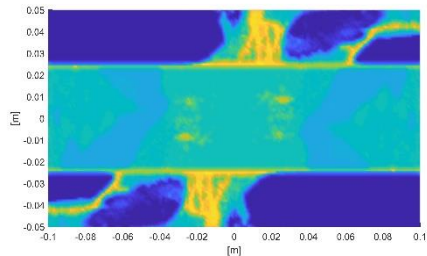
(4) 4th/-45°

Fig.3.18 Damage cloud at 2000 steps

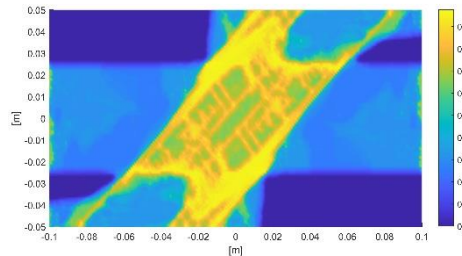
In the first three layers, the damage had been carried out along the fiber direction to the edge of the laminate, especially in the third layer is the most obvious, because the fiber of this layer is parallel to the short side direction, the fiber length is the

shortest; also the fiber direction is parallel to the direction of the cylindrical bus, which means that the damage of this layer is the easiest to carry out, and the damage is the most This was confirmed by the final test results.

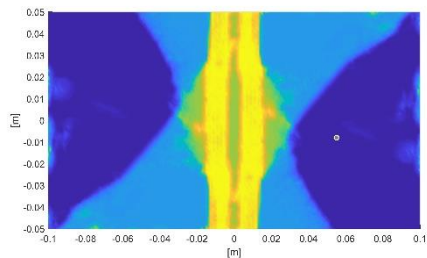
(5) 3000 step



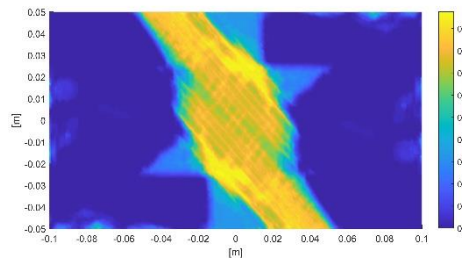
(1) 1<sup>st</sup>/0°



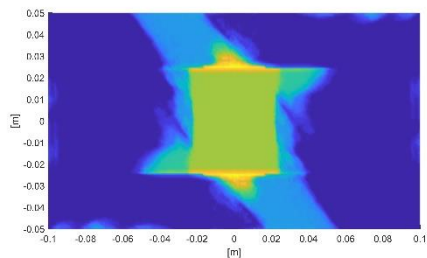
(2) 2<sup>nd</sup>/45°



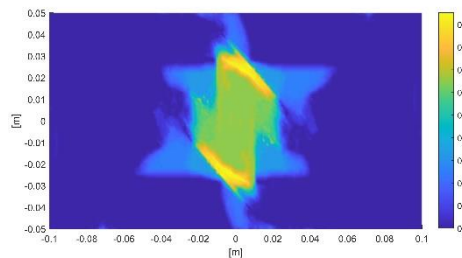
(3) 3<sup>rd</sup>/0°



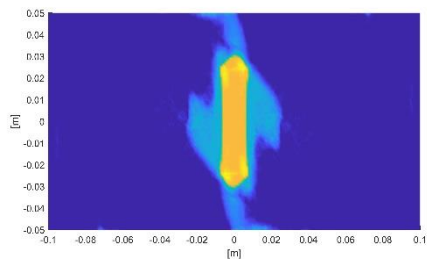
(4) 4<sup>th</sup>/-45°



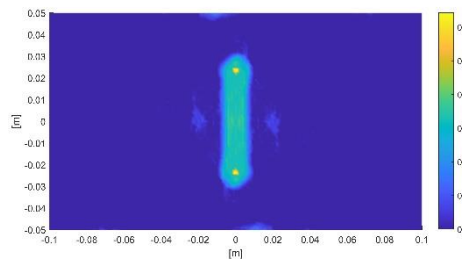
(5) 5<sup>th</sup>/0°



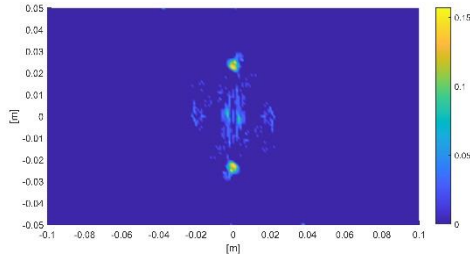
(6) 6<sup>th</sup>/-45°



(7) 7<sup>th</sup>/90°



(8) 8<sup>th</sup>/45°



(9) 9th/0°

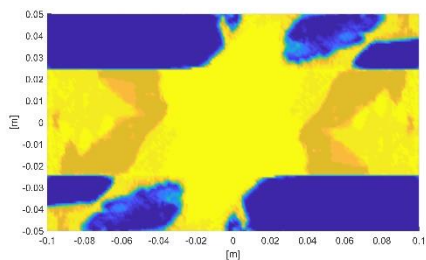
Fig.3.19 Damage cloud at 3000 steps

At 3000 steps, the column almost completely invaded the laminate, and the bottom layer of the laminate (layer 9) started to show damage, and the location of the damage was concentrated in the contact position between the two, especially the location of the top and bottom surface of the column was the most obvious, which is consistent with the previous conclusions.

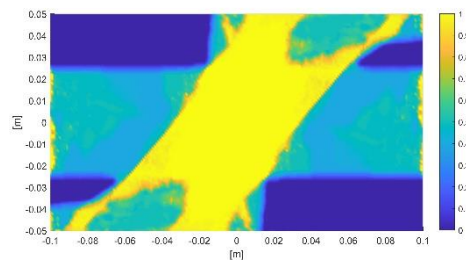
In the first four layers, the damage cracks were roughly spider-webbed in layers 2 to 4, where the damage evolution was more obvious; at this point, the damage was carried out along the fiber direction to the edge of the laminate, indicating that the matrix of the layer was almost completely fractured at this point and the layer of fiber-reinforced composite had lost its load-bearing capacity.

**Simulation results of interlayer damage**

Here, we define interlaminar damage as the fracture of the "interlaminar bond" between the two adjacent layers above and below a given layer. We have introduced interlaminar bonds to describe the interlaminar action, so that the results of interlaminar damage can also be obtained, as shown in the following figure.



(1) 1<sup>st</sup>/0°



(2) 2<sup>nd</sup>/45°

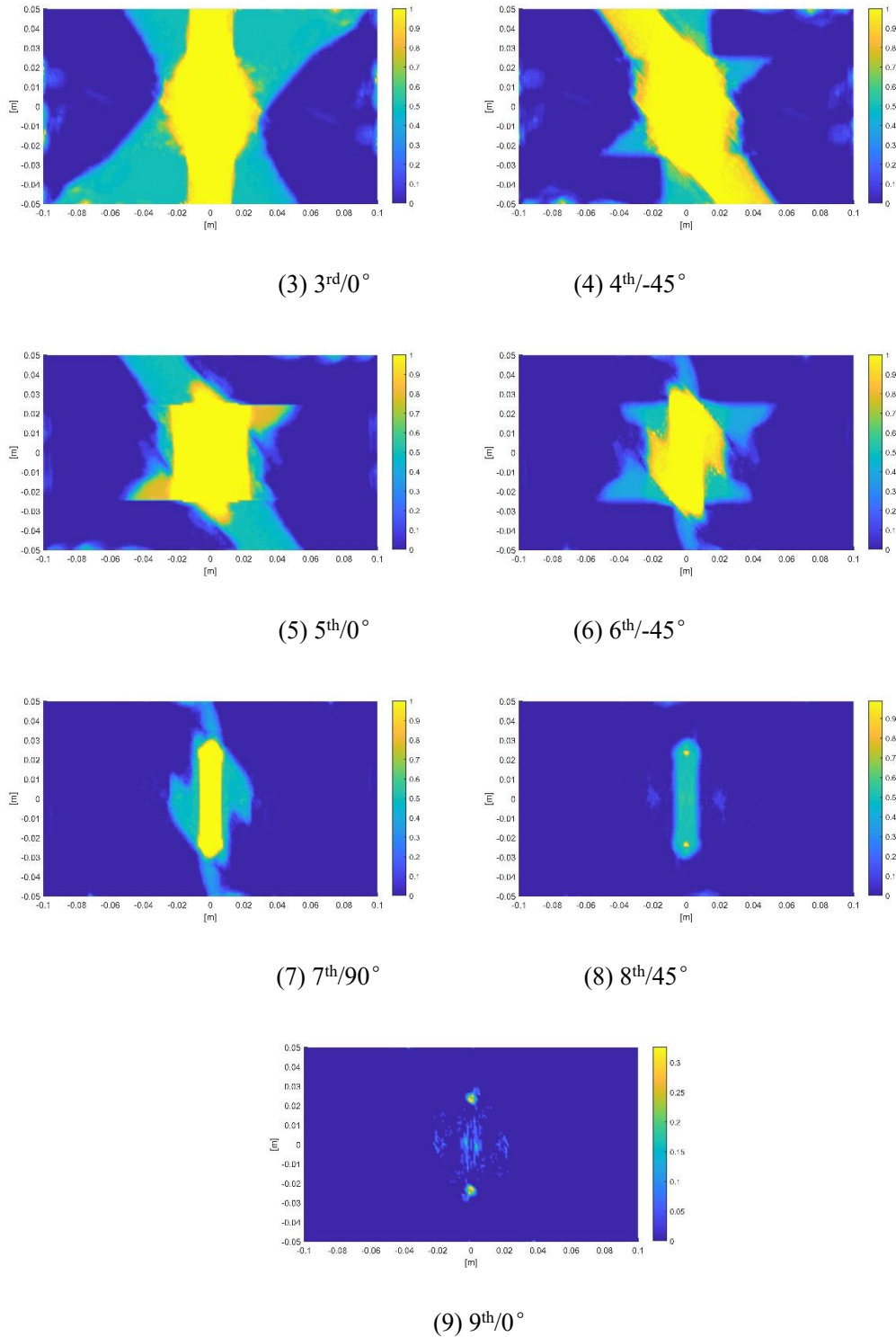


Fig.3.20 Schematic diagram of interlaminar damage of composite laminates

Observing the above damage contour diagram, we can find that the interlaminar damage evolution form of laminate is similar to that of intra-laminar damage and overall damage, but the interlaminar damage tends to be more uniform and blocky.

**Deformation of laminate**

In addition, we can obtain the displacement of each material point on the laminate in the vertical direction, and thus we can obtain the vertical deformation of the laminate. Taking the vertical displacement of each material point at 3000 steps as a variable, we can plot the deformation of the laminate as shown below:

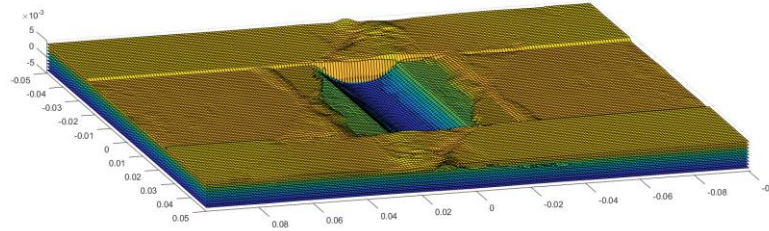


Fig.3.21 Vertical deformation of laminated panels

Observing the above images, it can be found that the laminate undergoes significant deformation under the impact, and the most obvious is the contact area with the impactor, where the deformation profile is "cylindrical", i.e., consistent with the shape of the impactor. At the same time, the deformation shows an obvious "groove" shape, i.e., the deformation of the laminate is deeper on the impacted side and shallower on the back side, which is consistent with the findings of the related literature [24]

### 3.7.2 Simulation results of round ball impact damage

Based on the above procedure, we replaced the impactor from a cylinder to a rigid sphere, with the geometric parameters of the sphere as described before and the rest of the parameters remaining the same.

Considering the symmetry of laminate layup, we choose two different typical working conditions to show the simulation results of impact damage under different shapes.

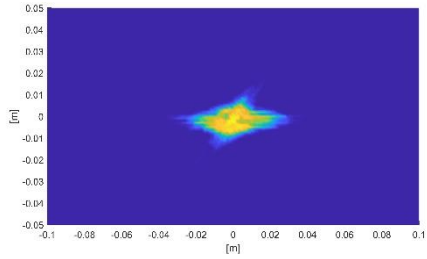
**Case 1** ( $v_x=0\text{m/s}$ ,  $v_y=24\text{m/s}$ ,  $v_z=32\text{m/s}$ ):

In the 1<sup>st</sup> case, we set the initial velocity as  $v_x=0\text{m/s}$ ,  $v_y=24\text{m/s}$ ,  $v_z=32\text{m/s}$ , which is equivalent to  $v=40\text{m/s}$ ,  $\alpha=36.5^\circ$ ,  $\alpha$  is the angle between the velocity and the normal direction of the laminate, i.e. the angle with the surface of the laminate is  $63.5^\circ$ . The rest of the initial conditions remain the same as the previous test.

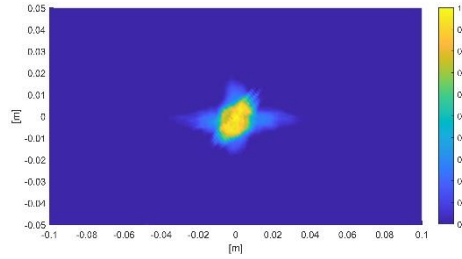
In order to demonstrate the results of the development of damage at different stages, the results of damage evolution at two different stages were selected, 1000 steps and 3000 steps, the former at the early stage of the impact effect, and the latter at

the late stage of the impact effect, and the results of damage evolution at the two stages are shown in the following figure:

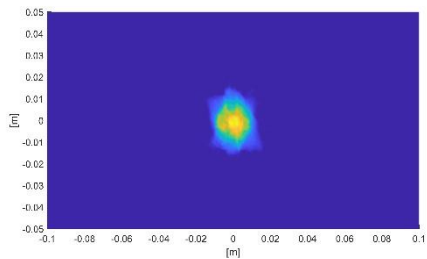
1000 step:



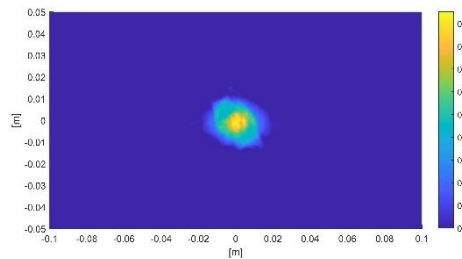
(1) 1st/0°



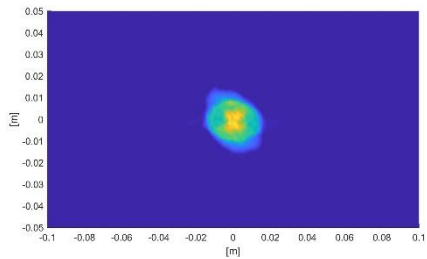
(2) 2nd/45°



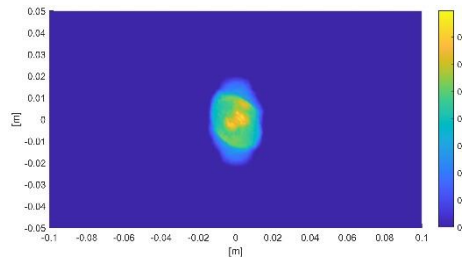
(3) 3rd/0°



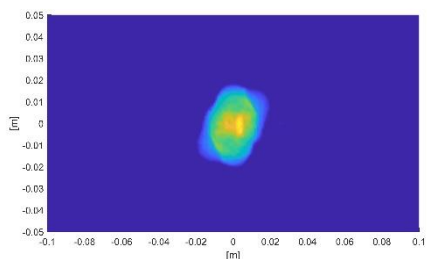
(4) 4th/-45°



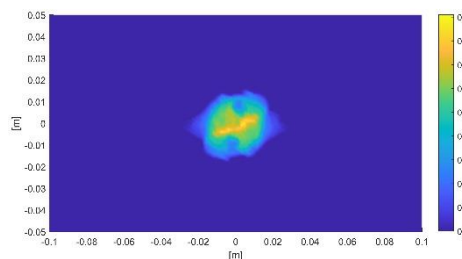
(5) 5th/0°



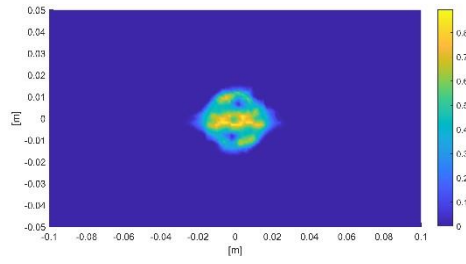
(6) 6th/-45°



(7) 7th/90°



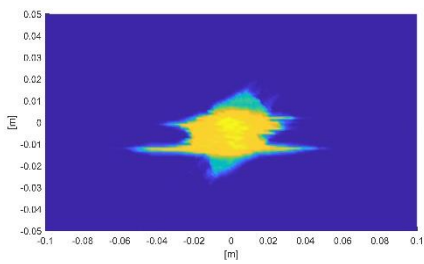
(8) 8th/45°



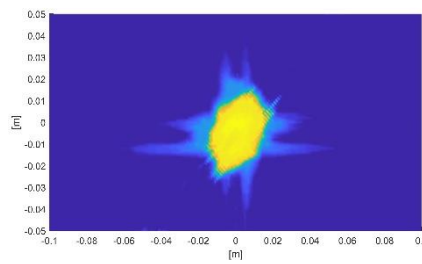
(9) 9<sup>th</sup>/0°

Fig.3.22 Schematic diagram of the overall damage to the composite laminate

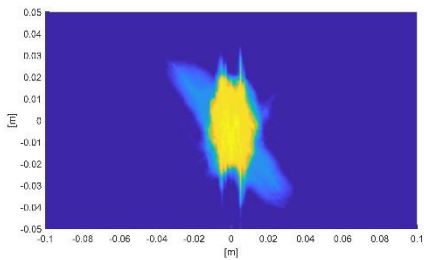
3000 step:



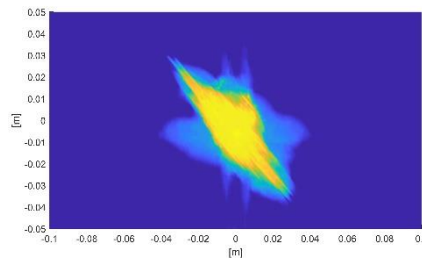
(1) 1<sup>st</sup>/0°



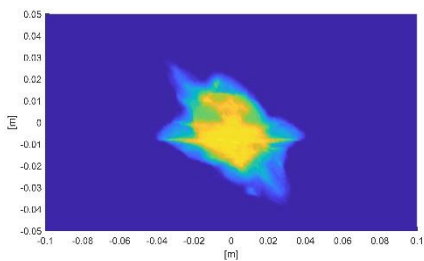
(2) 2<sup>nd</sup>/45°



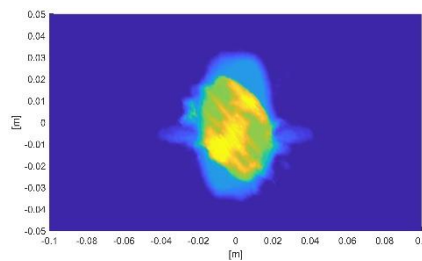
(3) 3<sup>rd</sup>/0°



(4) 4<sup>th</sup>/-45°



(5) 5<sup>th</sup>/0°



(6) 6<sup>th</sup>/-45°

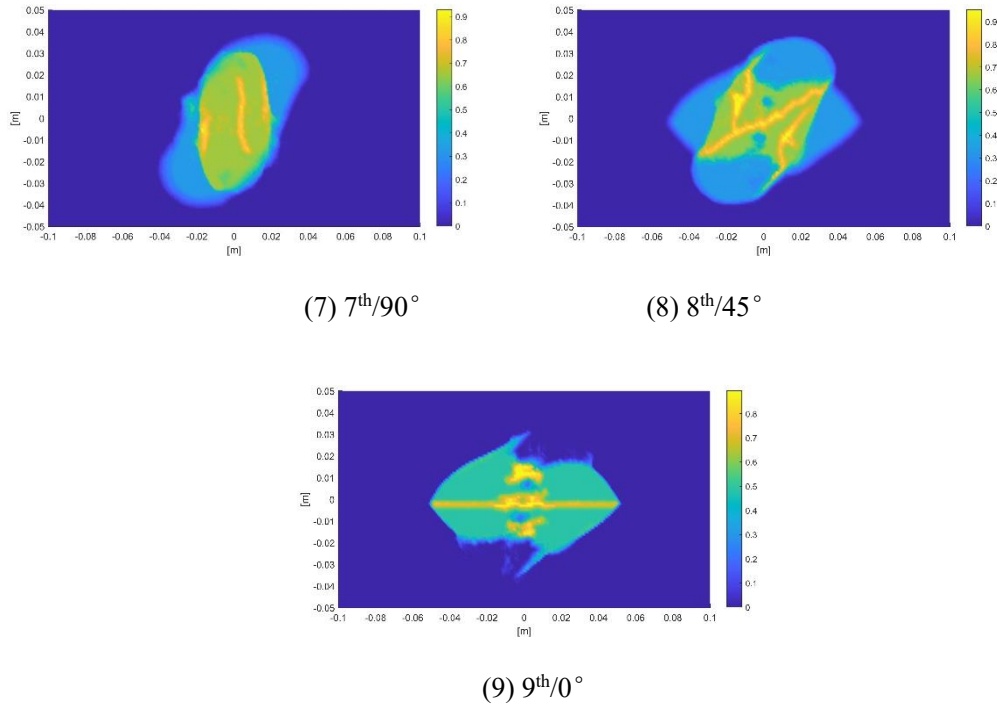


Fig.3.23 Schematic diagram of the overall damage to the composite laminate

### Deformation of laminate

In addition, we can get the displacement of each material point on the laminate in the vertical direction, and thus we can get the vertical deformation of the laminate. Taking the vertical displacement of each material point at 3000 steps as a variable, the deformation of the laminate can be plotted as shown below:

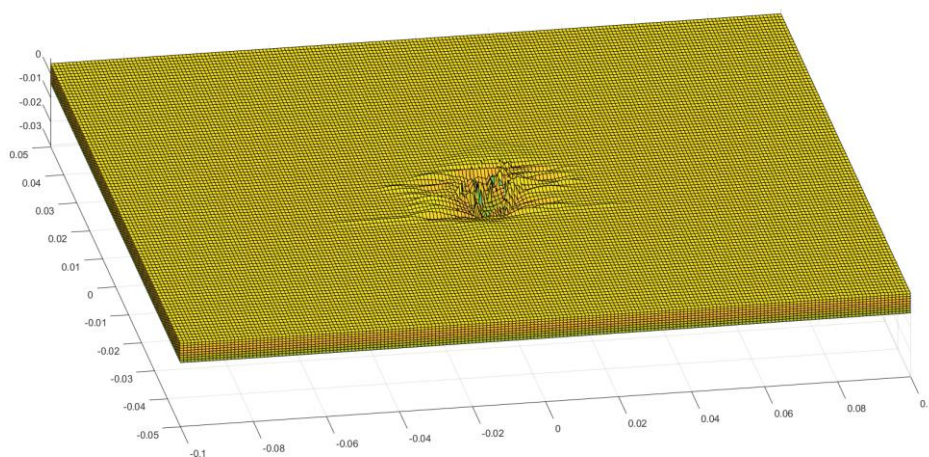


Fig.3.24 Vertical deformation of laminated panels

Observing the above damage evolution and deformation, it can be found that at

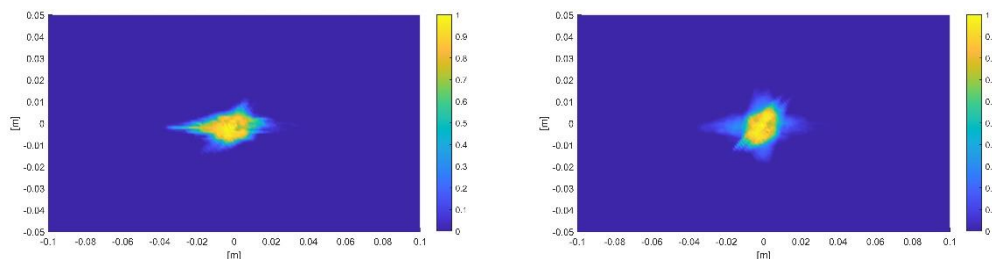
1000 steps, the normal travel of the impactor is short, estimated to be about 3 mm based on the initial velocity, and only the first three layers of the model produce contact with the laminate; at this time, the overall damage situation of the laminate is shallow, and the damage area of each layer is small and almost concentrated at the contact position between the impactor and the laminate, which is roughly circular, i.e., the damage shape is roughly the same as the impactor; when the program enters 3000 steps, the rigid round ball almost completely invades the laminate, and at the same time, comparing the results of 1000 steps, it can be clearly observed that the damage area increases significantly, and the damage of each layer is carried out roughly along the fiber direction, which is consistent with the results of other related literature.

Comparing the results under the action of cylindrical impact, it can be found that there is a clear relationship between the damage development and the motion parameters (velocity, angle) of the impactor. In the cylindrical impact experiment, the impact velocity of the impactor is perpendicular to the plate surface, which means that the velocity is spatially symmetric, and the damage evolution is also symmetrically distributed considering the symmetry of the laminate lay-up direction; while in this test, the motion parameters of the impactor do not have symmetry, so the damage development also shows a certain generality and correlation with the velocity magnitude and direction. The sphere has a horizontal velocity pointing in the negative direction of the  $y$ -axis and parallel to the direction of the plate; therefore, the damage is more pronounced in the negative position of the  $y$ -axis than in the positive position, i.e., the damage arises roughly in the direction of travel of the impactor.

**Case 2** ( $v_x=18\text{m/s}$ ,  $v_y=24\text{m/s}$ ,  $v_z=32\text{m/s}$ ):

In this condition, the initial velocity  $v_x=18\text{m/s}$ ,  $v_y=24\text{m/s}$ ,  $v_z=32\text{m/s}$ , i.e., the velocity along the  $x$ -axis is increased, and the rest of the initial conditions are the same as above, showing the damage evolution results for 1000 steps and 3000 steps as well.

1000 step 时:



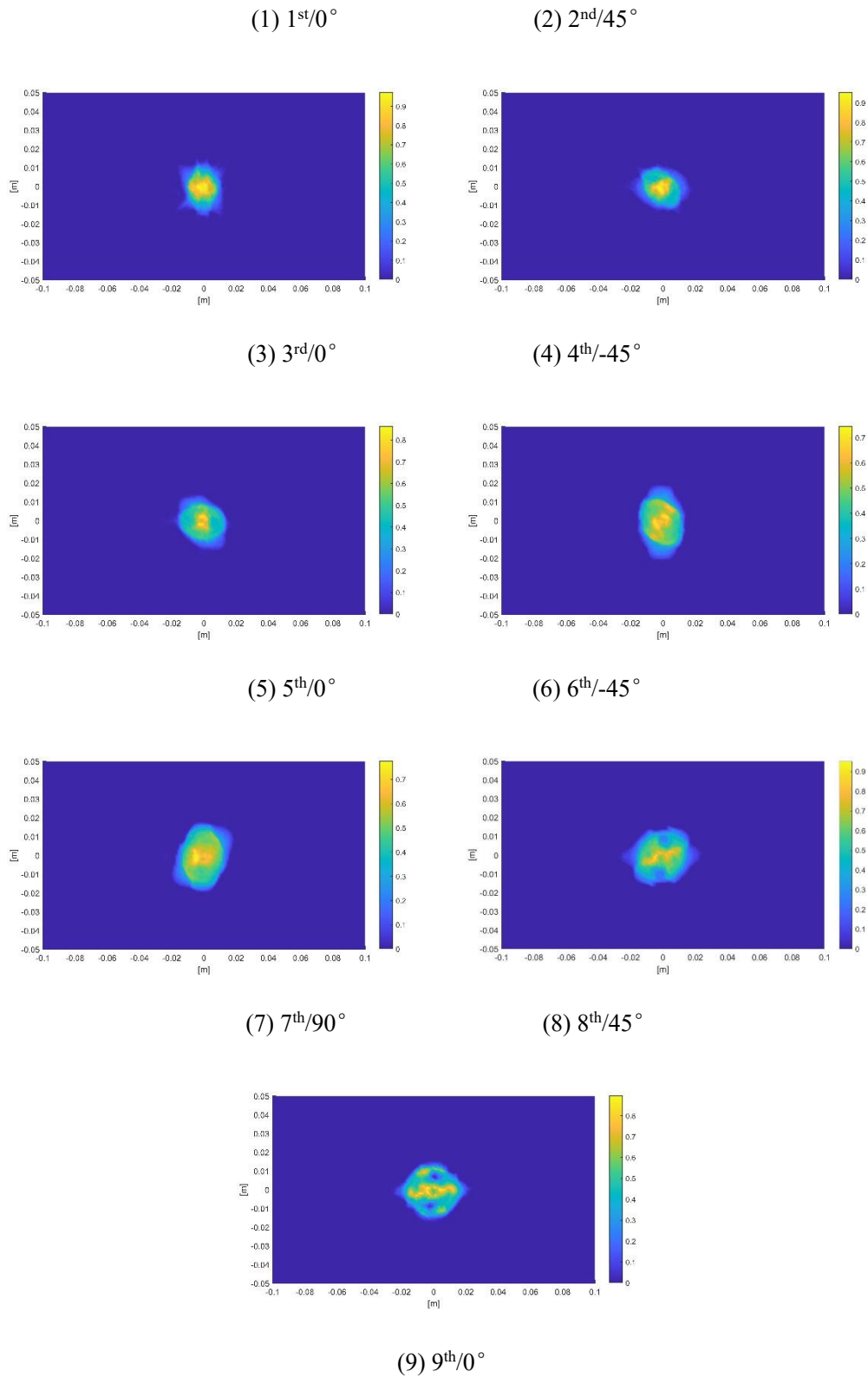
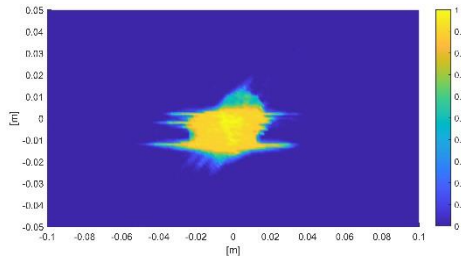
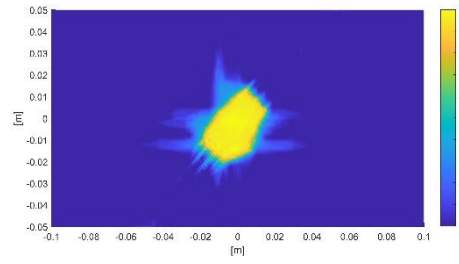


Fig.3.25 Schematic diagram of the overall damage to the composite laminate

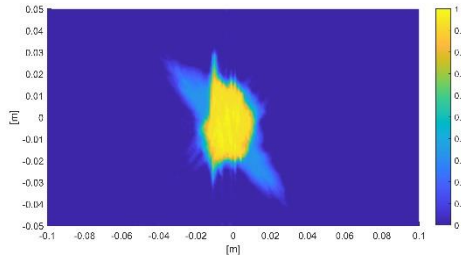
3000 step:



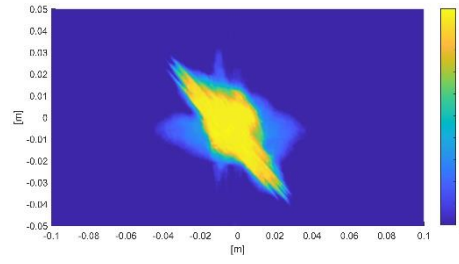
(1) 1<sup>st</sup>/0°



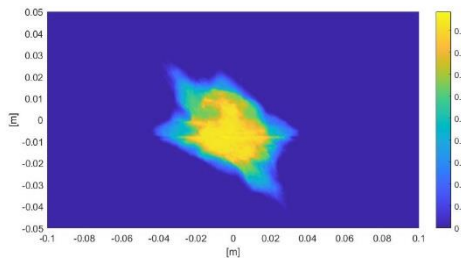
(2) 2<sup>nd</sup>/45°



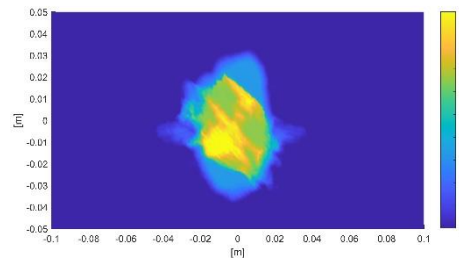
(3) 3<sup>rd</sup>/0°



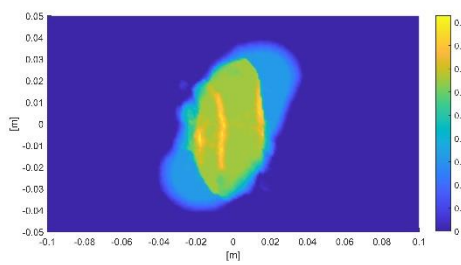
(4) 4<sup>th</sup>/45°



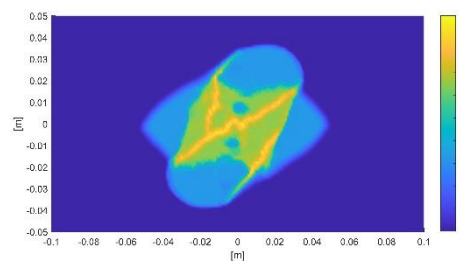
(5) 5<sup>th</sup>/0°



(6) 6<sup>th</sup>/45°



(7) 7<sup>th</sup>/90°



(8) 8<sup>th</sup>/45°

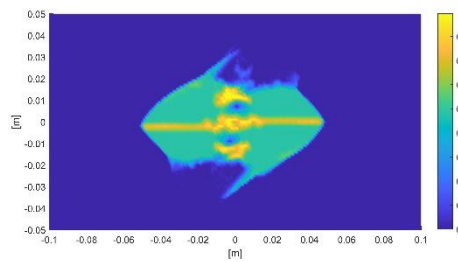


Fig.3.26 Schematic diagram of the overall damage to the composite laminate

Observing the overall damage contour of the above laminate, we can find that the damage is carried out similarly to that under the action of cylindrical impact.

At 1000 steps, the ball as the impact object has limited travel, the damage to the laminate has not yet been carried out, and the more serious damage is almost always concentrated in the contact area between the ball and the laminate.

Also, due to the spatial asymmetry of the impact velocity, the damage is carried out more irregularly in the plane, but the overall conclusion remains the same, i.e., more pronounced damage occurs in the direction of travel of the impactor.

### 3.8 Summary of this chapter

This chapter focuses on the simulation of impact damage of composite laminates based on peridynamics, with specific work on:

(1) A more concise surface correction factor for composite materials is proposed. The traditional peridynamics method faces the problem of "surface effect", which means that the near-field range is often incomplete for the material points in the boundary region, which leads to large calculation errors.

(2) To address the problem of discontinuous mechanics of composite laminate impact damage, an analytical model of rigid body impact damage evolution of composite laminate based on the peridynamics theory was established, and a corresponding PD calculation program was developed. Based on this model, the damage evolution of the composite laminate is simulated under different impact conditions (shape, velocity and angle of the impactor). During the simulation, the impactor is assumed to be rigid, i.e., only rigid body displacement occurs, and no deformation occurs in itself. During the impact process, we record the results of the laminate at different time steps, analyze the evolution of the impact damage and the deformation of the laminate, and obtain the damage law of the laminate under the action of rigid body impact, i.e., the damage is carried out roughly along the normal direction of each ply fiber, the fracture of the matrix precedes the fracture of the fiber, the damage area increases with the increase of the impact velocity, and its shape is consistent with the shape of the impactor.

## Chapter 4 Deep Learning Based Impact Condition Identification

### 4.1 Introduction

In the previous chapter, we simulated the impact action of a rigid body on a laminate under different working conditions through an analytical model of laminate impact damage evolution based on peridynamics, and analyzed the development and form of laminate impact damage. We found that the damage evolution of a laminate is not only related to its own properties and parameters, including factors such as layup direction, geometry, and material properties, but also to the impact working conditions, such as velocity, angle, and position of the contact area. Therefore, for this phenomenon, we consider an "Inverse solution" - based on the damage evolution of a plywood layer, we infer the size and direction of the impact it was subjected to in the first place. This is a very practical problem in engineering, i.e., some structures represented by composite laminates are often subjected to impacts from the outside, in different directions and at different speeds, such as front windshields or shells of cars and airplanes, which may be hit by birds or rocks, thus causing accidents. The study of this phenomenon will help to analyze and restore the working conditions when such accidents occur, and provide some theories and evidence for a series of subsequent improvement measures or engineering studies. However, since the impact damage evolution of composite laminates presents complex nonlinear characteristics, the identification of impact conditions encounters great challenges, so we address this problem by trying to identify unknown impact conditions using deep learning methods.

### 4.2 Introduction to Deep Learning Theorys

Deep learning<sup>[95]</sup> is a way of Machine Learning (ML), and the main research directions of machine learning include decision trees, random forests, and deep learning. Its ideas have existed for almost centuries, and as early as the 17th century, Thomas Bayes, Pierre-Simon Laplace and others proposed some derivations and

conclusions about the method of least squares (Ordinary least squares), and these theories also constitute the most These theories form one of the core and essential theoretical foundations of machine learning theory today.

In the 1950s, Alan Turing, the father of computer science, asked in one of his papers<sup>[93]</sup> "Can machines think?" (Can machines think?), asking whether machines could learn and become self-aware like the human brain. This question continues to plague today's academic community and has, in part, inspired today's work on deep learning. At the beginning of this century, Hinton et al. formally introduced the concept of Deep Learning (DL). Meanwhile, with the dramatic improvement of computer hardware and the birth and practical application of some network models (e.g., AlexNet<sup>[94]</sup> proposed by Hinton in 2012), deep learning has made great progress and become the most popular research direction in machine One of the hottest research directions in the field of learning has intersected with almost all disciplinary disciplines, and algorithms refined by deep learning have shone in the fields of finance, medicine, autonomous driving, drones, and even art, with notable results. Today, deep learning is the most widely used term in science, engineering, and even the online community.

Deep learning discovers the intrinsic distribution of data by combining low-level features to form more abstract categories or features of higher-level representational attributes that can inform the study of similar features in other data. The essence is to learn from sample data to discover its intrinsic patterns and levels of representation, and the information obtained from this learning process can be of great help in the interpretation of data such as text, images, and sounds. The ultimate goal of deep learning is to enable computers to learn analytically like humans, and to train various types of data to perform subsequent predictions, including recognition, classification, regression, etc.

As one of the methods in deep learning theory, neural networks are one of the popular research at present, and many researches related to deep learning are carried out on neural networks. Typical neural network models include fully connected neural networks (FNN), convolutional neural networks (CNN), recurrent neural networks (RNN), and so on. Each of these networks has its own characteristics and strengths, and it is often necessary to select the appropriate network according to the specific research problem.

At present, the code of deep learning is mainly presented in the form of Python

language. At present, there are already a large number of libraries and platforms developed for deep learning internationally, and these libraries and platforms constitute the development framework of deep learning, and the related development work can be carried out on the basis of the above framework, among which some more popular frameworks have been widely popularized and applied, abroad, including TensorFlow developed by Google, Caffe developed by UC Berkeley Caffe developed by Google, Theano developed by Polytechnic Institute of Montreal, PyTorch launched by Facebook AI Institute, etc. In addition, domestic research development frameworks include the deep learning platform Flying Paddle (PaddlePaddle) launched by Baidu with years of deep learning technology and business applications, Jittor developed by Tsinghua University, MindSpore launched by Huawei, etc.

TensorFlow developed by Google is one of the most widely used frameworks, and the computational libraries, software packages and other related data materials based on this framework are the most complete, so the deep learning models in this paper are all developed and built based on TensorFlow.

### 4.3 Model Selection

As mentioned earlier, the development of deep learning so far has given birth to a large number of network models, including the classical BP model, CNN model, RNN model, FNN model, GAN model, etc. These models have different characteristics and are also applicable to different practical problems, and choosing a suitable class of network models is our first job.

#### 4.3.1 Common Network Models

##### 1. Fully connected network, FNN

A fully connected neural network is one of the most traditional neural networks in which two neurons in any two adjacent layers are interconnected, and its structure is shown in the following figure:

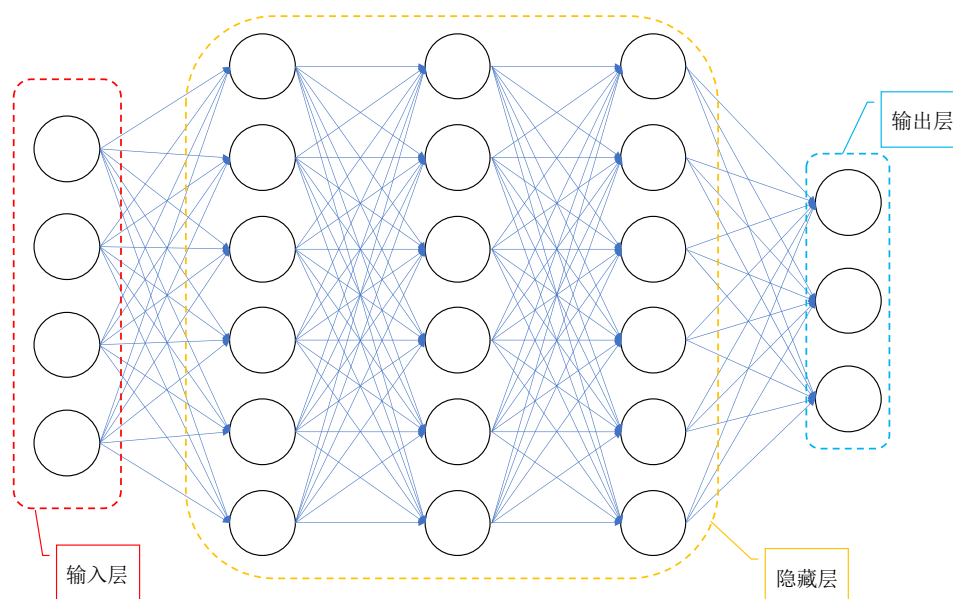


Fig. 4.1 Fully connected neural network model

In each iteration, the data in the input layer is first passed one-way until the output, the error is calculated, and then the parameters are updated by the back propagation algorithm and a second iteration is performed, cyclically advancing the above process until the final error converges.

## 2. Convolutional Neural Network, CNN

Convolutional neural networks (CNNs) are a clever combination of computer science and mathematics, and have now become a highly influential part of the computer vision field, with a wide range of applications in many areas, such as image recognition and behavior classification.

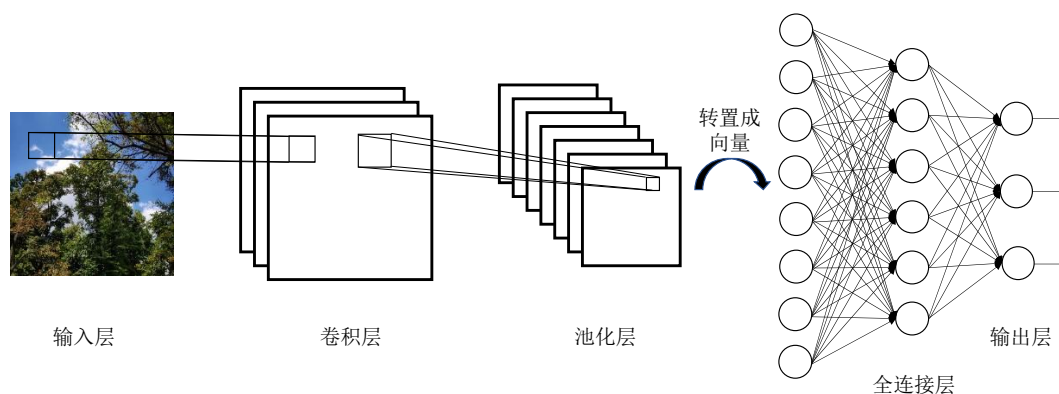


Fig.4.2 卷积神经网络模型

## 3. Recurrent Neural Network, RNN

Recurrent neural networks are also known as recurrent neural networks. Such

networks can be used to deal with a more specific class of problems where there is a clear Sequence relationship between feature data, a typical example being the language used by humans. Almost all languages contain certain grammatical rules, which means that words can only be arranged in a specific order to produce a specific meaning, and different orders often mean different meanings. Therefore, recurrent neural networks are born.

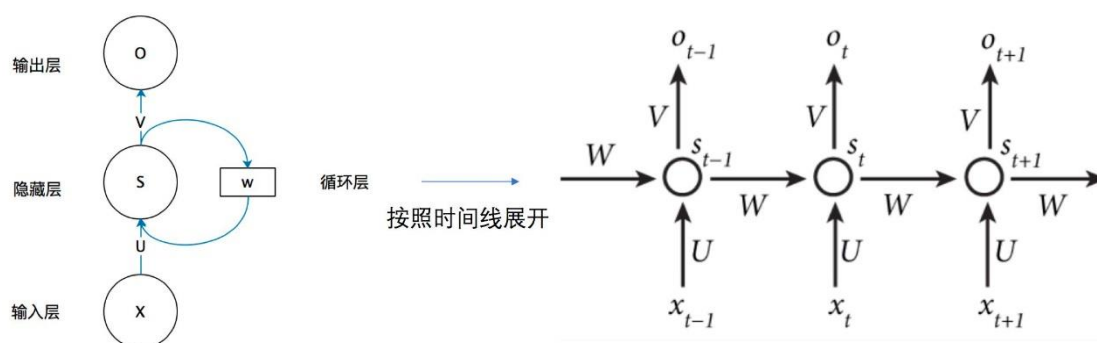


Fig.4.3 Schematic diagram of the recurrent neural network timeline

### Comparison of the models

We list the characteristics and the most important usage scenarios of the above three neural networks in the following table:

Table4.1 Comparison of three types of neural networks

	FNN	CNN	RNN
Features	Connections exist between each neuron on two adjacent layers of the network, with a simple structure and wide applicability, but a large number of parameters	CNN can significantly reduce the number of parameters to be measured compared to FNN by extracting and enhancing data features through convolution and pooling operations	There is a recurrent layer, i.e., the output of this layer and the sample data are used together as the input of the next layer, so there is a memory function for the sample data
The type of problem suitable	In terms of principle and	Suitable when the input data is two-	Such as text recognition, natural

for	structure, the most traditional FNN is suitable for all problems	dimensional, such as image recognition, face recognition, etc.	language processing, text padding, time series related problems	Select
<b>Selection</b>		✓		

As described in the table above, we consider the damage data of the laminate as a multi-channel number of pictures, so the convolutional neural network is best suited for our work.

### 4.3.2 Convolutional neural network and image recognition

Deep learning theory has a wide range of applications and has yielded numerous results in search techniques, data mining, machine translation, natural language processing, multimedia learning, speech, recommendation and personalization techniques, and other related fields.

Image recognition, on the other hand, is a technical area of great interest to deep learning. Image recognition refers to the technology of using computers to process, analyze and understand images in order to recognize various targets and objects with different patterns, which is a practical application of deep learning algorithms. At this stage, image recognition technology is generally divided into face recognition and commodity recognition. Face recognition is mainly used in security inspection, identity verification and mobile payment; commodity recognition is mainly used in the process of commodity circulation, especially in the unmanned retail field such as unmanned shelves and intelligent retail cabinets.

The traditional image recognition process is divided into four steps: image acquisition → image pre-processing → feature extraction → image recognition, as shown in the following figure:

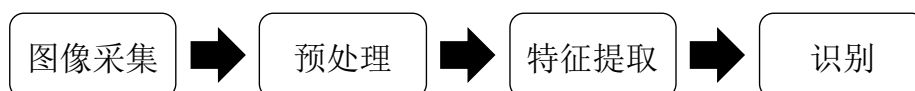


Fig.4.4 Image recognition process

Convolutional neural networks (CNN), recurrent neural networks (RNN), RNN-based long-short term memory model (LSTM), deep confidence networks, generative adversarial nets (GAN) and other common network structures are widely used in the field of image recognition. The traditional classical models have not disappeared, but are being updated, and there are many related researches. Hinton, a leading figure in deep learning, and his student Alex Krizhevsky designed a new model called AlexNet<sup>[94]</sup> based on the traditional convolutional neural network (CNN), and applied ReLU, Dropout and LRN techniques in CNN for the first time, and applied the model to super large-scale image recognition. achieved better recognition accuracy than traditional networks and won the championship in the ImageNet competition in 2012; after that, results born on this basis began to emerge. Domestic scholars Zhou et al<sup>[96]</sup> developed a set of migration learning algorithms based on AlexNet and applied them to image recognition in industrial environments, solving the problems of complex maintenance and poor environmental adaptability of traditional methods. In 2013, Zeiler's team<sup>[97]</sup> further updated AlexNet in that year's ImageNet competition. Google, Microsoft, Facebook, and other Internet giants Google's AI team<sup>[97]</sup> designed and proposed the model of GoogleNet in 2014, which further reduced the error rate of image recognition to about 6.7%.

### **Channel**

Channel is a very important concept in image theory, initially referring to the display scheme of a computer or print for pictures, the former mainly being the RGB channel and the latter commonly being the CMYK channel. The essence of a two-dimensional image is a collection of pixel dots, each of which displays only one color, which in turn is a superposition of the grayscale values of the R (red), G (green) and B (blue) color channels.

Take RGB channel as an example, for any picture, each of its pixel points is displayed through a three-dimensional array (R,G,B) to show the corresponding color, where R,G,B that represents the value of the three color channels of red, green and blue, known as grayscale value, the range is [0,255], the operation of the channel is reversible, that is, a picture can be separated into three channels on the sub-picture, and the three sub-pictures can also be be superimposed into the original picture in some way, as shown in the following figure.:

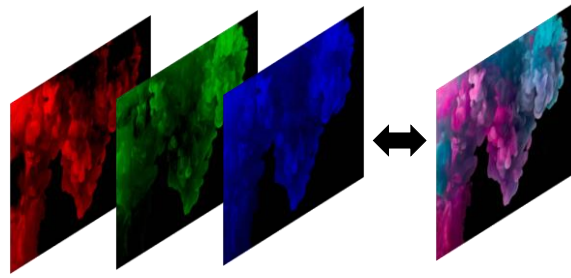


Fig.4.5 RGB channel

Based on this theory, we propose a channel division method for laminate damage, i.e., the damage of each layer is input to the neural network as a channel, and the damage is divided as shown in the following figure:

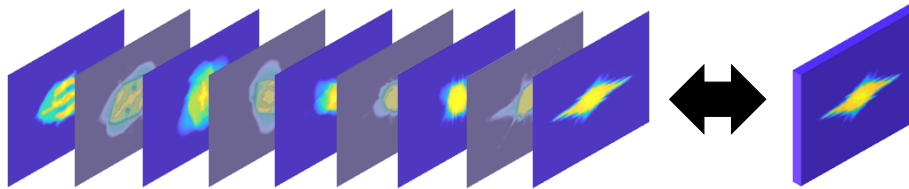


Fig.4.6 Damage channel division

### Convolutional layer

Convolutional layers are the core of convolutional neural networks. When the number of layers of fully connected neural networks increases and the number of neurons in the hidden layer gradually increases, the number of parameters to be optimized also increases exponentially, which is a great test for the computer's computational power. Convolution operation avoids this crisis. Take image recognition as an example, there is often a lot of repetitive or useless information in the image summary, so we apply convolution to the image, the essence of which is to extract the significant features (such as edges) in the image to reduce the number of features and thus the number of parameters.

The principle of the convolution operation can be represented in the following figure:

Take a  $4 \times 4$  grayscale image, the number in the image represents the grayscale value of the pixel, 0 is all black and 255 is all white. We take a  $3 \times 3$  convolution kernel to convolve the image with a step size of 1, i.e., the convolution kernel moves to the right or down one at a time, and the convolution operation can be shown as follows:

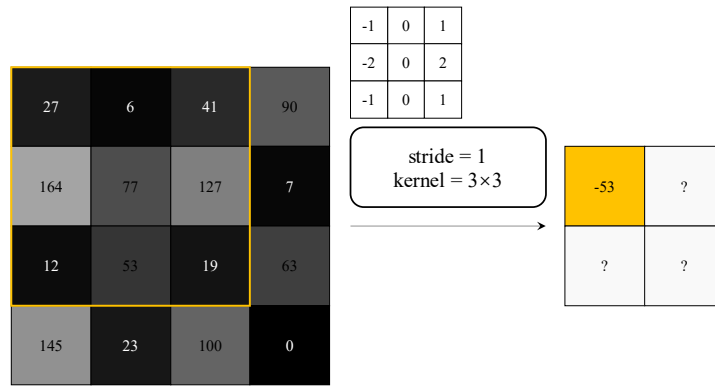


Fig.4.7 Schematic diagram of convolution operation

The size of the image obtained after the convolution operation is related to the size of the convolution kernel, the step size of the convolution operation, etc., and satisfies the following equation:

$$o = \left\lfloor \frac{n + 2p - f}{s} \right\rfloor + 1 \quad (4.1)$$

Where, the input image size is  $n \times n$ ; the convolution kernel size is  $f \times f$ ; the thickness of the fill layer is  $p$ ; the step is  $s$ ; the size of the output image is  $o$ ; “ $\lfloor \ \rfloor$ ” is the downward rounding sign.

Observe the above process, and then combine with the above formula, we can find that after the convolution operation of the original 4x4 grayscale image, the image size becomes 2x2, which also means that some grayscale information of the original image edges is lost, and in most cases, we want to keep the image size unchanged after the convolution operation. To meet this requirement, we try to expand the image size by filling "0" value points around the original image, as shown in the following figure:

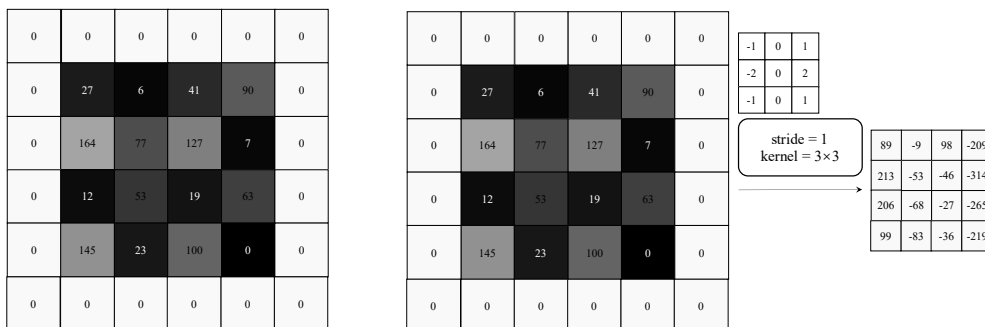


Fig.4.8 Diagram of filling operation

With this method, an image of the same size as the original image can be obtained after the convolution operation.

**Pooling layer**

Pooling is necessary in convolutional neural networks, especially when the amount of data is large, and pooling is also called Downsampled. Too much data in the input model often means too many parameters, which means it is very easy to cause overfitting. Therefore, we consider introducing a pooling layer to downsample the features, compress the number of data and parameters, reduce overfitting, and improve the fault tolerance of the model.

The two common pooling methods used today include Max pooling and Average pooling.

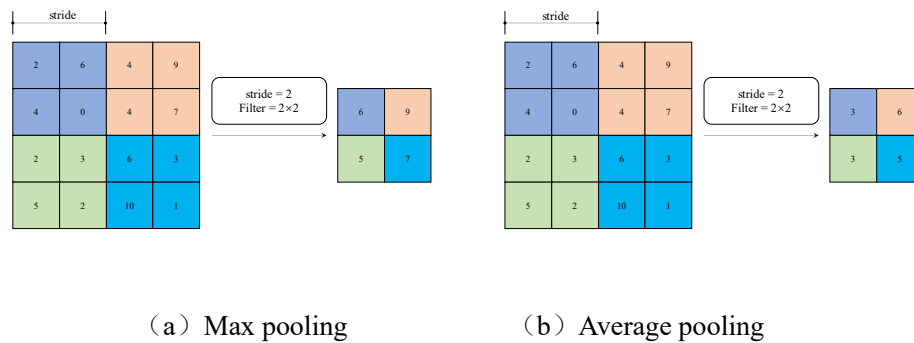


Fig.4.9 Pooling

In general, the two pooling methods do not have an essential effect on the results. In this paper, we consider using maximum pooling.

**4.4 Convolutional neural network construction**

We build our impact work recognition network on the basis of classical image classification convolutional neural network, and before that we need to determine some parameters in the network.

**4.4.1 Activation Function**

The activation function is a very important concept in deep learning networks and is also known as the "transfer function" in artificial neural network theory. It acts

directly on the neuron, mapping its original linear input to the output.

For neurons that do not add an activation function, we call them "Perceptron", which is a very primitive learning network that is also capable of performing some learning and regression work, and whose principle can be represented in the following figure:

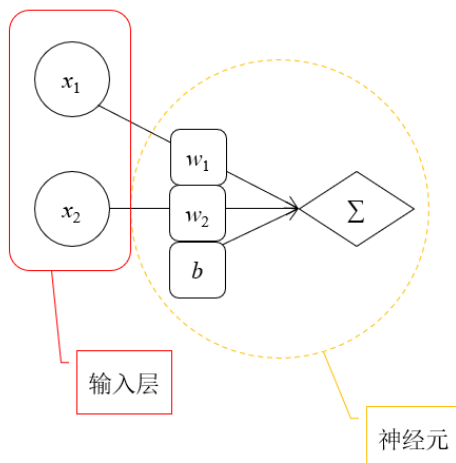


Fig.4.10 Perceptron model

在 In the above figure, the input layer elements  $x_1$ 、 $x_2$  with weights  $w_1$ 、 $w_2$  and bias  $b$ , are transformed by a simple linear transformation to obtain the output of this neuron  $\Sigma$ , i.e.:

$$\Sigma = [w_1 \quad w_2] \cdot \begin{bmatrix} x_1 \\ x_2 \end{bmatrix} + b \quad (4.2)$$

From the above figure and a simple mathematical derivation, it is clear that if only the perceptron model exists in the network, the model remains linear even if the number of neurons and hidden layers is increased. This model is then extremely biased when fitting nonlinear events.

Therefore, the most important point of the activation function is to introduce nonlinear properties into the network, so that our network can learn and understand those complex nonlinear models.

Activation functions commonly used in deep learning include:

### 1. Sigmoid

$$f(x) = \frac{1}{1 + e^{-x}} \quad (4.3)$$

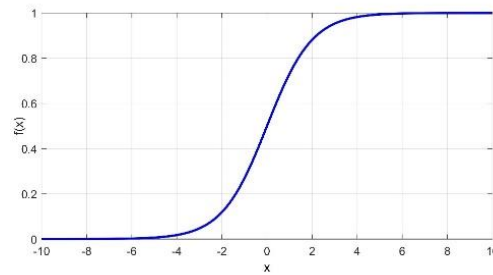


Fig.4.11 Schematic diagram of the Sigmoid function

The Sigmoid function is also known as the "logistic function" and is also known as the S-shaped growth curve in the field of biology. As a very common activation function, it can map the continuous value of the input to the output of the interval. This feature makes the Sigmoid function extremely useful for binary classification problems, i.e., to determine the class of the input by judging the magnitude of the function value and 0.5.

Sigmoid was once widely used, though in recent years it has been used less and less frequently because of some of its inherent drawbacks. One is that it tends to lead to gradient explosion and gradient disappearance when gradients are passed backwards in deep learning networks; the second is that its parsing formula contains power operations, which can significantly reduce the training efficiency of the computer for larger data sets.

In addition, the output values of Sigmoid are all greater than 0, making the output not zero-centered, which in a way causes the "bias phenomenon".

## 2. Tanh

The Tanh function is mathematically known as the "hyperbolic tangent function" and has the following functional equation:

$$f(x) = \frac{e^x - e^{-x}}{e^x + e^{-x}} \quad (4.4)$$

The image of the function is shown below:

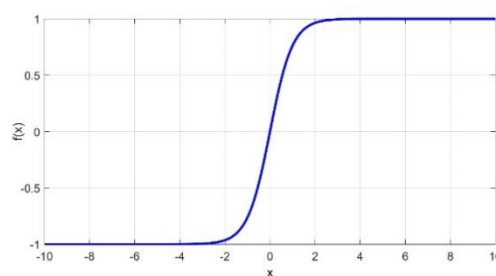


Fig.4.12 Schematic diagram of Tanh function

From the above function image, it can be seen that the Tanh function maps the input to the interval  $(-1,1)$  and, according to the symmetry of the image, implies that the output of the Tanh function is a distribution with 0 as the mean. Compared with the Sigmoid function, the problem that the latter is not zero-centered is solved, and the problems of power operation and gradient disappearance still exist. the Tanh function has a similar image trend to the Sigmoid function, which means that the function is also applicable to the binary classification problem. combining the above advantages, disadvantages and common points, we will be accustomed to using the Sigmoid function on occasions when it can be Tanh function instead.

### 3. ReLU(Rectified Linear Unit)

The ReLU function is a very simple function to take the maximum value with the following functional equation:

$$f(x) = \max(0, x) \quad (4.5)$$

The image of the function is shown below:

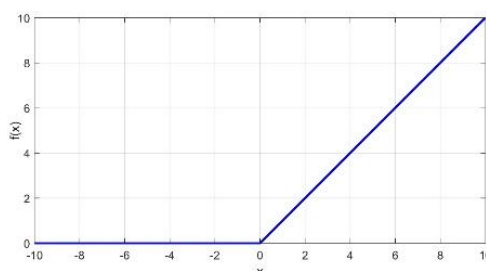


Fig.4.13 Schematic diagram of the ReLU function

The ReLU function is essentially a take maximum function in mathematics - for positive values, the function value is equal to itself, and for negative values it is 0. ReLU is currently the most widely used activation function in deep learning, especially in convolutional neural network models, and almost all such models use ReLU as the hidden layer ReLU is the most widely used activation function in deep learning.

Thanks to the simple form of ReLU, it converges faster than the first two and solves the problem of gradient vanishing at the same time. But the ReLU function also has two problems. One is that it is not fully interval derivable, and the derivative function is not continuous at the origin; second, its output is still not a distribution with 0 as the mean; third, ReLU maps all negative inputs to 0, meaning that it ignores

the contribution of negative features.

In the model of this paper, we use ReLU as the activation function in all the two convolutional layers except the final linear output layer.

#### 4.4.2 Hyperparameter setting

Hyperparameter refers to a set of parameters that need to be specified before the network starts training. It is different from another type of parameters that need to be updated through learning, because once the hyperparameter is specified, it will not be changed during training. Therefore, the setting of hyperparameters is also a very important issue in the construction of deep learning networks. The hyperparameters involved in deep learning include Learning rate, Batch size, etc. In a broad sense, hyperparameters also include non-numerical parameters such as Loss function, Optimizer, etc.

Since the hyperparameters need to be set before the network starts iterative training and will not be modified during the training process, and since the training of deep networks is generally time-consuming, selecting a better set of hyperparameters as much as possible can significantly improve the learning efficiency and of deep learning networks.

A series of hyperparameters are determined in this paper as follows:

##### 1. Learning rate

The learning rate determines the magnitude of parameter updates during each iteration of training:

$$\theta_{j+1} = \theta_j - \alpha \cdot \nabla \quad (4.6)$$

Where  $\theta_{j+1}$ 、 $\theta_j$ ——parameters to be learned;

$\alpha$ ——Learning rate;

$\nabla$ —— $\frac{\partial loss}{\partial \theta}$ , the partial derivatives of the loss function with respect to the

parameters.

The effect of learning rate on training is shown in the following figure.:

Learning rate too small:

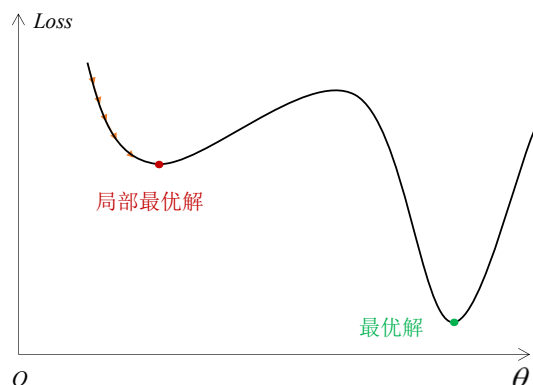


Fig.4.14 Learning rate too small

As shown above, when the learning rate is too small, the training process iterates slowly and tends to fall into a local optimum solution, i.e., the loss function converges when the gradient decreases to a very small value.

When the learning rate is too high:

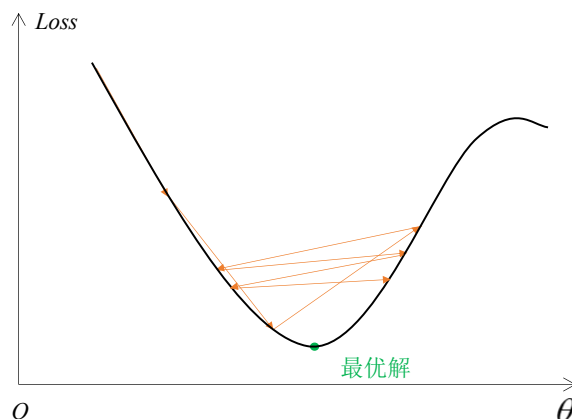


Fig.4.15 Excessive learning rate

And when the learning rate is too large, the gradient oscillates repeatedly around the optimal solution and sometimes fails to converge. Therefore, it is crucial to choose an appropriate learning rate.

In deep learning, we use a very basic strategy of choosing the learning rate, i.e., choosing a larger learning rate at the beginning of training to make the gradient converge to the optimal solution first, and then using a smaller learning rate to converge to the optimal solution. Therefore, we consider the "exponential decay learning rate" to describe this kind of adjustment. TensorFlow framework provides the corresponding function `tf.train.exponential_decay`. based on this function, the learning rate is adjusted during the iterative process by the following equation:

$$Lr = Lr\_base \times Lr\_decay^{\frac{global\_step}{decay\_step}} \quad (4.7)$$

## 2. Batch size

Batch size refers to the number of samples selected for training at one time. In particular, when the total sample size is extremely large, it is not physically possible to feed all samples into the model at once. In addition to this factor, the batch size also affects the degree of optimization and training speed of the model, and an inappropriate batch size may cause the model to converge to a local optimum.

## 3. loss function

The loss function can quantitatively evaluate the degree of difference between the recognition result of the model and the true value. Generally speaking, the smaller the loss function is, the stronger the model is and the better the performance is. The loss function used varies for different models. For example, for a series of classification problems such as image recognition problems, we tend to use the cross-entropy loss function, while for continuous output problems such as regression, we use the mean square error (MSE) loss function.

## 4. Optimizer

The optimizer is a class of algorithms used to find the optimal solution in deep learning network models. Its main role is to guide the parameters of the loss function to update the appropriate size in the right direction during the backpropagation process of deep learning, so that the updated parameters can keep the loss function value close to the global minimum.

The most central optimization idea of almost all optimizers is the use of gradient descent (Gradient descent). Currently, the commonly used optimizer algorithms include Stochastic gradient descent (SGD), Adaptive learning rate algorithm (AdaGrad), etc. In this paper, we use the Adam optimizer based on the self-using learning rate algorithm, which is also a widely used optimizer in deep learning. Adam is a set of the aforementioned methods, and its main advantages include:

- Simple implementation, efficient computation and low memory requirements.
- The update of the parameters is not affected by the scaling transformation of the gradient.
- Suitable for scenarios with large-scale data and parameters, etc.

## 5. Dropout

Dropout technique was first introduced in AlexNet in 2012 by Hinton and his team, the titan of deep learning. This technique means that during the training process

of a neural network, for each layer of neurons, a portion of the neurons are randomly dropped according to a ratio (called "Dropout rate") set by the implementation. The main purpose of introducing dropout is to prevent overfitting of the convolutional neural network during training, as shown in the following figure:

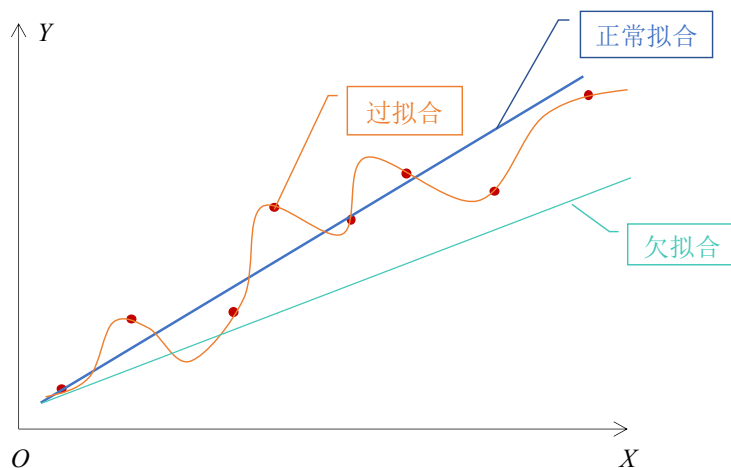


Fig.4.16 Normal fit, underfitting and overfitting

overfitting means that the model learns the features of the data in the training set excessively and is less sensitive to the unexpected data features in the training set. During the training process, although the loss function is converged to a very low level, however, the real recognition ability of the model is poor.

A comparison of the neural network with and without the dropout added is shown below:

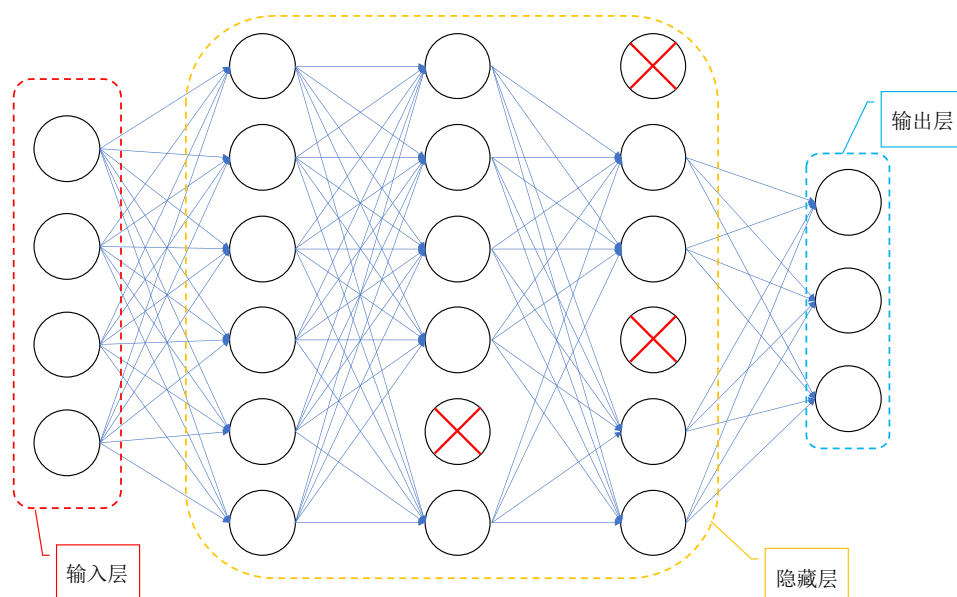


Fig.4.17 Adding dropout

Through the above comparison, it can be noted that the network after dropout is more streamlined than the original network, thus reducing the probability of overfitting.

After clarifying the above concept, and after several rounds of attempts, we finally selected the hyperparameter settings as shown in the following table:

Table6.2 Hyperparameter setting table

Hyperparameter	Value
Learning rate base	0.001
Learning rate decay	0.99
Training set	1440
Validation set	180
Test set	180
Batch size	18
Training epoch	3000
Dropout rate	0.025/0.2
Loss function	MSE
Activation function	ReLU
Optimizer	Adam

### 4. 4. 3 Network Structure

After determining the neural network type and all hyperparameters in the network, we can draw the neural network structure of the response, as shown below:

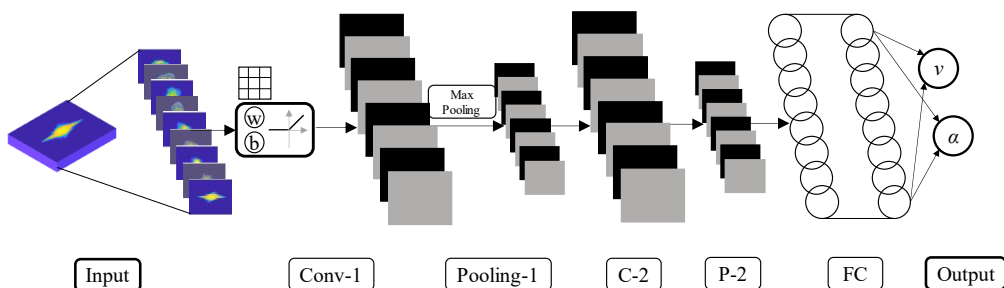


Fig.4.18 Neural network structure diagram

In the first fully connected layer, we set up with 1024 neurons, and in the second fully connected layer, with 256 neurons.

## 4.5 Impact condition identification

The main content of this chapter is deep learning-based impact condition recognition, and the computational flow of this part is shown in the following figure:

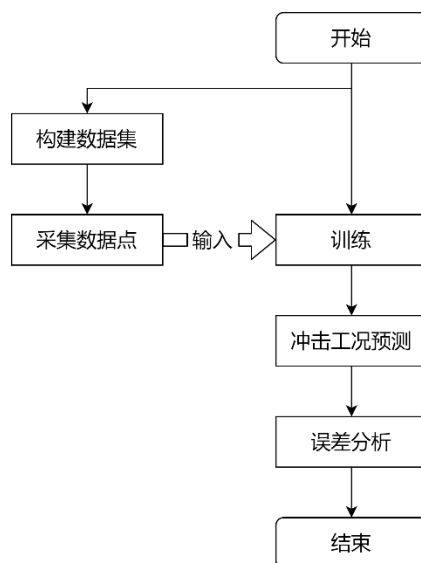


Fig.4.19 Calculation flow of this chapter

### 4.5.1 Dataset construction and partitioning

#### 1. Dataset construction and partitioning

First, we specify the coordinate system settings for the laminate as shown below:

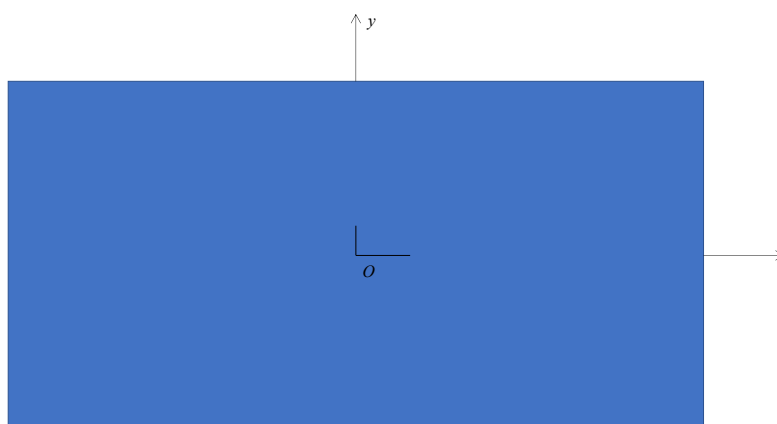


Fig.4.20 Coordinate system setting of laminate model

After that, we construct the data set based on the calculation procedure in the

previous chapter by modifying the ball impact velocity and angle, where the velocity is from 30 to 70 in size with a step size of 5, for a total of 10 groups. The angles range from  $0^\circ$  (perpendicular to the plate) to  $85^\circ$  (almost parallel to the plate) in steps of  $5^\circ$ , for a total of 18 sets. The following figure shows:

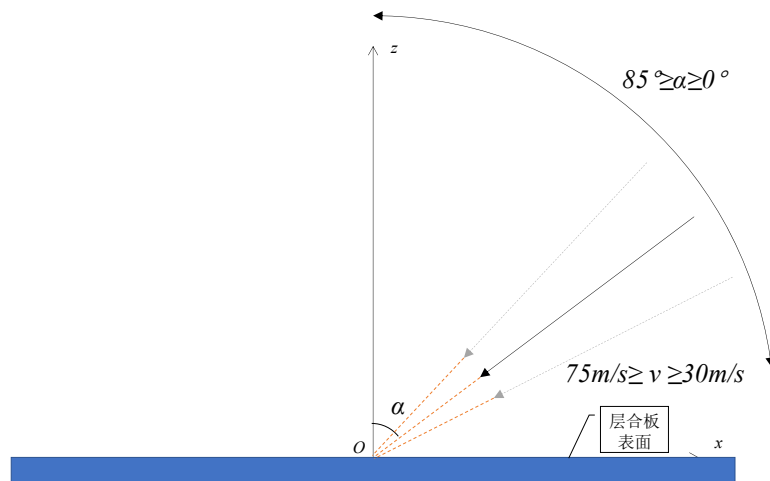


Fig.4.21 Schematic diagram of speed and angle

## 2. Data enhancement

With the combination of speed and angle described above, we can obtain a sample set consisting of 180 data sets. According to the experience related to deep learning, this amount of data is low, therefore, we consider obtaining more data by the method of Data augmentation.

The traditional data enhancement methods include SMOTE (Synthetic Minority Over-sampling Technique) method, adding noise (Gaussian noise, pretzel noise, Poisson noise, etc.), and the traditional data augmentation methods are used to expand the number of sample data sets (Data set) when they are small. Sample pairing method, Mix up method, etc.

In this paper, we consider data enhancement by adding "Salt and Pepper" to the data.

"Pepper noise" is divided into "pepper noise" and "salt noise", which refer to white dots with a gray value of 1 and black dots with a gray value of 0, respectively. We add a given percentage of noise to the image by controlling the value of signal-to-noise ratio (SNR).

In this paper, we set  $\text{SNR}=0.99$ , and add noise to all damage images according to this ratio, i.e. "pepper noise" or "salt noise" is added to 1 out of every 100 data. The damage contour after adding noise is shown in the following figure:

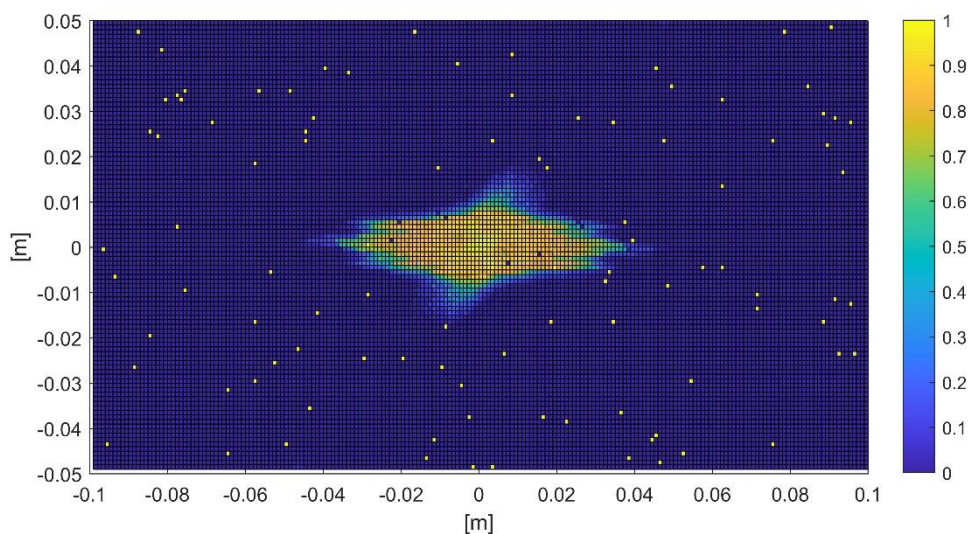
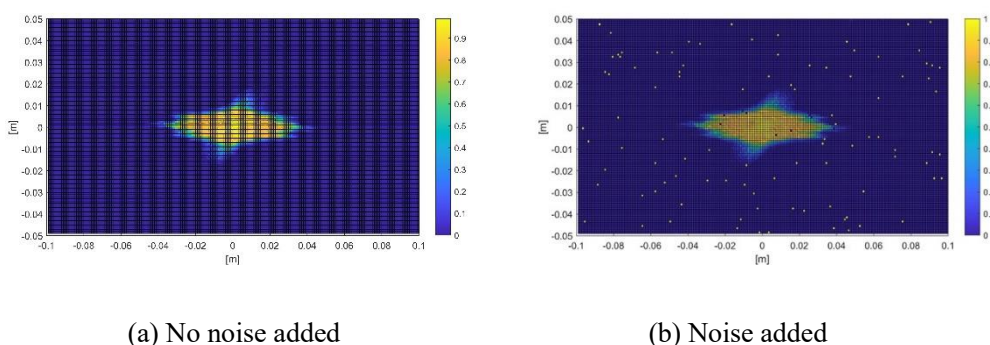


Fig.4.22 Damage contour after adding noise to layer 1 in case 1 ( $v=30\text{m/s}$ ,  $\alpha=0^\circ$ )

A comparison with the original image is shown below:



(a) No noise added

(b) Noise added

Fig.4.23 "Pepper noise" effect diagram

The yellow and blue dots in the figure are the added "pretzel noise", which accounts for 1% of the total number of points. This percentage is very small and will not blur the features of the damage contour. The above operation was repeated 10 times for each damage image, as shown in the following figure:

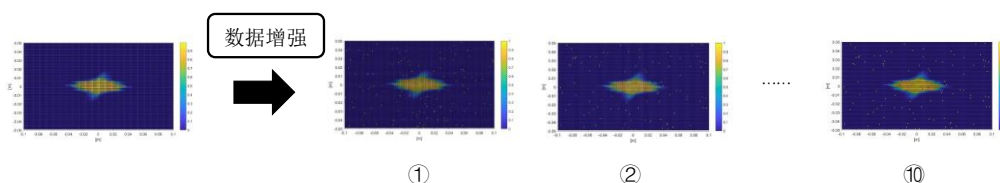


Fig.4.24 Data enhancement

Then, for each condition, we can obtain 10 different sets of noise added damage contours, which can expand the sample capacity from 180 to 1800 sets, thus achieving the effect of data enhancement.

### **3. Partitioning of the data set**

With the initial construction and data augmentation described above, we obtained 1800 sets of sample data, and these constitute our subsequent deep learning dataset.

According to the deep learning theory, we need to divide the 1800 sets of data into three groups, i.e. Training set, Validation set and Test set.

The three data sets serve the following purposes.

(1) Training set: the training set is input into the model at the beginning of the phase for training, helping the model to keep updating its parameters during the training process; in terms of quantity, it accounts for the largest share of the data set.

(2) Validation set: The main function of the validation set is to prevent the model from "overfitting" and to verify that the model has sufficient generalization ability, i.e., similar sensitivity to different data sets.

(3) Test set: The role of the test set is to test the recognition ability of the model using the trained model after the training is finished.

According to the related literature, the ratio of the three data sets can be set to 8:1:1. According to this ratio, we randomly select 1440 sets as the training set and input them into the constructed neural network for training; then randomly select 180 sets as the validation set to verify the generalization ability of the model after each round of training to prevent overfitting; and the last 180 sets as the test set to test the accuracy of the model after the training is completed. model recognition accuracy.

In the aforementioned division of material points, the laminate was divided into more than 180,000 material points in total. However, according to the damage evolution contour obtained in the previous section, almost all the damage of the plate is concentrated in its central area, i.e., the area in contact with the impactor and its peripheral part, while the other areas, especially its edge areas, hardly produce any damage. Based on this, we consider cutting the original laminate by cutting off 20% of the length of each side of the plate, and selecting only the damage data of the material points in the central part as the input of the neural network.

The discarded areas have zero damage values, so they do not affect the distribution of the damage data, and at the same time, the amount of input data is reduced by about 40%, which also improves the computational efficiency. The

laminates are cut as shown in the following figure.:

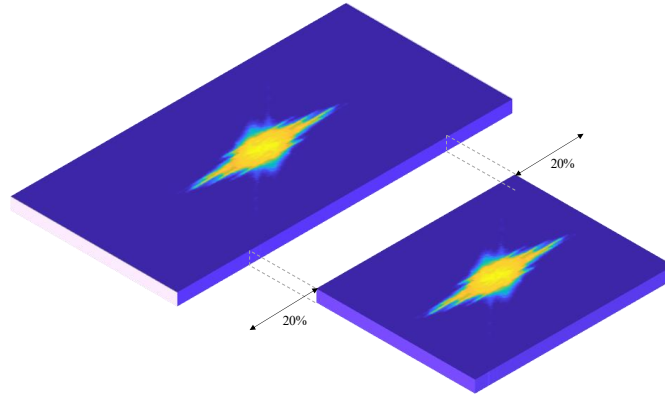


Fig.4.25 Schematic diagram of laminate cutting

#### 4.5.2 Identification based on the whole dataset

After building the model and getting the training data set, we can input 144 sets of training set data into the input layer of the model and start the training. After 3000 rounds of iterative training, the time-course curves of the damage functions of the training and validation sets can be plotted as shown below:

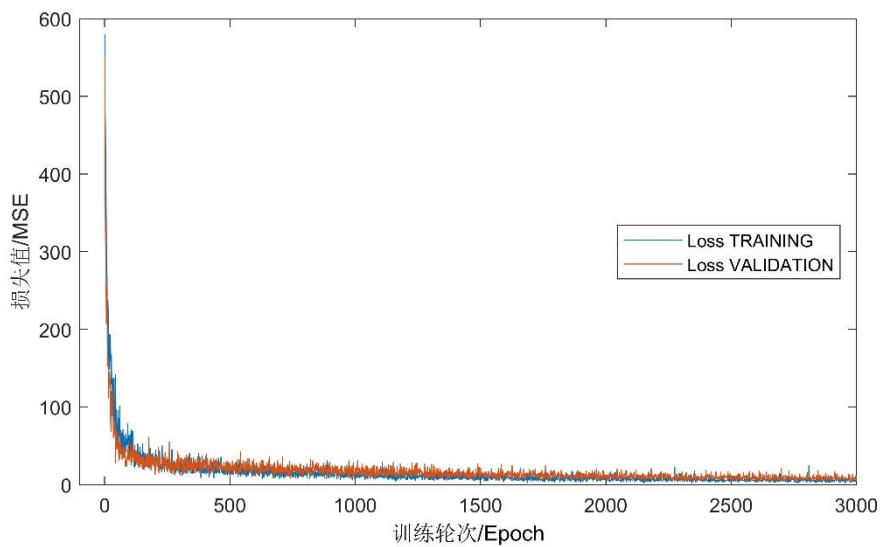


Fig.4.26 Training loss for the training and validation sets

Observing the loss function curves, we can find that after 3000 rounds of

iterative training, the loss functions of both have converged to very small values.

Unlike the classification problem, we define the accuracy rate in this paper as follows: the recognition result is considered accurate when the absolute error between the recognition result and the true value is not greater than  $5 (^\circ / m/s)$ .

Based on the above definitions, an image of the 3000-round accuracy time course curve can be plotted as shown below:

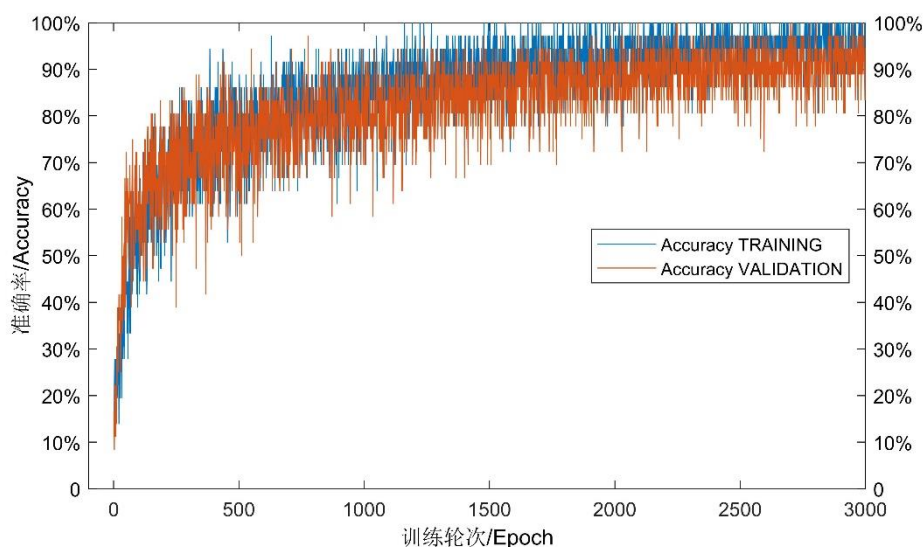


Fig.4.27 Accuracy of training set and validation set

After 3000 rounds of training, the accuracy of both the training and validation sets reached about 95%, indicating that the model has a high recognition accuracy and no "overfitting" phenomenon.

We used the trained model to recognize the remaining 180 test sets and selected 18 of them to show the recognition results as follows:

Table4.7 Table of identification results

No.	$v [m/s]$	$\alpha [^\circ]$
1	64.98	35.96
2	54.90	47.32
3	60.47	78.04
4	58.06	80.45
5	74.09	54.50
6	37.82	22.84

7	56.65	18.78
8	53.26	34.64
9	45.73	10.42
10	75.96	60.93
11	69.48	55.46
12	46.91	22.58
13	63.77	10.87
14	57.56	51.56
15	35.84	48.01
16	51.32	53.99
17	35.16	10.84
18	62.13	25.73

The label values (true values) corresponding to each working condition are shown in the following table:

Table4.8 Table of label values

No.	$v[m/s]$	$\alpha[^\circ]$
1	65	35
2	55	50
3	65	80
4	60	80
5	75	55
6	35	20
7	55	20
8	55	35
9	45	10
10	75	60
11	70	55
12	45	20
13	60	10
14	60	60
15	35	45
16	50	55
17	35	10

18

60

25

From there we can calculate the relative error as shown in the following table:

Table4.9 Relative error table

No.	$\nu$	$\alpha$
1	0.04%	2.74%
2	0.18%	5.35%
3	6.96%	2.45%
4	3.23%	0.57%
5	1.21%	0.91%
6	8.06%	14.21%
7	3.00%	6.08%
8	3.17%	1.02%
9	1.63%	4.17%
10	1.28%	1.54%
11	0.74%	0.84%
12	4.24%	12.92%
13	6.28%	8.66%
14	4.07%	14.06%
15	2.41%	6.69%
16	2.65%	1.84%
17	0.45%	8.37%
18	3.55%	2.90%
Average	2.95%	5.30%

The absolute errors are shown in the following table.:

Table4.10 Absolute error table

No.	$\nu [m/s]$	$\alpha [^\circ]$
1	0.02	0.96
2	0.10	2.68
3	4.53	1.96
4	1.94	0.45
5	0.91	0.50
6	2.82	2.84
7	1.65	1.22

8	1.74	0.36
9	0.73	0.42
10	0.96	0.93
11	0.52	0.46
12	1.91	2.58
13	3.77	0.87
14	2.44	8.44
15	0.84	3.01
16	1.32	1.01
17	0.16	0.84
18	2.13	0.73
Average	1.58	1.68
Standard deviation	1.24	1.92

Reading the data in the error table, we can get, in the speed identification results, the maximum relative error is located in working condition 6, 8.06%, the minimum error is located in working condition 1, only 0.04%, the average relative error is 2.95%; the maximum absolute error is located in working condition 3, 4.53  $m/s$ , the minimum error is located in working condition 1, only 0.02  $m/s$ , the average absolute error is 1.58  $m/s$ .

In the angle identification results, the maximum relative error is also located in working condition 6, 14.21%, the minimum is located in working condition 4, only 0.57%, the average relative error is 5.30%; the maximum absolute error is 8.44° , the minimum is only 0.5°, the average absolute error is 1.68°.

Analyzing the above error data, we find that for the vast majority of results, the identification results have extremely small errors relative to the labeled values (true values). According to the accuracy formula proposed in this section, 18 sets of data, for a total of 36 sets of identification results, 35 sets will have an absolute error within 5[° / $m/s$ ], with an accuracy rate of 97.2%.

The above results prove that the fitting effect and recognition ability of the model have reached a high degree and meet the requirements of engineering practice.

### 4.5.3 Identification based on partial dataset

In practical engineering, due to the limitation of the technology level, we cannot

get the damage of all data points, so we started to study the change of the model accuracy when the number of samples in the input data set is reduced.

We consider the selection of material points by controlling the step size. The selection process is shown in the following figure:

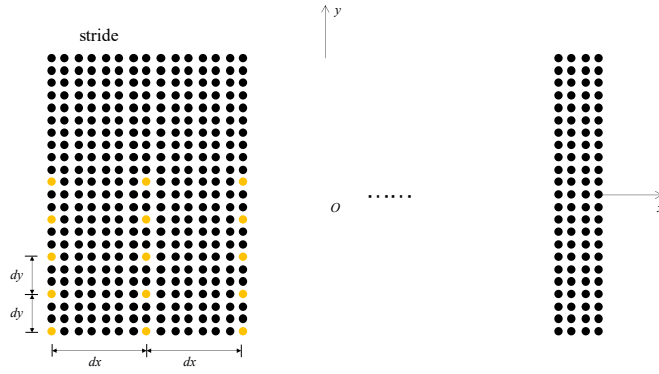


Fig.4.28 采样示意 Fig.

We start from the lower left corner and select a material point every  $dx$  points along the  $x$ -direction and every  $dy$  points along the  $y$ -direction. Since two pooling layers are set in our neural network structure, the dimension of the input matrix becomes 1/2 of the original one in the length and width direction for each pooling layer, i.e., both dimensions should be a multiple of 4. We control the dimensionality of the output data by the following equation:

$$m = \left\lfloor \frac{\left\lceil \frac{100}{dx} \right\rceil}{4} \right\rfloor \times 4 \quad (4.8)$$

$$n = \left\lfloor \frac{\left\lceil \frac{120}{dy} \right\rceil}{4} \right\rfloor \times 4 \quad (4.9)$$

where  $m$ ,  $n$  are the dimensions of the sampled matrix;  $dx$ ,  $dy$  are the sampling spacing in the  $x$  and  $y$  directions, respectively.

To investigate the relationship between the recognition error of the model and the sampling spacing based on data reduction, we adjusted the values of  $dx$ ,  $dy$  according to the data in the following table.:

Table4.11 Sampling spacing table

$dx$	$dy$
------	------

2	2
3	3
4	4
6	6
8	8

By adjusting the sampling spacing according to the above table and repeating the identification process in Section 4.3.2, we can obtain the variation of the loss functions of the training and test sets under each set of spacing as shown in the following figure:

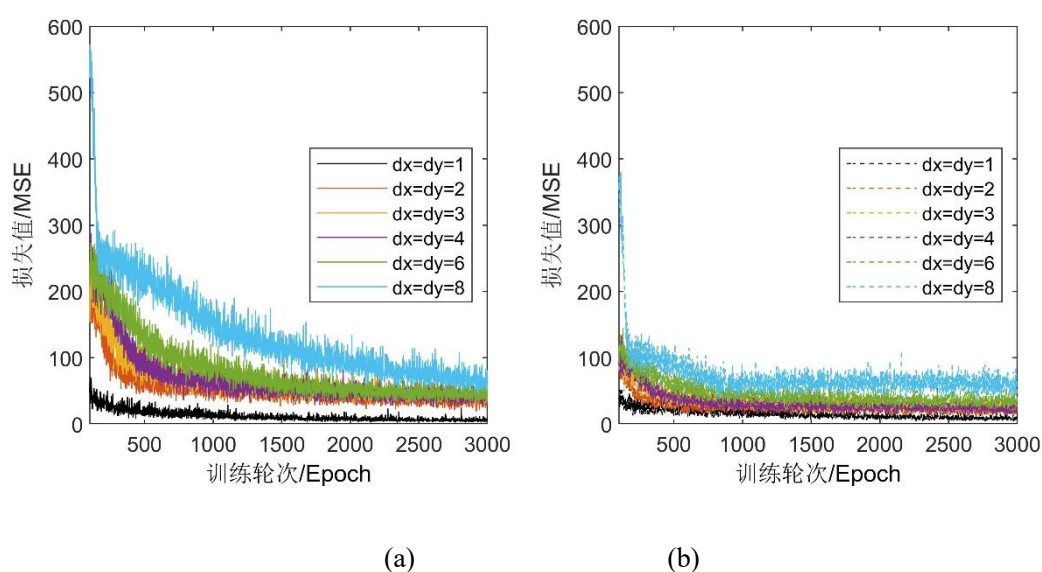
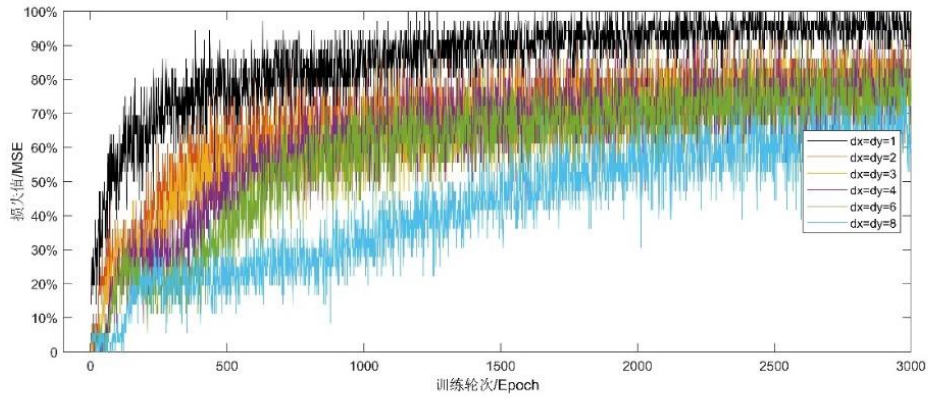


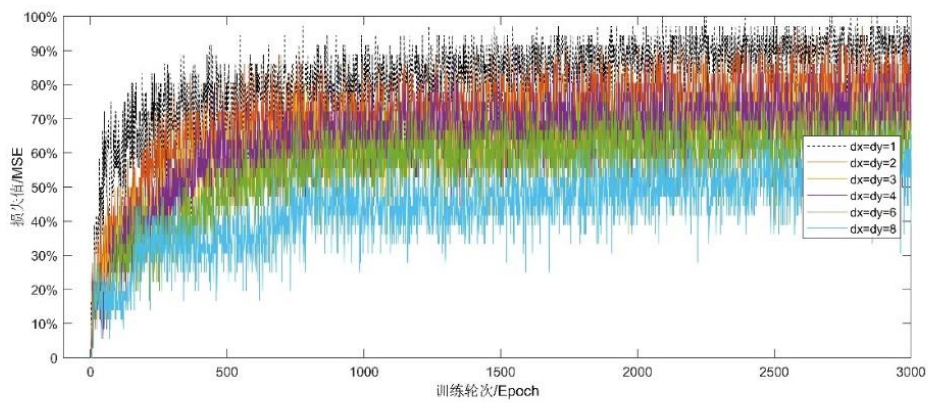
Fig.4.29 (a) Training set loss (b) Validation set loss

From the above images, it can be found that as the sampling spacing increases, the loss value obtained by the model convergence also gradually increases, and when the sampling spacing is taken  $(dx, dy)$  as  $(8, 8)$ , the loss value converges to about 60, which is nearly 10 times more than the initial value.

Also, the accuracy of the training and validation sets can be plotted as shown below:



(a)



(b)

Fig.4.30 (a) Training set accuracy (b) Validation set accuracy

Also, the change in accuracy of the training set can be plotted as shown in the following figure:

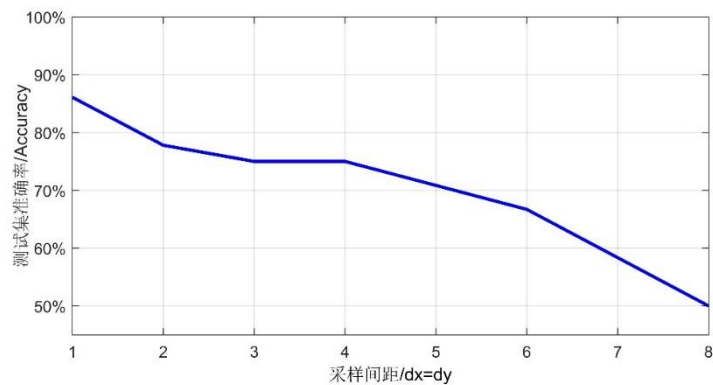


Fig.4.31 Training set accuracy

and the trend of the relative error is shown in the following figure.:

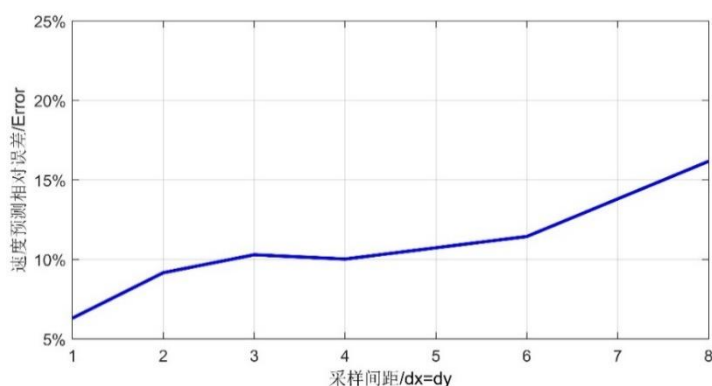


Fig.4.32 Speed relative error

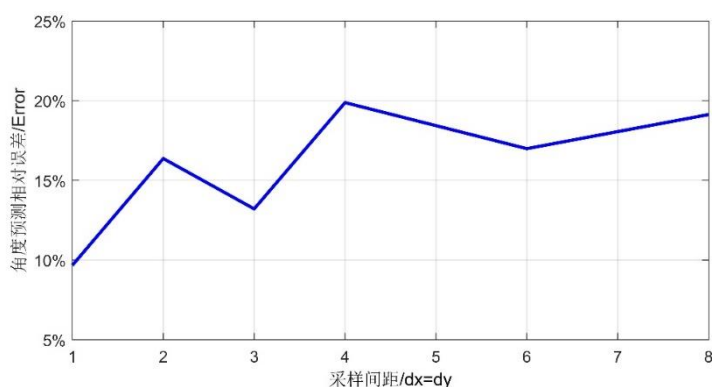


Fig.4.33 Angular relative error

Observing the above images, we can also draw similar conclusions, i.e., as the sampling spacing increases and the number of samples decreases, the model shows the following changes.

(1) Convergence of the damage function to a larger value, indicating a decrease in the optimization capability of the model and convergence to some less optimal local optimum point.

(2) The accuracy rate tends to decrease significantly, but the model still has an accuracy rate of about 75% when the selected material points are trained, while when the sampling spacing  $(dx, dy)$  is  $(8, 8)$ , the number of samples used as input is about 1/64 of the initial one, and for this order of magnitude, the recognition accuracy rate of the model has decreased to about 50%, which basically does not have practical application value.

In summary, constructing the dataset by sampling reduces the amount of input data and also significantly reduces the model recognition accuracy, but when the

amount of data is reduced to a certain degree (around in this paper), the model still has a high accuracy, and the amount of input data can be adjusted according to the actual needs.

#### 4.6 Summary of this chapter

In this chapter, we further investigate the inverse problem of identifying impact conditions from damage evolution data, which is of great importance and has wide application in engineering. At the same time, impact condition identification encounters great challenges due to the complex nonlinear characteristics of composite laminate impact damage evolution, and attempt to identify unknown impact conditions using deep learning methods.

To solve this problem, we first analyzed the type of damage data and the form of impact, and briefly reviewed and analyzed various types of neural network structures widely used in the current deep learning field, from which we selected the most suitable class of neural network structure, convolutional neural network (CNN), based on the characteristics of various models and the actual problem of this paper. ).

Then, we developed a deep learning-convolutional neural network (CNN)-based laminate impact recognition program in the framework of TensorFlow and Jupyter Notebook, inspired by image recognition techniques. Based on the PD program in Chapter 3, we expand the dataset to 1800 sets by modifying the velocity and angle of the impact and adding "pretzel noise", and the program uses this dataset for training and recognition of unknown conditions. The relative error of the final recognition result is controlled within 5%, and the recognition accuracy is over 90%, which has high application value.

After that, the damage evolution data of some material points were selected as the training set, and the changes of the model accuracy and error were analyzed under different sample numbers and patterns. It was found that the accuracy of the model decreased significantly as the number of samples decreased, and the error increased accordingly, indicating that the recognition ability of the model decreased significantly with the decrease of the number of samples, and it was also found that the model still had an accuracy of about 75% when the material points were selected as the input, while the accuracy of the model decreased to about 50% when only the damage data of the material points were selected as the input, indicating that The

model is unable to learn the effective information from the data, and this procedure does not have practical application value. It is necessary to further improve the accuracy by other means, such as increasing the number of hidden layers, modifying the network structure, and data enhancement.

## Chapter 5 Conclusion and Outlook

### 5.1 Conclusion

In this paper, we use the traditional peridynamics model and deep learning theory to investigate the relevant positive and negative problems based on the impact damage evolution of a composite laminate model. Firstly, for the problem of discontinuous mechanics of composite laminate impact damage, an analytical model of composite laminate rigid body impact damage evolution based on peridynamics theory is established, and the corresponding computational procedure is developed. Moreover, in order to solve the problem of incomplete near-field material points in the boundary region, an improved "Table surface correction factor" is proposed, which can improve the calculation accuracy. Based on the above results, a deep learning-convolutional neural network (CNN)-based impact condition recognition model is built to address the problem that the damage evolution of composite laminates exhibits complex nonlinear characteristics and the impact condition recognition encounters great challenges. A deep learning-convolutional neural network (CNN)-based impact condition recognition model was developed, and the laminate damage evolution data obtained under different impact conditions were used for training, and the recognition of unknown impact conditions was successfully achieved with high accuracy and precision. The specific research results are summarized as follows:

(1) The impact damage evolution of composite laminates is related to the impact conditions (shape of the impactor, impact velocity, direction) and the form of ply lay-up of the laminate. The damage tends to spread along the fiber direction of each ply, and the damage area of each ply of the laminate is larger for different impact conditions when the impactor volume is larger and the impact velocity is higher.

(2) The deep learning-convolutional neural network (CNN)-based impact condition recognition procedure can effectively identify the unknown impact conditions and control the recognition error within a small range with a high accuracy rate. We built a deep learning-convolutional neural network (CNN)-based laminate impact condition recognition program, and selected several sets of conditions that did not appear in the training and validation sets to test the recognition ability of the model, and found that the average error between the recognition results and the real

values was controlled at about 3%, and the accuracy of the recognition results reached about 90%, thus verifying the effectiveness and applicability of our recognition program. validity and applicability.

(3) The recognition accuracy of the model is related to the size of the sample. By selecting damage data from different locations of material points and studying the effect of sample size on the accuracy, it was found that the accuracy of the model began to decrease as the number of selected data points became smaller, while the error increased, indicating that the recognition ability of the model decreases as the number of samples decreases, and the model still has an accuracy of about 75% when 1/4 of the material points selected for training are selected, while the accuracy of the model is about 75% when the material points selected for training are selected. The accuracy of the model decreases to about 50% when 1/64 of the material points are selected for training, which is basically not applicable.

## 5.2 Outlook

In terms of the present results, the research work of this paper has achieved certain results and the accuracy of the relevant identification procedures is good, but there are still many defects and debatable points based on the above work, which are now briefly described as follows.

(1) The numerical method of PD is less efficient, the calculation of PD depends on the discretization of material points, for the finer the model, the more the number of material points and the number of "keys" involved in the calculation procedure, take this paper as an example, the laminate model in this paper is divided into 182,709 material points, the number of "keys" in each material point field is in hundreds. In this paper, for example, the laminate model is divided into 182,709 material points, and the number of "bonds" in each material point field is recorded in hundreds, and the whole model involves nearly 10 million PD bonds. For more detailed models, or when the model size is even larger, the number of keys will be even larger and the time required will also increase proportionally.

(2) Damage data collection and evaluation is more difficult. Due to technical and capability limitations, our work is limited to numerical values, especially in the methodological area of damage identification techniques. Damage identification is still a difficult problem in engineering, and there are numerous researches in related

fields. In particular, refined damage identification methods for small and micro structures and components still need to be researched and developed, and many structures are not visible and open to the outside, and are difficult to cut, thus making it difficult to discover and monitor their internal damage evolution; at the same time, there are difficulties in calibrating the damage degree of the test structure. The aforementioned difficulties also make it difficult to obtain training datasets for the neural networks we build, despite their notable efficiency and accuracy, and it is well known that a sufficiently large dataset is the basis for us to continuously update and improve the network structure. Therefore, the methodological field of damage recognition still needs further work and efforts from scholars.

(3) Attempts and applications of "state-based" peridynamics theory. "The "state-based" PD theory has been published for some isotropic single-media materials, in which the derivation of the physical quantities of such materials is given, but for each anisotropic material with composite materials as a proxy for Table, this method has not been studied in depth. Therefore, it is hoped that the near-field kinetic theory and the study of anisotropic materials will be further explored in the future.

(4) Other forms of network structures can be tried in the impact condition recognition procedure. Convolutional neural networks can formally match two-dimensional models such as plates better, but they cannot reflect the temporal properties of the impact; at the same time, due to the limited computational efficiency, the hidden layers of the network used in this paper are small, therefore, CNN with other forms of network structures (such as RNN with temporal correlation) can be tried to build deeper and more computationally efficient recognition procedures and algorithms.



## Reference

- [1] MADENCI E, OTERKUS E. Coupling of the peridynamic theory and finite element method[M]. Springer, New York, NY, 2014: 191-202.
- [2] FLORIN, BOBARU, YOUN, et al. Damage progression from impact in layered glass modeled with peridynamics[J]. Central European Journal of Engineering, 2012,2(4): 551-561.
- [3] BLESS S, CHEN T. Impact damage in layered glass[J]. International Journal of Fracture, 2010,162(1-2): 151-158.
- [4] AKBARI M J, KAZEMI S R. Peridynamic Analysis of Cracked Beam Under Impact[J]. JOURNAL OF MECHANICS, 2020,36(4): 1-13.
- [5] NING, LIU, DAHSIN, et al. Peridynamic modelling of impact damage in three-point bending beam with offset notch[J]. Applied Mathematics and Mechanics(English Edition), 2017,38(1): 103-114.
- [6] HA Y D, BOBARU F. Studies of dynamic crack propagation and crack branching with peridynamics[J]. International Journal of Fracture, 2010,162(1): 229-244.
- [7] WU Z, LIU D, XNGUYEN H, et al. Dynamic Fracture Process during Three-Point-Bending Impact on Polymethyl-Methacrylate Beams[J]. Global Journal of Researches in Engineering: A Mechanical and Mechanics Engineering, 2017,17(1):115-122.
- [8] LOYA J A, VILLA E I, FERNÁNDEZ-SÁEZ J. Crack-front propagation during three-point-bending tests of polymethyl-methacrylate beams[J]. Polymer Testing, 2010,29(1): 113-118.
- [9] BUTLER A E. Peridynamic prediction of compression and impact strength of carbon fiber reinforced plastic panels[J]. Transactions of the Japan Society of Mechanical Engineers, 2013,78: 83-94.
- [10] BABER F, HALL R, JUSTUSSON B, et al. An Improved Peridynamic Approach for Prediction of Low Velocity Impact Damage in Fiber Reinforced Composites[C]. AIAA Scitech 2021 Forum, 2021.
- [11] LE Q, BOBARU F. Surface corrections for peridynamic models in elasticity and fracture[J]. Computational Mechanics: Solids, Fluids, Fracture Transport Phenomena and Variational Methods, 2018,64(4): 499-518.
- [12] BARTLETT J, STORTI D. A Generalized Fictitious Node Approach for Surface Effect Correction in Peridynamic Simulation[J]. Journal of Peridynamics and Nonlocal Modeling, 2021(2): 70-81.
- [13] 黄丹, 乔丕忠, 章青, et al. 近场动力学方法及其应用[J]. 力学进展, 2010,40(4): 448-457.
- [14] 沈峰, 章青, 黄丹, et al. 冲击荷载作用下混凝土结构破坏过程的近场动力学模拟[J]. 工程力学, 2012(S1): 12-15.
- [15] 顾鑫, 章青, 黄丹. 基于常规状态近场动力学理论的含孔板破坏分析: 中国力学大会[C], 2015.
- [16] 郁杨天, 章青, 顾鑫. 含单边缺口混凝土梁冲击破坏的近场动力学模拟[J]. 工程力学, 2016(12): 85-90.
- [17] 沈峰, 章青, 黄丹, et al. 基于近场动力学理论的混凝土轴拉破坏过程模拟[J]. 计算力学学报, 2013,30(S1): 79-83.

- [18] 顾鑫, 章青, 黄丹. 基于近场动力学方法的混凝土板侵彻问题研究[J]. 振动与冲击, 2016,35(06): 52-58.
- [19] CHENG Z, HU Y, CHU L, et al. Peridynamic modeling of engineered cementitious composite with fiber effects[J]. *Engineering Fracture Mechanics*, 2021,245(11): 107601.
- [20] 熊伟鹏, 王超, 傅江妍, et al. 冰球冲击试验的近场动力学方法数值模拟[J]. 振动与冲击, 2020,39(7): 148-155.
- [21] 周小平, 王允腾, 钱七虎. 爆破荷载作用下岩石破坏特性的"共轭键"基近场动力学数值模拟研究[J]. *中国科学(物理学 力学 天文学)*, 2020,050(002): 48-60.
- [22] 郑国君, 陈瑞, 申国哲, et al. 改进的键基正交各向异性近场动力学模型[J]. *计算机辅助工程*, 2020,029(001): 1-8.
- [23] 张劲松. 基于近场动力学的冲击模拟方法研究[D]. 上海交通大学, 2015.
- [24] 王富伟, 黄再兴. 复合材料层合板冲击损伤近场动力学模型与分析[J]. *计算力学学报*, 2014,31(06): 709-713.
- [25] 秦洪远, 李玲, 王伟, et al. 基于改进型近场动力学方法的复合材料单向板变形与破坏分析[J]. *宇航材料工艺*, 2020(4): 19-23.
- [26] 赵天佑. 基于近场动力学的舰船复合材料结构冲击损伤研究[D]. 哈尔滨工程大学, 2019.
- [27] 苏伯阳, 李书欣, 刘立胜, et al. 湿热环境下复合材料冲击损伤的近场动力学模拟[J]. *科学技术与工程*, 2018,018(001): 201-206.
- [28] 陈晓烽, 王新峰. 基于近场动力学的复合材料平板低速冲击损伤研究[J]. *江苏航空*, 2019,156(01): 31-34.
- [29] 陈晓烽. 基于近场动力学的复合材料曲板冲击损伤研究[D]. 南京航空航天大学, 2019.
- [30] LIU J, XIE J, LI B, et al. Regularized Cubic B-spline Collocation Method with Modified L-curve Criterion for Impact Force Identification[J]. *IEEE Access*, 2020, 8: 36337-36349.
- [31] AB DE LJABER O, AVCI O, KIRANYAZ S, et al. Real-time vibration-based structural damage detection using one-dimensional convolutional neural networks[J]. *Journal of Sound & Vibration*, 2017,388: 154-170.
- [32] LI H, LI Z, XIAO Z, et al. Development of an integrated model for prediction of impact and vibration response of hybrid fiber metal laminates with a viscoelastic layer[J]. *International Journal of Mechanical Sciences*, 2021(3): 106298.
- [33] CHONG M, ABRAHAM A, PAPRYCKI M. Traffic Accident Analysis Using Machine Learning Paradigms.[J]. *Informatica*, 2005, 29(1):89-98.
- [34] KALHORI H, TASHAKORI S, HALKON B. Experimental Study on Impact Force Identification on a Multi-Storey Tower Structure Using Different Transducers[J]. *Vibration*, 2021, 4(1), 101-116.
- [35] KALHORI H, ALAMDARI M M, LI B, et al. Concurrent Identification of Impact Location and Force Magnitude on a Composite Panel[J]. *International Journal of Structural Stability and Dynamics*, 2020, 20(10): 2042004.
- [36] KAWABATA N, HAYATA H, HU N, et al. Modal Measurements Using Strain Sensors and Application to Impact Force Identification[J]. *Inverse Problems in Engineering Mechanics IV*, 2003: 85-94.
- [37] LI T. Machine Learning-Based Inverse Solution for Predictions of Impact Conditions during Car Collisions[D]. UC Berkeley, 2019.
- [38] 方际澄. 冰球冲击层压板的载荷与分层响应识别[D]. 上海交通大学, 2019.
- [39] 朱向阳, 郭旭, 赫亮. 复合材料层合板低速冲击载荷定位研究[J]. *航空计算技术*, 2018,48(06):

- 29-31.
- [40] 严刚, 孙浩. 基于贝叶斯压缩感知的复合材料结构冲击载荷识别研究[J]. 振动工程学报, 2018,31(03): 483-489.
- [41] 贾方, 刘升. 基于交替方向乘子法的冲击载荷识别[J]. 锻压技术, 2014,39(09): 86-91.
- [42] 苏永振, 袁慎芳, 王瑜. 基于多重信号分类算法的复合材料冲击定位[J]. 复合材料学报, 2010,27(03): 105-110.
- [43] 李守巨, 刘迎曦, 何翔, et al. 基于人工神经网络的爆炸冲击荷载参数识别方法[J]. 岩石力学与工程学报, 2003,22(11): 1870.
- [44] 郭松, 何顶顶. 基于小波包变换及相关系数法的复合材料层合板冲击位置识别研究[J]. 航天器环境工程, 2017,34(05): 464-470.
- [45] 王利恒. 基于应变信号的复合材料层合板低速冲击损伤识别研究[J]. 工程力学, 2014,31(02): 230-236.
- [46] 沈观林, 胡更开. 复合材料力学[M]. 清华大学出版社, 2006.
- [47] MADENCI E, OTERKUS E. Peridynamic Theory and Its Applications[J]. Springer, New York, 2014,10.1007/978-1-4614-8465-3.
- [48] 束德林. 工程材料力学性能[M]. 机械工业出版社, 2004.
- [49] 徐芝纶. 弹性力学简明教程[M]. 高 et al教育出版社, 2013.
- [50] SILLING S A, ASKARI E. A meshfree method based on the peridynamic model of solid mechanics[J]. Computers & Structures, 2005,83(17-18): 1526-1535.
- [51] 谢国森. 基于深度学习的Fig. 像识别算法研究[D]. 中国科学院大学, 2016.
- [52] 张国云, 郭龙源, 吴健辉, et al. 计算机视觉与Fig. 像识别[M]. 科学出版社, 2012.
- [53] 孙海英. Fig. 像高斯噪声及椒盐噪声去噪算法研究[D]. 复旦大学, 2012.
- [54] 刘正兴. 计算固体力学[M]. 上海交通大学出版社, 2010.
- [55] 谢多夫. 连续介质力学[M]. 高 et al教育出版社, 2007.
- [56] ARNOLD V, ARNOLD V, ARNOLD V I, et al. Mathematical methods of classical mechanics[J]. Advances in Mathematics, 1983,49(1): 106.
- [57] SILLING S A, EPTON M, WECKNER O, et al. Peridynamic States and Constitutive Modeling[J]. Journal of Elasticity, 2007,88(2): 151-184.
- [58] SILLING S A, LEHOUCQ R B. Convergence of Peridynamics to Classical Elasticity Theory[J]. Journal of Elasticity, 2008,93(1): 13-37.
- [59] SILLING S A. Reformulation of elasticity theory for discontinuities and long-range forces[J]. Journal of Mechanics Physics of Solids, 2000,48(1): 175-209.
- [60] CABOT G P, BA ANT Z P. Nonlocal Damage Theory[J]. Journal of Engineering Mechanics, 1987,113(10): 1512-1533.
- [61] REDDY J N. Nonlocal theories for bending, buckling and vibration of beams[J]. International Journal of Engineering Science, 2007,45(2-8): 288-307.
- [62] XIA S, LI G, HAO L. A nonlocal damage theory[J]. International Journal of Fracture, 1987,34(4): 239-250.
- [63] 樊康旗, 贾建援. 经典分子动力学模拟的主要技术[J]. 微纳电子技术, 2005,42(3): 133-138.
- [64] BHUSHAN B. Molecular Dynamics Method[M]. Encyclopedia of Nanotechnology, 2012.
- [65] 阎守胜. 固体物理基础[M]. 北京大学出版社, 2011.
- [66] 哈尔滨工业大学理论力学教研室. 理论力学[M]. 理论力学, 1997.
- [67] 朗道, 栗弗席兹, 李俊峰. 理论物理学教程:力学[M]. 高 et al教育出版社, 2007.
- [68] LANDAU L D, PITAEVSKII L P, LIFSHITZ E M, et al. Course of theoretical physics[M].

- Elsevier, 2013.
- [69] 秦洪远, 黄丹, 章青. 混凝土复合型裂纹扩展的非局部近场动力学建模分析[J]. 计算力学学报, 2017,34(03): 274-279.
- [70] 秦洪远, 韩志腾, 黄丹. 含初始裂纹巴西圆盘劈裂问题的非局部近场动力学建模[J]. 固体力学学报, 2017,38(06): 483-491.
- [71] 沈峰, 田磊, 章青, et al. 基于DIP技术的混凝土非均质近场动力学模型研究[J]. 郑州大学学报(理学版), 2018,50(04): 112-116.
- [72] 白小敏, 唐建群, 巩建鸣. 不同过电位下一维点蚀的近场动力学数值模拟[J]. 南京工业大学学报(自然科学版), 2017,39(06): 91-98.
- [73] ZHANG G, LE Q, LOGHIN A, et al. Validation of a peridynamic model for fatigue cracking[J]. *Engineering Fracture Mechanics*, 2016,162: 76-94.
- [74] BABER F, GUVEN I. Solder joint fatigue life prediction using peridynamic approach[J]. *Microelectronics Reliability*, 2017,79: 20-31.
- [75] SILLING S A. Reformulation of elasticity theory for discontinuities and long-range forces[J]. *Journal of the mechanics and physics of solids*, 2000,48(1): 175-209.
- [76] 黄丹, 卢广达, 章青. 准静态变形破坏的近场动力学分析[J]. 计算力学学报, 2016,33(05): 657-662.
- [77] 李波, 李遇春, 吴晓涵. 混凝土试件劈裂抗拉强度的数值研究[J]. 结构工程师, 2016,32(03): 45-49.
- [78] 马鹏飞, 李树忱, 周慧颖, et al. 岩石材料裂纹扩展的改进近场动力学方法模拟[J]. 岩土力学, 2019,40(10): 4111-4119.
- [79] 郁杨天, 章青, 顾鑫. 近场动力学微极模型在求解静力学问题中的应用[J]. 力学季刊, 2017,38(01): 50-57.
- [80] 石宏顺, 钱松荣, 原群盛, et al. 基于近场动力学理论的准脆性材料的本构力函数的构建[J]. 计算力学学报, 2017,34(04): 422-427.
- [81] 胡祎乐. 基于近场动力学的FRP层压板建模与分析[D]. 上海交通大学, 2013.
- [82] 秦洪远, 黄丹, 刘一鸣, et al. 基于改进型近场动力学方法的多裂纹扩展分析[J]. 工程力学, 2017,34(12): 31-38.
- [83] 刘肃肃, 余音. 复材非线性及渐进损伤的态型近场动力学模拟[J]. 浙江大学学报(工学版), 2016,50(05): 993-1000.
- [84] SILLING S A, LEHOUCQ R B. Peridynamic Theory of Solid Mechanics[J]. *Advances in Applied Mechanics*, 2010,44(10): 73-168.
- [85] 刘新东, 郝际平. 张量分析[M]. 国防工业出版社, 2009.
- [86] HAN F, LUBINEAU G, AZDOUD Y, et al. A morphing approach to couple state-based peridynamics with classical continuum mechanics[J]. *Computer Methods in Applied Mechanics and Engineering*, 2016,301: 336-358.
- [87] ZHANG H, QIAO P. A state-based peridynamic model for quantitative fracture analysis[J]. *International Journal of Fracture*, 2018,211(1-2): 217-235.
- [88] SHANG S, QIN X, LI H, et al. An application of non-ordinary state-based peridynamics theory in cutting process modelling of unidirectional carbon fiber reinforced polymer material[J]. *Composite Structures*, 2019,226: 111194.
- [89] 王联, 王慕秋. 常差分方程[M]. 新疆大学出版社, 1991.
- [90] 丁同仁, 李承治. 常微分方程教程[M]. 高等教育出版社, 2004.
- [91] 沈峰, 章青, 黄丹, et al. 基于近场动力学方法的结构准静态变形的定量计算[J]. 重庆大学

- 学报, 2016,39(05): 49-55.
- [92] 郭帅, 焦学健, 李丽君, et al. 近场动力学方法研究复合材料失效的进展[J]. 材料导报, 2019,33(05): 826-833.
- [93] TURING A M. Computing machinery and intelligence[M]//Parsing the turing test. Springer, Dordrecht, 2009: 23-65.
- [94] KRIZHEVSKY A, SUTSKEVER I, HINTON G. ImageNet Classification with Deep Convolutional Neural Networks[J]. Advances in neural information processing systems, 2012,25(2): 1097-1105.
- [95] 周志华. 机器学习[M]. 清华大学出版社, 2016.
- [96] 周曼, 刘志勇, 陈梦迟, et al. 基于AlexNet的迁移学习在流程工业Fig. 像识别中的应用[J]. 工业控制计算机, 2018,31(11): 84-86.
- [97] ZEILER M D, FERGUS R. Visualizing and Understanding Convolutional Neural Networks[C]. European Conference on Computer Vision. Springer, Cham, 2014: 818-833.
- [98] SZEGEDY C, WEI L, JIA Y, et al. Going Deeper with Convolutions[C]. Proceedings of the IEEE Conference on Computer Vision and Pattern Recognition. 2015: 1-9.

